THE MIKER TECHNIQUE FOR DETERMINING

VAPOR PRESSURES AT HIGH TEMPERATURE

By

Eugene Albert Elphingstone

Bachelor of Science

Arkansas State University

Jonesboro, Arkansas

1965

Submitted to the Faculty of the Graduate College
of the Oklahoma State University
in partial fulfullment of the requirements
for the Degree of
MASTER OF SCIENCE
May, 1969

THE MIKER TECHNIQUE FOR DETERMINING

VAPOR PRESSURES AT HIGH TEMPERATURE

Thesis Approved:

_____
Thesis Adviser

_____

_____
Dean of the Graduate College

ACKNOWLEDGMENTS

The author wishes to express his thanks to his thesis advisor, Dr. R. D. Freeman, for his patient counsel during this investigation.

Acknowledgment is made to the Oklahoma State University Chemistry Department for teaching assistantships, to the Aeronautical Systems Division, Wright-Patterson Air Force Base, Ohio, to the Dow Chemical Company, and to the National Aeronautic and Space Administration for financial support.

Special thanks are extended to Mr. Heinz Hall and his associates in the Physics-Chemistry Shop for counsel in designing and then construction of the experimental apparatus.

Mr. Larry Jones and Mr. Ron Morrison are thanked for their assistance with the electrical components in the experimental apparatus.

Finally, thanks to my wife, Frances, who typed the rough drafts of the thesis.

TABLE OF CONTENTS

LIST OF TABLES

LIST OF FIGURES

LIST OF FIGURES (Continued)

CHAPTER I

Introduction

"All substances evaporate. They do so by different types of re-
actions and at vastly different pressures. The temperatures required
may be very high; but ultimately, all evaporate."[1] Thus, Professor
Gilles has described the scope of high temperature chemistry. In other
words, this area of chemistry includes any and all substances that are
considered non-volatile near room temperature.

If one wished to set limits on the temperature range that is de-
fined as high temperature, he might choose the range of 1000 $^{\circ}$K to 100,
000,000 $^{\circ}$K as indicated by Beckett[2]. A range of 1000 $^{\circ}$K to 6000 $^{\circ}$K
might be considered moderately high temperature.

Most of the work done in this field has been in the range of 1000
$^{\circ}$K to 2000 $^{\circ}$K. This is the temperature range that this work will be con-
cerned with.

The complexity of the reactions and ultimately the reactivity of
all materials at high temperature make work even in the 1000 $^{\circ}$K to 2000
$^{\circ}$K range extremely difficult.

The materials used in this temperature range are limited first by
their physical and chemical properties and second by their availability
at reasonable costs and in a suitable physical form. This latter prob-
lem is a technical one. An example is graphite cloth[3] which has pro-
perties much more suitable than solid carbon for resistance furnaces.

1

The materials commonly used now are tungsten, molybdenum, titanium, graphite (various forms and types), just to name a few.

One approach to determining the high temperature properties of materials is to measure their vapor pressures. There are two indirect methods widely used to measure vapor pressures at high temperature. They are the Knudsen effusion technique[4,5,6,7] and the Langmuir "free evaporation" technique[8,9].

The Langmuir technique involves measuring the rate of escape of atoms and/or molecules from a surface and will not be discussed here in detail. Conversely, the Knudsen technique involves measuring the rate of escape of atoms and/or molecules through an orifice. The work to be presented here is just one modification of the Knudsen technique.

In the Knudsen effusion technique one determines the weight lost during a specified time at a known temperature. Using this information along with some physical parameters of the effusion cell, one may calculate the vapor pressure of the material being studied. This work can be very simply done because one only needs a furnace, vacuum system and Knudsen cell. There is, however, one drastic shortcoming of this technique. To calculate the vapor pressure of a material, one must know the average molecular weight of the effusing vapors[10]. Since monomers, dimers, trimers, etc., are very common at high temperature, one needs to revert to some supplimentary method to determine the average molecular weight for the effusing vapors at a given temperature. The mass spectrometer used in conjunction with a Knudsen cell is one accepted method for determining the nature of the vapor species[11].

There is a second technique developed by Volmer, et. al.[12] This technique involves suspension of an effusion cell from a fine torsion

fiber. The cell may have two or four orifices in its sides; effusion from the cell causes some angular rotation of it. This technique has been given the mnemonic designation "Torker"[10] technique (torsion-Knudsen effusion-recoil). Weight loss from the cell may be determined as in the regular Knudsen effusion technique by weighing the cell before and after an experimental run or the cell may be suspended from a balance. Using either technique, one can easily calculate the vapor pressure using the standard Knudsen equation[10].

$$P_K = (2\pi RT/M)^{\frac{1}{2}} \dot{g}/\sum_i a_i W_i \qquad (1)$$

where T = temperature of cell in degrees Kelvin

M = average molecular weight of effusing vapors

R = gas constant

$\dot{g}$ = rate of effusion of sample

a_i = area of the ith orifice

W_i = transmission probability for i^{th} (non-ideal) orifice.

The unique feature of this technique is that one may simultaneously determine the vapor pressure of a material by observing the angular deflection of the torsion cell on the end of the torsion fiber that has previously been calibrated. This pressure is often referred to as the recoil pressure P_R and, if the system is at equilibrium, should be equal to the Knudsen pressure. The equation for the recoil pressure is[10]

$$P_R = 2\emptyset D/\sum_i a_i l_i \qquad (2)$$

where l_i = the lengths of the moment arms about the fiber

a_i = the orifice areas

$\emptyset$ = angular deflection

D = torsion constant for the fiber.

By inspection of the equations 1 and 2, one can see that only P_K needs the average molecular weight of the effusing molecules M for calculation. P_R is determined strictly from the torsion cell and fiber parameters, which may be determined independently of the experiment, and the angular deflection of the cell during the run. Thus, if one equates P_K and P_R, M may be determined by using both sets of experimental data and then inserted into equation 1 to obtain P_K. Equating P_K and P_R, one gets

$$M = \pi RT/2D^2 \emptyset^2 \left[\sum_{i=1}^{n} (g/a_i W_i) \sum_i (al)_i \right]^2 \qquad (3)$$

There are several problems that have been encountered in this technique. These include induction furnace-cell interaction[13,14], difficulty in obtaining a null position[14], temperature gradients in the cell[15], etc. Some other difficulties that are inherent in the technique are:

1. A torsion fiber is usually very fragile and requires extreme care in handling at all times; this can be bothersome since the cell must be removed periodically.

2. A convenient system in which one can measure weight loss and recoil simultaneously requires operation in vacuum of two separate, highly sensitive, measuring systems, an analytical balance and a torsion balance.

This technique is, however, very useful for high temperature chemistry in the 1000 ^{o}K to 2000 ^{o}K range. A review of this and other techniques used in high temperature chemistry is now available in book

form[16].

As a result of the difficulties encountered in work with the Torker technique, a new technique has been devised that hopefully incorporates the better features of the older technique and alleviates some of the inherent problems mentioned. The theory supporting this new technique follows in the next chapter.

There are two basic problems to be elucidated in this thesis. The first is to show that the technique to be presented in Chapter II can be used to determine the vapor pressure and average molecular weight of the effusing vapors at high temperature. The second problem is unavoidably intertwined with the first. It is to check the correction factors for non-ideal conical orifices at high temperature.

CHAPTER II

THE MIKER TECHNIQUE

The technique used in determining the vapor pressures at high temperature which is presented in this thesis is referred to as the "Microbalance-Inverted Knudsen Effusion-Recoil" or Miker technique. This technique was first presented by R. D. Freeman and J. E. Bennett[17] in this laboratory.

As shown in Figure 1, this technique involves hanging an effusion cell from one end of a microbalance, heating the cell to some appropriate temperature and measuring the rate at which the sample effuses through the cells' orifice. The recoil pressure is determined by the apparent change in weight of the cell as the furnace is turned off. This technique is very similar to that used today by many investigators in Torker work. The outstanding difference between the two techniques is the position of the orifice in the effusion cell. In the Torker technique, the orifices are located in the sides of the effusion cell; in the Miker technique, the orifice is located in the bottom of the effusion cell for one set of measurements and in the sides of the effusion cell for a second measurement.

There are three unique features of this technique and this particular experiment that should be appreciated before continuing.

First, the vapors effusing from the cell are directed away from the hang down wire and the effusion area is well defined (i.e. the area of

6
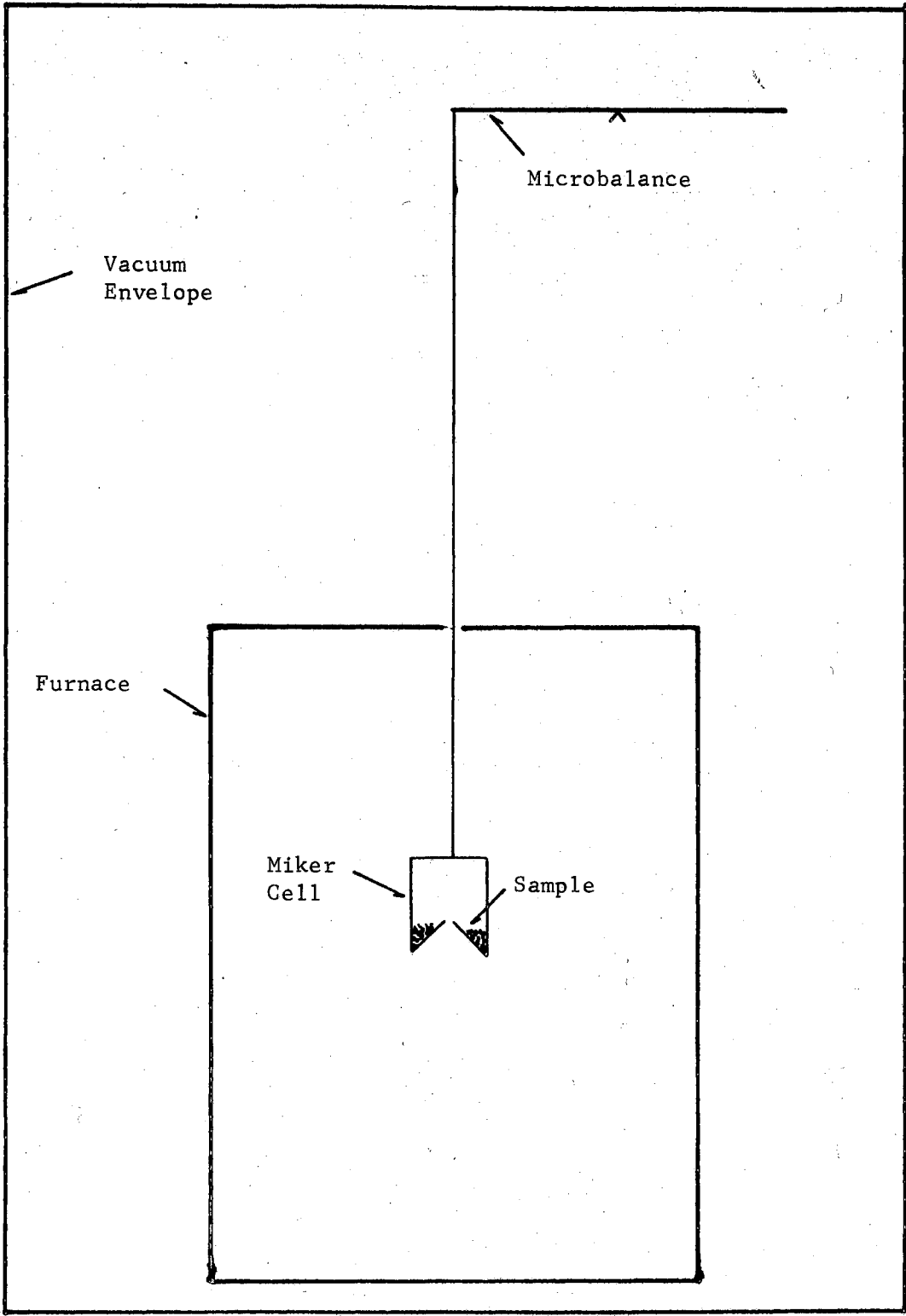
Figure 1. Schematic Representation of Apparatus for Miker Technique.

the orifice).

Second, the weight loss per unit time and the so-called recoil force can both be measured as weight changes by the microbalance. In the Torker technique, the weight loss of the cell can be monitered with the cell hanging from a balance, but the recoil given the cell by the molecules effusing through the orifice must be measured as an angular rotation of the cell hanging from a calibrated torsion fiber. In the Miker technique, the recoil given to the cell via the effusing molecules is in the upward direction and is sensed as an apparent incremental weight loss of the effusion cell as long as a particular rate of effusion continues.

The third feature of this experiment is the shape of the effusion orifice. As contrasted to the razor thin, small diameter, cylindrical ideal effusion cell orifice, a rather long conical orifice is used. Ideally, the small end of the conical orifice is as well defined as machining and the angle of the cone will allow. A theoretical treatment for effusion through such an orifice is given by Freeman[19] and Edwards[18] while the experimental work on effusion through conical orifices by R. Erbar[20] is just being completed in this laboratory.

If one uses a modified form of the Knudsen equation,

$$P_K = (2\pi RT/M)^{\frac{1}{2}} \dot{g}/aW \qquad (4)$$

he can readily determine the Knudsen pressure if he has experimentally obtained; $\dot{g}$, the rate of effusion; T, the absolute temperature of the cell; M, the average molecular weight of the effusing vapors; a, the area of the orifice; and W, the transmission probability for the given orifice geometry.

The Recoil Force and the Recoil Pressure

The recoil force is the reaction force given the Knudsen cell by the effusing vapors. To determine the force exerted on the Knudsen cell, one must understand the effusion process.

The accepted description for ideal effusion in the molecular flow range (<0.1mbar) is the "cosine law of effusion"[7], which may be stated as follows: the number dN_ω of molecules which cross an incremental plane surface ds per second and flow into an incremental solid angle $d\omega$ which lies at the angle θ from the normal to the surface is given by (as shown in Figure 2)

$$dN_\omega = \sigma \nu ds \cos\theta\, d\omega, \tag{5}$$

where ν is the molecular flux (molecules per unit area and per unit time) incident on the surface and σ is the proportionality constant. If one chooses as the z axis the axis of the orifice of the effusion cell, $d\omega$ may be transferred into spherical coordinates,

$$d\omega = \sin\theta\, d\theta\, d\phi. \tag{6}$$

Since the orifice, and presumably effusion, are symmetrical about the z axis, we may integrate over all ϕ and obtain

$$d\omega = 2\pi \sin\theta\, d\theta. \tag{7}$$

Thus, the cosine law of effusion in spherical coordinates is

$$dN_\omega = 2\pi\sigma\nu\, ds\, \sin\theta \cos\theta\, d\theta. \tag{8}$$

We shall now relate the recoil force to the rate of transfer of momentum across the plane of the orifice.

Using the physical analog to be presented later, the rate of transfer of momentum $\underline{p}$ for those molecules which have speed $\underline{c}$ and which
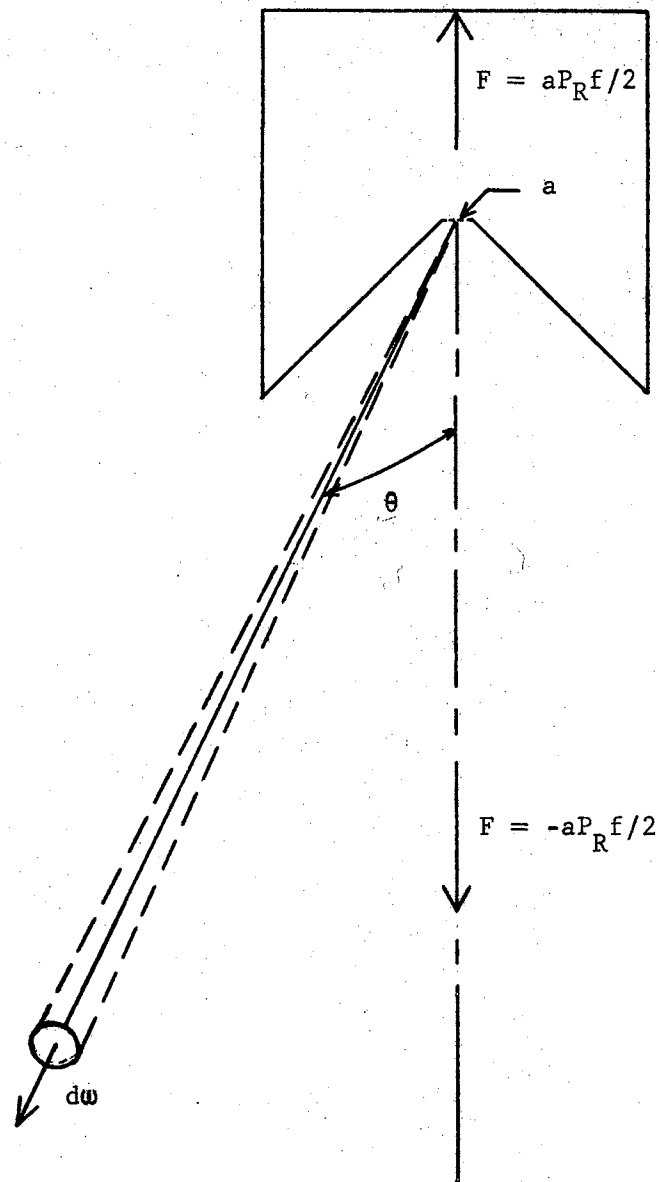
Figure 2. Momentum Transfer by Molecular Flow from a Conical Orifice

effuse through elemental area ds into dω at an angle θ with the z axis
is

$$dp^*/dt = mc \, dN_\omega^*$$ (9)

where the asterisk indicates that we refer only to those molecules with
speed c. Since effusion is symmetrical about the z axis (normal to the
orifice plane), the non-vertical momentum components cancel each other.
Thus, the resultant momentum transfer in the vertical direction is

$$dp^*/dt = mc \cos \theta \, dN_\omega^*.$$ (10)

This is the momentum transferred across a plane (the orifice) by the
effusing molecules. Microscopically, this momentum transfer is inter-
preted as that which would be detected by impingement and condensation
of the effusing molecules upon a susceptor surface.

It has been proposed by Freeman[10] and Bennett[17] that the law of
conservation of momentum here requires that an equal and opposite re-
action force be given to the cell via these effusing molecules, or

$$dF_\omega^* = mc \cos \theta \, dN_\omega^*$$ (11)

$$dF_\omega^* = dp^*/dt$$ (12)

Integration of ds over the orifice area a, and conversion to
spherical coordinates, give

$$dF_\omega^* = 2mca\nu^* \sin \theta \cos^2 \theta \, d\theta$$ (13)

Integration of dF_ω^* over θ from 0 to θ and substitution of $\nu^* = n^* c/4$
(Kennard 21), where n^* is the number density of the gas, give

$$F_\theta^* = an^* mc^2 (1-\cos^3\theta)/6 \qquad (14)$$

F_θ^* is the recoil force which results from the vertical vector component of those molecules effusing in a cone of included angle θ to the z axis with speed c. To extend this force exerted by molecules with speed c, we need only sum equation 14 over all speeds

$$F_\theta = \sum_{c\,=\,o}^{\infty} F_\theta^* = a(1-\cos^3\theta)\left(\frac{mn}{6}\right) \sum_{c\,=\,o}^{\infty} (n^*/n)c^2 \qquad (15)$$

$$= a(1-\cos^3\theta)\, nm\, \overline{c^2}/6 \qquad (16)$$

where $\overline{c^2}$ is the mean of the square of the speeds.

Using further results from kinetic theory[21],

$$P = nm\, \overline{c^2}/3 \qquad (17)$$

and

$$\overline{c^2} = \overline{c}^2 \left(\frac{3\pi}{8}\right) \qquad (18)$$

we have,

$$F_\theta = a(1-\cos^3\theta)P/2 = \pi\, Nm\overline{c}(1-\cos^3\theta)/4 \qquad (19)$$

where $N = \nu\underline{a}$ is the number of molecules per second entering the orifice.

The pressure determined by measurement of the recoil force is designated P_R, and

$$P_R = 2F_\theta/a(1-\cos^3\theta) \qquad (20)$$

If one now wishes to determine the total recoil force $\underline{F}$, he need only substitute $\theta = \pi/2$ in equation 20.

Upon doing the substitution $\theta = \pi/2$, one gets

$$F_R = aP_R/2 = \pi \, Nm \, \bar{c}/4 \qquad (21)$$

Correction Factors f and W

In practice, the recoil pressure equation is written as

$$P_R = 2 \, F_R/af \qquad (22)$$

where f is referred to as the recoil force correction factor. This factor compensates for the non-ideality of the orifice and is determined strictly by geometric parameters of the orifice. In the effusion process, an orifice with a finite length has some diminution of molecular flow (W correction factor) as well as partial collimation of the velocity vectors of the effusing molecules (f correction factor).

The effusion correction factor (W) used in the Knudsen equation and the recoil force correction factor (f) have been derived and tabulated by Freeman and Edwards[18] for conical orifices. The physical parameters under which the tabulation is listed are (1) the angle (T) of the cone of the orifice measured from the center axis and (2) the length to radius ratio (radius of smallest end) L/r of the orifice.

Assuming 'cosine law' distribution[18] may be somewhat inconsistent with the work of Wang and Wahlbeck[22] in terms of their high temperature work in verifying the cosine law of distribution. They found that the angle of incidence is very close to the angle of reflection for a long orifice and thus small angle of incidence. This reasoning was presented as an explanation for the somewhat p-orbital shaped distribution seen with a long orifice as contrasted to the cosine law distribution of the

shorter, near ideal, orifice.

Determination of M^*

The recoil force acting on the cell is measured by the microbalance as an apparent change in mass of the Knudsen cell; the measured change in mass and the desired recoil force are related by the gravitational constant g,

$$F_R = mg \tag{23}$$

$$P_R = 2mg/af. \tag{24}$$

Thus, one can determine the recoil pressure by measuring the recoil mass of the effusion cell, if the area of the orifice, f, and g are known. It is important to note that this determination is independent of the molecular weight of the effusing vapors.

If we assume that equilibrium pressure conditions exist inside the cell, we can say that the recoil pressure and Knudsen pressure are equal,

$$P_K = P_R = \dot{g}(2\pi RT/M)^{\frac{1}{2}}/aW \tag{25}$$

or

$$2mg/af = \dot{g}(2\pi RT/M)^{\frac{1}{2}}/aW \tag{26}$$

This equation relates directly the recoil pressure, which is determined independently of the molecular weight of the effusing molecules, and the Knudsen pressure, which is inversely proportional to the square root of the molecular weight of the effusing species. Solving this equation for the average molecular weight of effusing vapors (M) in terms of the experimentally measured variables, one gets

$$M = \frac{\pi RT}{2g^2} \frac{\dot{g}^2 f^2}{m^2 W^2} \tag{27}$$

Freeman[10] has shown that an equivalent is to <u>assume</u> a value $\underline{M}_K$ for $\underline{M}$ in the Knudsen equation, and calculate $\underline{P}_K$ from the rate of effusion data. Then $\underline{P}_K$ and $\underline{P}_R$ are related to give a value for $\underline{M}^*$.

$$M_K = P_K^2 a^2/2\pi \dot{g}^2 RT \tag{28}$$

$$M^* = P_R^2 a^2/2\pi \dot{g}^2 RT \tag{29}$$

$$M^* = M_K(P_K/P_R)^2 \tag{30}$$

Once one has determined the average molecular weight of the effusing molecules, he can estimate directly the complexity of the effusing vapors (i.e. percent monomer, dimer, trimer, etc.). Freeman[10] has shown that, if we require the total pressure $\underline{P}_K$ ($=\Sigma P_{Kj}$;) to be calculable from the total rate of effusion $\underline{\dot{g}}(=\Sigma \dot{g}_j$;) of all $\underline{s}$ components in the vapor, then

$$P_{Kj} = (\dot{g}_j/aW)(2\pi RT/M_j)^{\frac{1}{2}} \tag{31}$$

or $$(\dot{g}/aW)(2\pi RT/M^*)^{\frac{1}{2}} = \sum_{j=1}^{s}(\dot{g}_j/aW)(2\pi RT/M_j)^{\frac{1}{2}} \tag{32}$$

which can be simplified to

$$M^* = \left(\sum_{j=1}^{s}(\dot{g}_j/\dot{g})M_j^{-\frac{1}{2}}\right)^{-2} \tag{33}$$

If we let $\dot{g}_j/\dot{g} = m_j$, the mass fraction of the jth component,

$$M^* = (\sum_{j=1}^{s} m_j M_j^{-\frac{1}{2}})^{-2} \tag{34}$$

where $\underline{M}^*$ is now a weighted average molecular weight of vapor in the cell.

Effusion During the Cooling Period

Ideally, one heats the cell to some temperature, effusion begins and is monitered in some manner as weight lost per second from the Miker cell. To measure the recoil force, one would like to cool the cell instantaneously to a temperature at which, for all practical purposes, effusion ceases. In practice, this is impossible to accomplish, so that in the time required for the cell to cool, some mass effuses. Figure 3 shows graphically the two weight changes which occur simultaneously in the cooling Miker cell.

The most significant weight change is the recoil mass $(\underline{m}_r)$. This is an apparent increase in weight of the cell as a result of removal of the reaction force of the effusing molecules. The second weight change, which occurs simultaneously, corresponds to the effusion during cooling $(\underline{m}_c)$. These two weight changes are opposite in direction and the algebraic difference of the two will give one the ideal recoil mass $(\underline{m}_i)$.

$$m_i = m_r - m_c \tag{35}$$

There are two techniques for determining $\underline{m}_c$. One is a theoretical calculation from the known effusion rate and rate of cooling of the cell as proposed by Bennett[17] and Freeman[13]. The second technique involves measuring the effusion during cooling from an effusion cell with orifi-
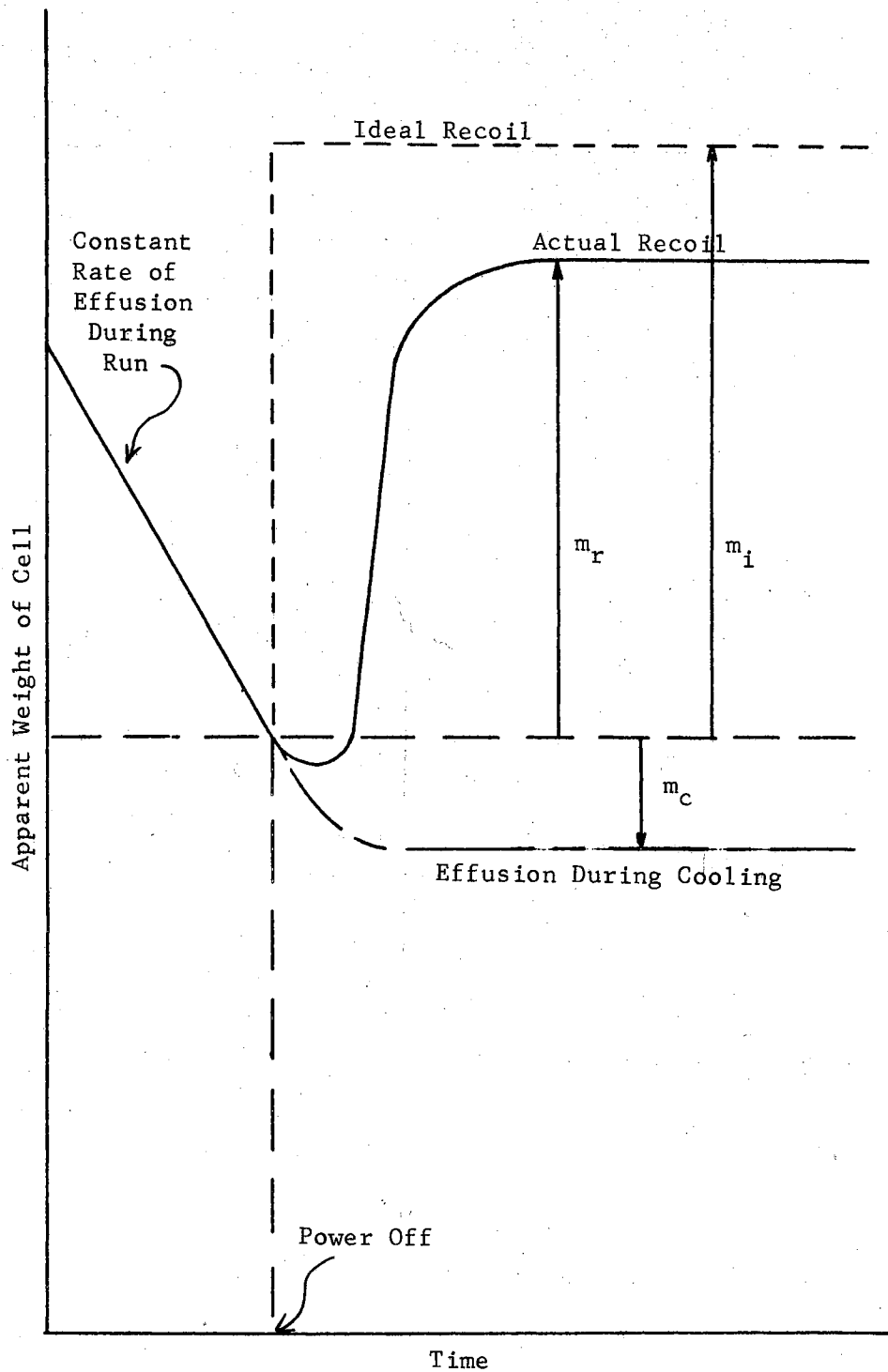
Figure 3. The Effect on the Recoil Mass of Effusion Which
Occurs During the Cooling Period

ces in its sides and extrapolating these experimental results at known

temperatures and rates of effusion to other cells.[*]

One may again rewrite the recoil pressure equation,

$$P_R = 2m_i g/af = 2(m_c + m_r) g/af \tag{36}$$

There is one other force that will be considered in detail in

Chapter IV. This is the so called pseudo-recoil force, which is spurious

and which arises from unintentional and undesired interactions between

various parts of the system.

To summarize, the rate of effusion, the apparent recoil force, the

effusion during cooling and the temperature of the cell need to be de-

termined in the experiment. One also needs the area of the orifice and

the correction factors $\underline{f}$ and $\underline{W}$.

―――――――――――――

[*]Appendix A

CHAPTER III

THE EXPERIMENTAL APPARATUS: MECHANICAL AND ELECTRONIC

The Vacuum System

The vacuum system profile is shown in Figure 4. The system consists of four main parts; the manifold, the balance chamber, the furnace chamber and the vacuum pumps.

The manifold connects and supports the other three components of the vacuum system. It is made of 5.5-inch diameter and 0.1875-inch thick steel pipe welded together and then Nickel-plated to prevent rust. Standard O-ring flanges connect the other system components. The manifold is supported by a saddle of 0.5-inch steel plates and T-beams on a 23" by 23" by 36" high concrete block built into the basement floor of the building. These precautions to eliminate vibrations to the microbalance were unsuccessful until the oil diffusion pump, to be discussed later, was fixed firmly to this concrete block. As indicated in Figure 4, the manifold has a flange for an ionization vacuum gauge (Miller-OSU ionization gauge) and for a helium leak detector (Mikros LD 100), and has cooling coils on the end just above the furnace chamber.

The furnace chamber, the region in which the actual experiment occurs, consists of two main parts. The first to be considered is the top plate which is attached to the manifold; this plate is 12 inches in outer diameter 0.5-inch thick steel. It contains an O-ring groove and attaches to the manifold flange with steel allen screws. In addition
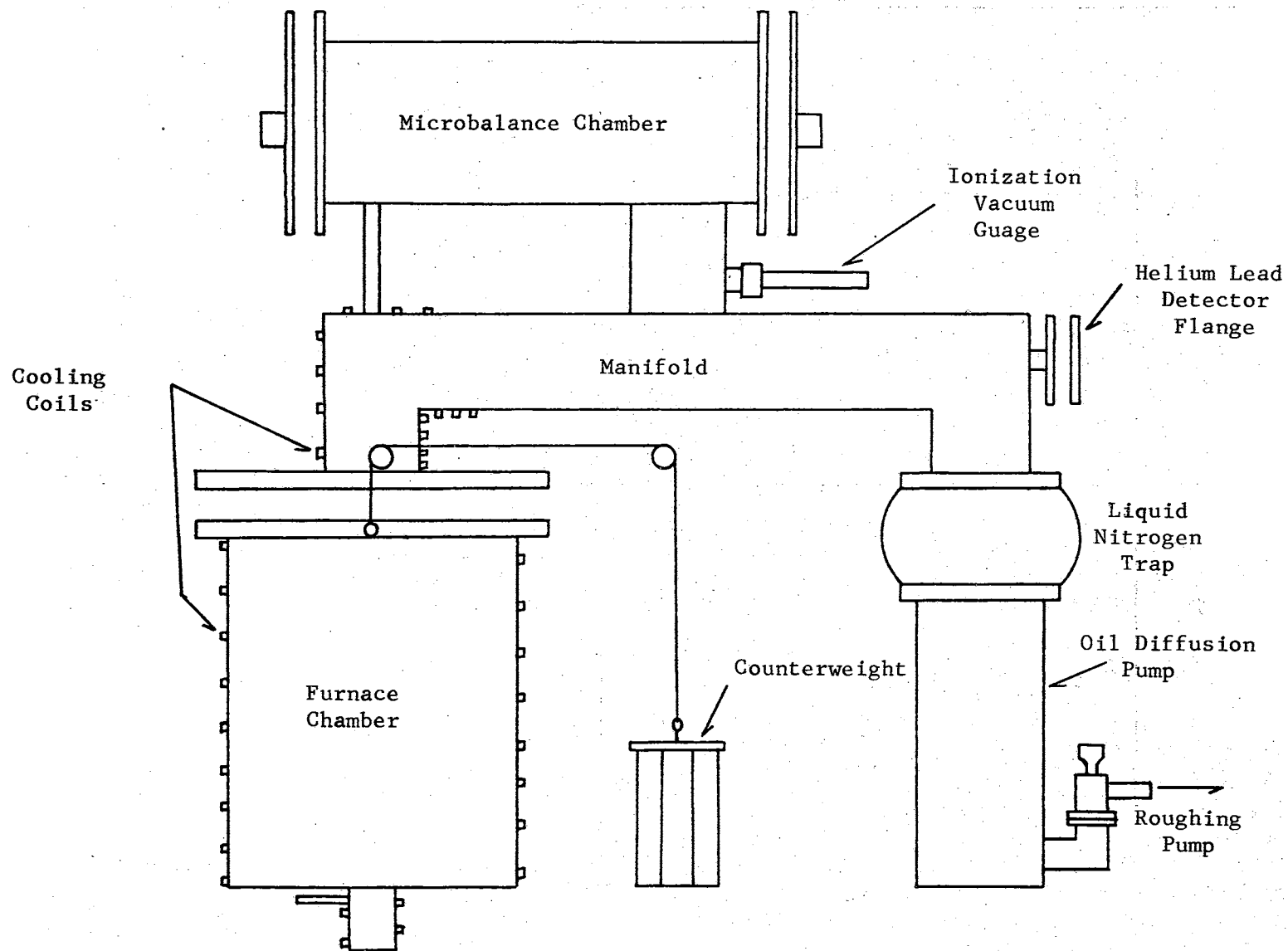
Figure 4.   Schematic Representation of Vacuum System (Not to Scale)

to acting as a step-down from the 10-inch furnace chamber to the 5.5-inch manifold, the top plate provides a convenient place for the furnace electrical connections. Five 0.5-inch diameter access holes are drilled through the plate; small (4/40) screw holes around each access hole permit mounting of electrical feedthroughs or cover plates. The access holes are in a 180° arc, spaced approximately 45° apart. The two holes 180° apart are now used for the furnace current feedthroughs which will be described later, and the other three holes are either capped or used for a ceramic insulated, thermocouple feed through. The final feature of the top plate is a copper cooling coil softsoldered to the plate; the O-rings must be cooled while the furnace is on. After being built, the entire plate was Nickel-plated.

The furnace chamber is a 10-inch outer diameter, 0.25-inch thick, steel pipe with a steel plate welded on as the bottom. The most unusual feature of the furnace chamber is the prism that is mounted (from the outside) in a well in the bottom of the chamber, and the shutter that keeps the prism from being coated with the vapor of the material being studied. The prism acts as a vacuum window and allows one to view the black body orifice in the bottom of the Miker Cell with an optical pyrometer mounted horizontally. The shutter mechanism is designed such that when the electromagnet in Figure 5 is energized, the soft iron rod is drawn into the coil, and the shutter opens. When the electromagnet is de-energized, the shutter closes under gravitational force, and pulls the soft iron rod out of the electromagnet. Of course, the shutter must be unbalanced when open so that it will close when the electromagnet is de-energized. Activation of the shutter requires 40 volts across a 200-ohm coil, and produces sufficient heating of the shutter mechanism to

To Miker Cell

Shutter

Coil

Coil

O-Ring

Soft Iron
Rod

Optical
Pyrometer

Prism

Inch
0   1   2
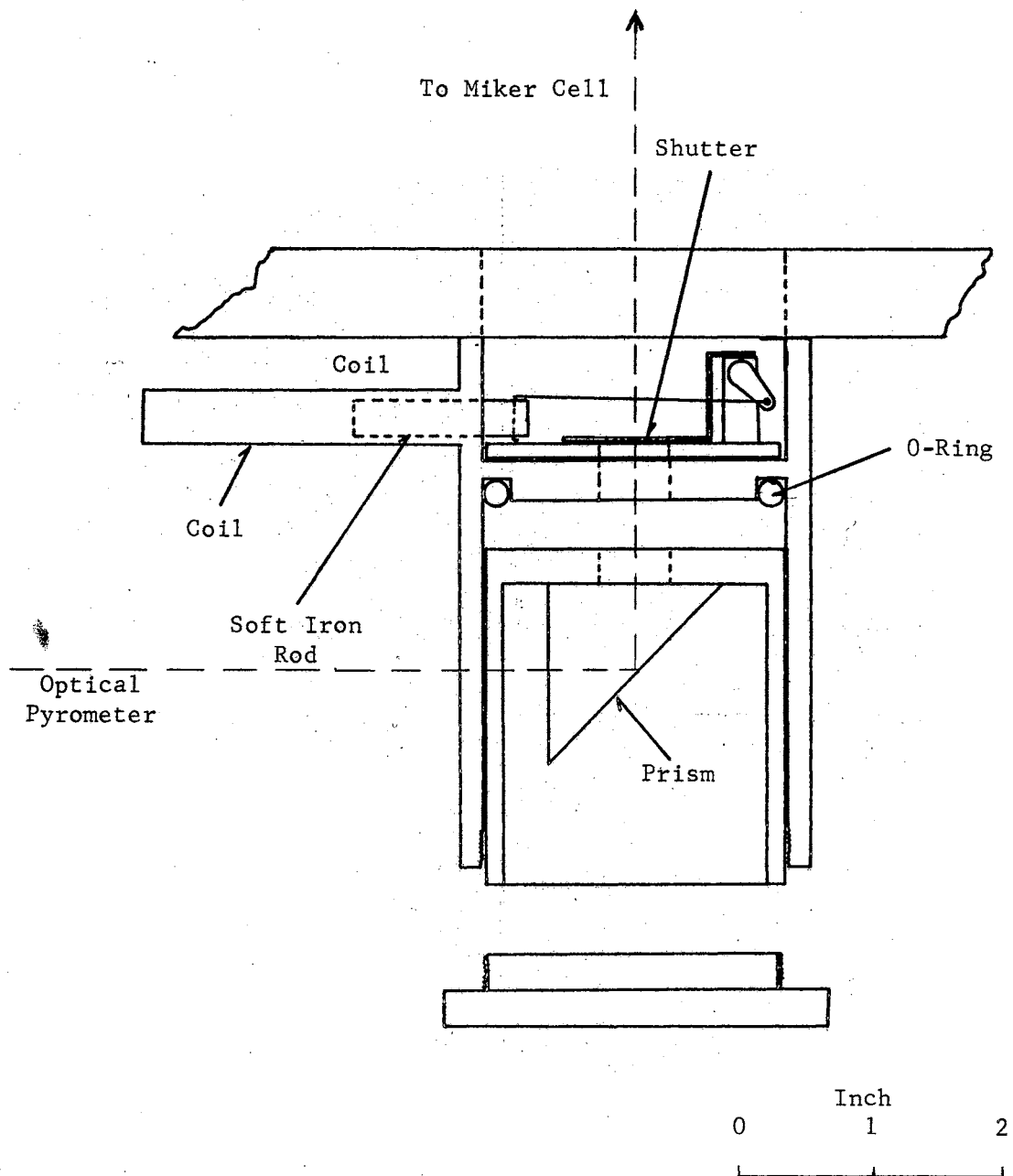
Figure 5.   The Shutter Mechanism and Prism in the Bottom
of the Furnace Chamber

cause the shutter, on occasion, to stick open. Therefore, the shutter coil has a cooling coil of Tygon tubing around it.

The cooling coils on the furnace chamber are 0.25-inch square copper tubing soft-soldered into place. These coils allow furnace powers of 3600 watts in the winter and perhaps 3000 watts in the summer without undue temperature rise on the outside surface of the can. After the can was completed, it too was Nickel-plated to prevent rust.

The microbalance chamber is made of 6-inch diameter brass pipe (0.1875-inch walls) with brazed flanges, and has brass end plates. A 4.5-inch and a 0.93-inch diameter flange connect this chamber to the manifold. Primary pumping takes place through the larger connection and the smaller connection accomodates the suspension wire that connects the Miker Cell in the furnace chamber to the end of the microbalance. In the bottom of the balance chamber are two longitudinal tracks on which the balance may be slid into position from the cell end of the chamber. A micrometer screw is mounted on the top of the chamber such that one can transmit vertical motion through a copper bellows into the vacuum system. A ceramic insulated, seven terminal, electrical feed through carries electrical connections into the vacuum system. The final point is that there are three quartz windows in the chamber. The two windows in the end plates are strictly for observational purposes and must be shielded to exclude external room light from the chamber. The top port is essential in that it is part of the optical system for the null sensing device used to control the balance automatically.

Two vacuum pumps and a liquid nitrogen nitrogen trap are used to evacuate the system. A Welch Duo Seal (Model No. 1402) mechanical pump, mounted on rubber cushions to minimize the vibrations transmitted

through the floor to the microbalance, evacuates the system to less than

50 μbar. A Consolidated Vacuum Corporation Model 720, 4-inch, oil dif-

fusion pump evacuates the system to 1.0×10^{-8} bar or less. Finally, a

Granville-Phillips Cryosorb 250, stainless steel, 4-inch, liquid nitro-

gen trap holds the system pressure in the 10^{-9} bar range while the fur-

nace is on.

It was observed that the oil diffusion pump, and the manifold, acted

as a lever through which mechanical pump vibrations were transmitted

through the metal vacuum system to the microbalance beam. The amplitude

of the vibration was reduced almost 90% by attaching the end of the

lever, the oil diffusion pump, securely to the concrete block on which

the system rests.

The Furnace

As discussed in Chapter II, the Miker Cell ideally should cool from

some high temperature to room temperature instantaneously. This is im-

possible to obtain experimentally, but the furnace material and design

used in this experiment very closely approximates that for instantaneous

cooling. When power to the furnace is terminated instantaneously, the

Miker Cell has been observed experimentally to cool from $1250^{\circ}C$ to 1100°

C in six seconds.

The material used in the fabrication of the furnace is a standard

material used in high temperature work, graphite. The unique properties

of the furnace can be attributed solely to the type of graphite used,

graphite cloth. The frame for the furnace is Type ZTG (National Carbon

Company) graphite machined to the proper size and form. These forms are

clearly shown in Figures 6 and 7. The two electrical terminals are the

top forms of the furnace. The heating elements are graphite cloth or tape, 0.5-inch wide with a resistance of about 3 ohms per foot. There are three lengths of tape, in parallel, going to the base of the furnace from each of the two electrical terminals; at the base of the furnace the two sets of three elements are connected in series. Since the length of the furnace is approximately six inches, the overall furnace resistance is about one ohm. A resistance of one ohm is very high for a graphite furnace, 10 to 20 times higher than the resistance of a solid graphite element of similar dimensions[17]. Carbon also has a unique advantage over a metal heating element in that it has a negative coefficient of resistance, which means its resistance decreases (slightly) with increasing temperature, rather than increasing as in a metal.

The high current, vacuum feedthroughs for the furnace are unique. Several designs were tried, but none were successful except the design in Figure 8. The usual electrical vacuum feedthrough consists of a metal electrode insulated from a vacuum fitting with glass or epoxy or ceramic or various mixtures of these. At high current, the electrode heats up and if the coefficient of expansion of the electrode and the insulator are not the same, a vacuum leak will form at the interface of the two materials. The electrode may be water-cooled with some sort of a jacket, but this is usually restricted to the external part of the electrode and the vacuum-sealed part may still heat. In the design of Figure 8, the feedthrough consists of a copper tube with a plate divider pushed about 0.5-inch from one end and caps with threaded rods soldered onto the ends and 0.25-inch copper tubing soldered into the appropriate water ports near the top of the feedthrough. The feedthrough is then insulated from the furnace chamber top plate with a Teflon spacer.

Graphite Cloth

Molybdenum
Screws

Top

Molybdenum
Screws

0   Inch   1
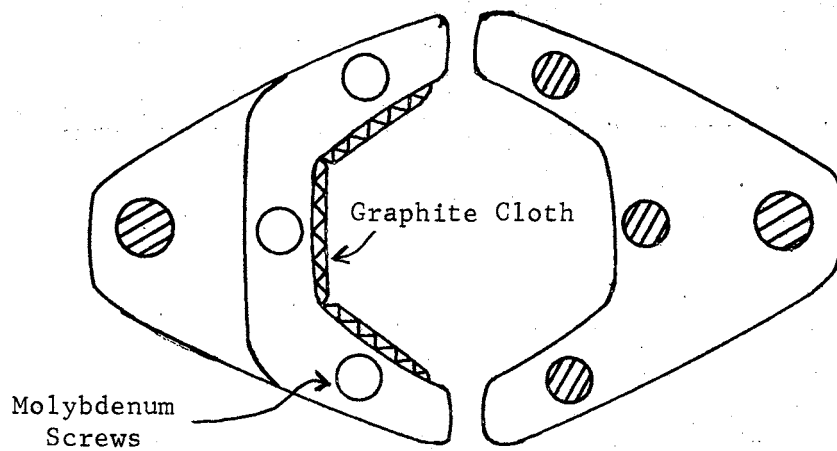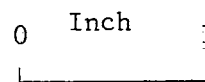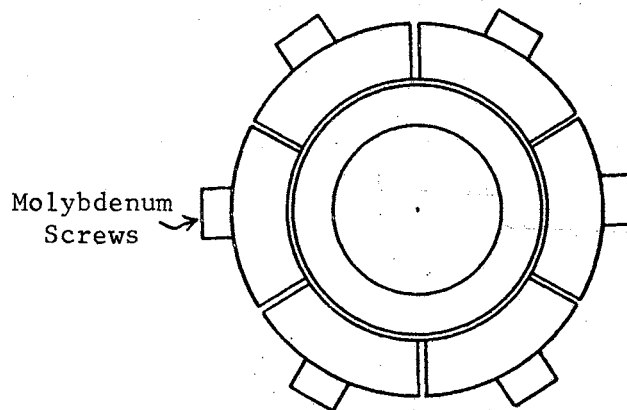
Bottom

Figure 6. Furnace Frame: Top and Bottom
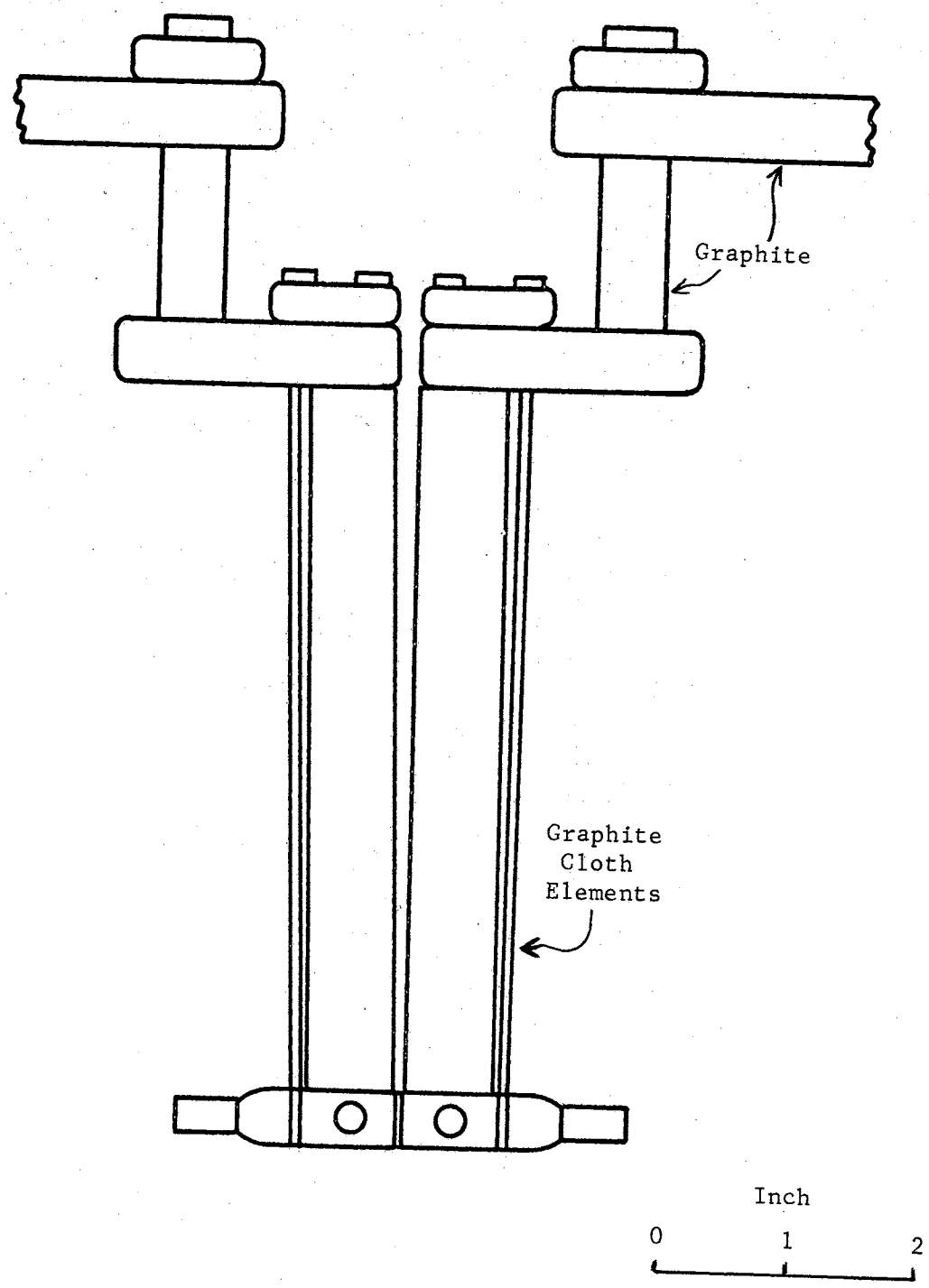
Figure 7. Side View of the Furnace

Water
Out

Water
In

O-Rings

Teflon

Vacuum
Wall

Inch

0   0.5   1
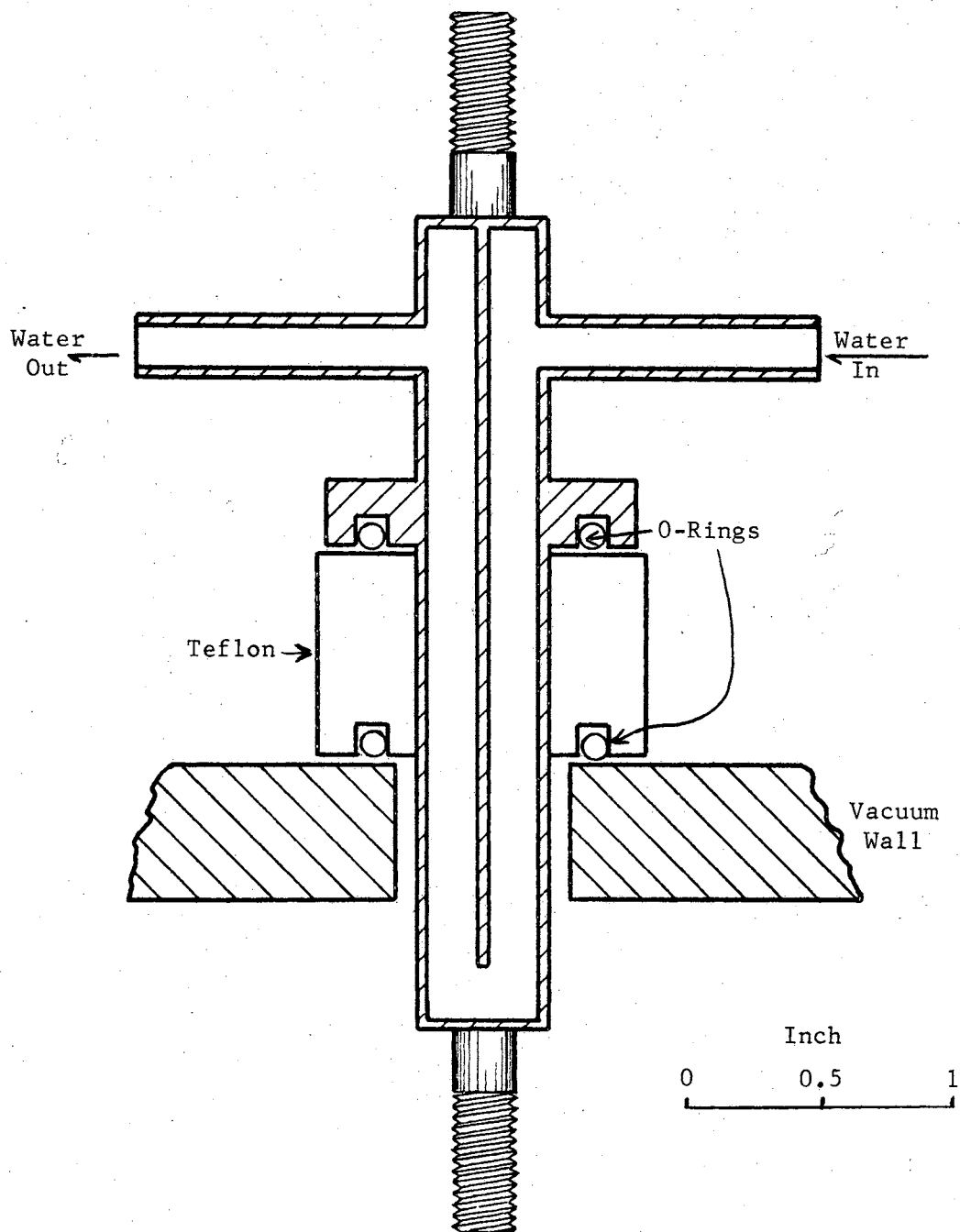
Figure 8.   The High Current Vacuum Feedthrough

0-rings are placed between the plate and the spacer, and the spacer and the feedthrough flange for a vacuum seal. All three parts are held together with six 6-32 allen head screws. The feedthrough is made entirely of copper; the various parts are soldered together. With vacuum grease on the 0-rings, the feedthroughs have been leak tested with a helium leak detector to less than 1×10^{-9} bar.

There is another problem associated with the furnace that will be discussed again in Chapters IV and V with the results of the first experimental run. This problem was simply that magnetic fields generated around the high current ac furnace leads interacted with the small magnets on the microbalance. As the furnace was turned on, there would be a change in the rest point of the balance. As the furnace was turned off, the initial rest point would be restored. The magnitude and direction of this change in rest point varied with the position of the furnace current leads with respect to the balance chamber. Furthermore, the changes appeared to be directly proportional to the furnace current which indicated that the change was due to some microbalance-furnace interaction.

The solution to the problem is indicated in Figure 9. There were two necessary modifications. First, the furnace leads themselves were twisted tightly, from the furnace to the furnace power supply, and from the power supply to the 100 A circuit breaker box in the lab. This was done to make the leads very symmetrical so that the electromagnetic fields produced would cancel. Ninety percent of the problem was eliminated with this change. There remained a smaller interaction that appeared to be due to assymetry of the furnace leads connected to the feedthroughs. The solution to this problem is shown in Figure 10. An

Inch

| 0 | 1 | 2 | 3 |
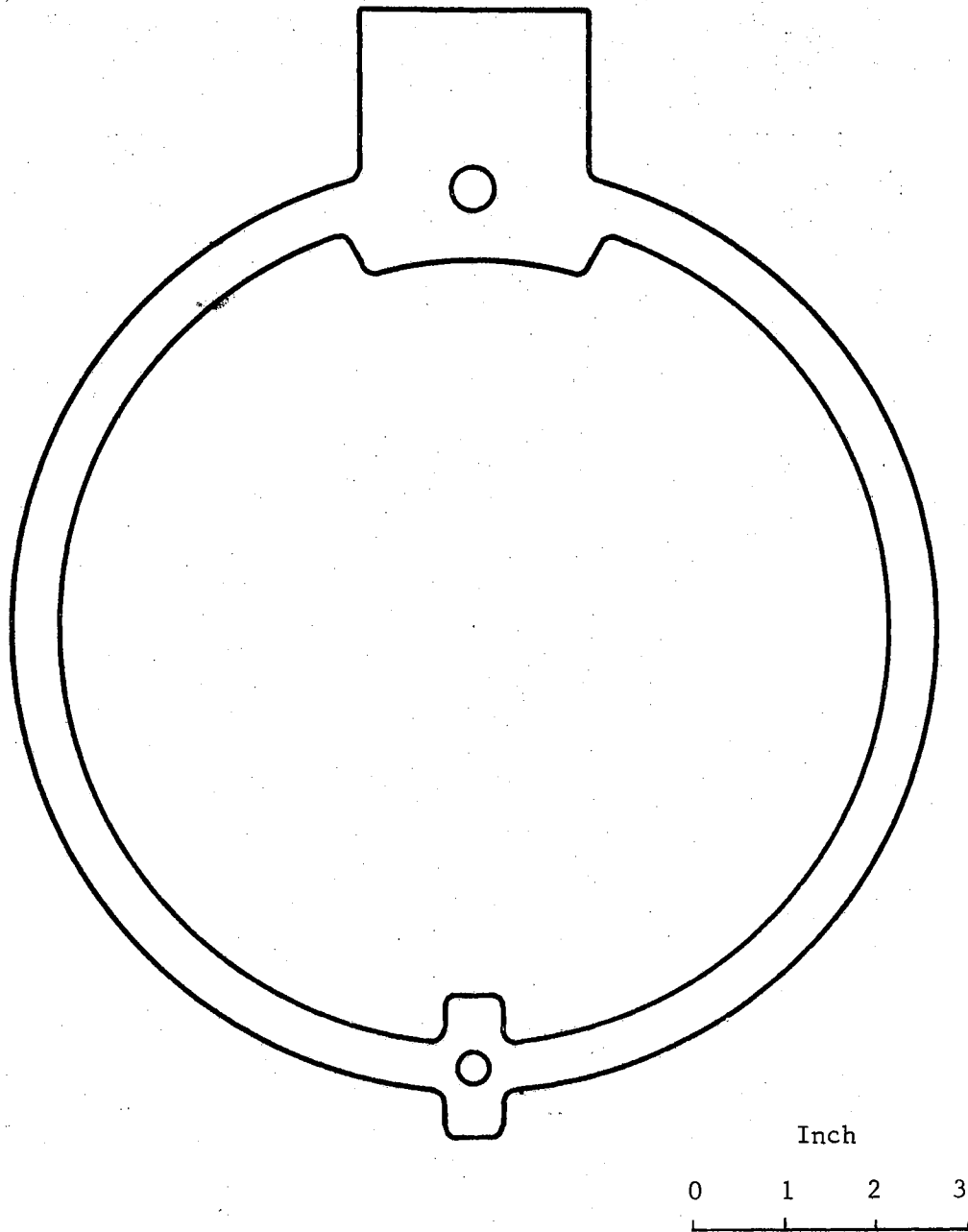
Figure 9. Aluminum Ring Used for Symmetrical Distribution
of Furnace Current to Vacuum Feedthroughs
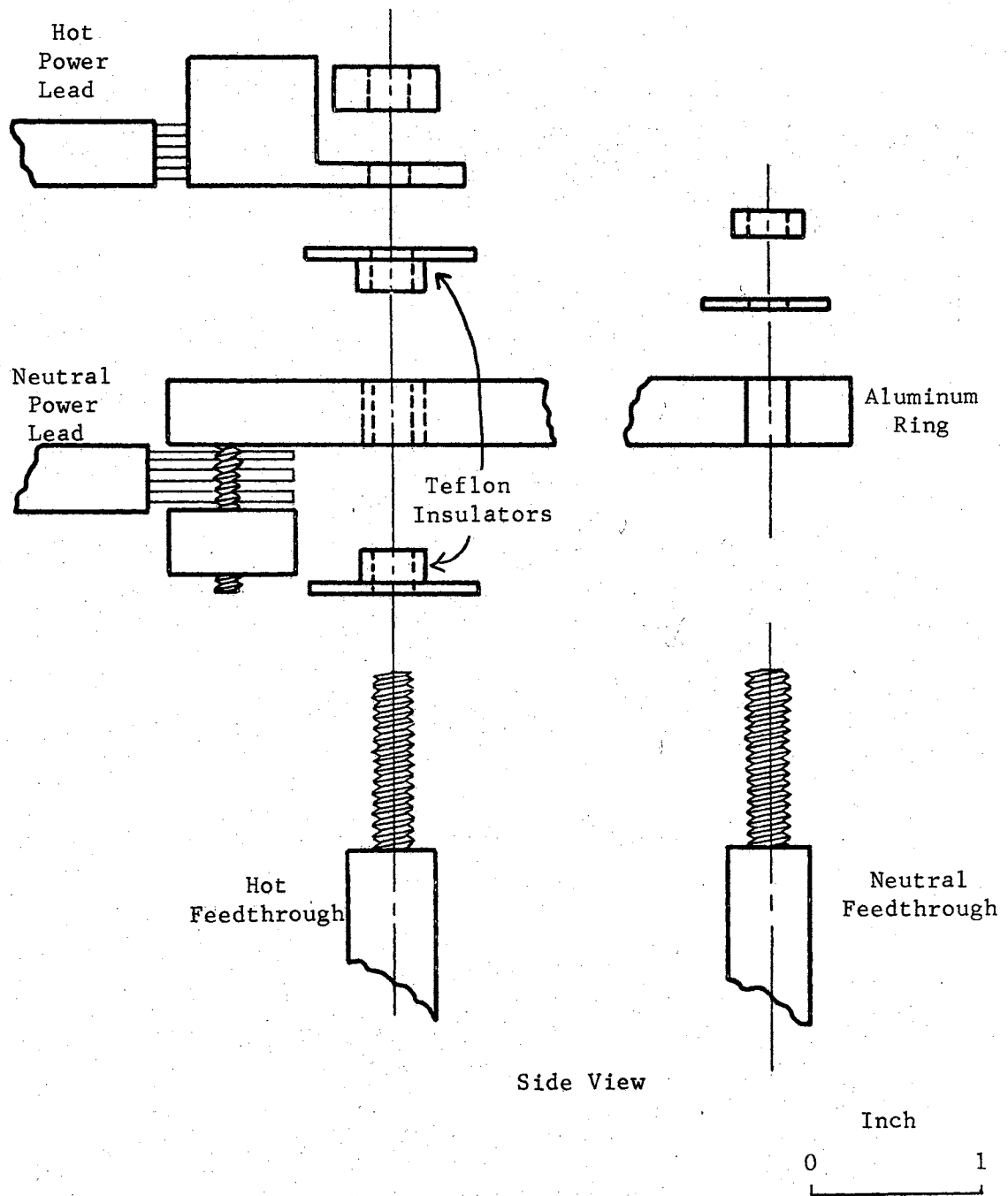
Figure 10. Method Used to Connect Furnace Power Supply Leads to
Aluminum Ring (Figure 9) and High Current Vacuum
Feedthroughs

aluminum ring was machined as shown in the drawing. This ring fits over the top studs of both feedthroughs, but is insulated from one with a Teflon sleeve and washer. One power lead is connected to the feedthrough insulated from the aluminum ring and the other to the aluminum ring. The connections are made very close to one another so that the power leads are the same length. The current to the feedthrough connected to the ring is divided evenly through both sides of the ring which is symmetrical about the end of the manifold.

In general, for the furnace described in this section, a temperature of 850 $^\circ$C is observed at 30 A furnace current, 1100 $^\circ$C at 40 A, 1200 $^\circ$C at 44 A and 1286 $^\circ$C at 50 A.

The Miker Cell

The two Miker Cell designs are shown in Figures 11 and 12. Both cell designs are made of high purity, high density, grade ZTG graphite. The cell with the orifice in the bottom was used for vapor pressure and recoil force measurements. Two design modifications have been made over previous cells[17]. The major change is that the new cell has thicker walls, about 0.110 inch thick on the sides and 0.080 inch thick on the top and bottom of the cell. Several workers have reported diffusion of samples through graphite cell walls at high temperatures and we hoped to eliminate, or minimize, the effect of this phenomenom. The second feature of the new cell design is that it has two seals around the threads. The cells were machined such that there would be a simultaneous seal at the top of the inside of the cell and just below the concealed threads on the outside of the cell.

The double-orifice cell differs from the other cells in that it has
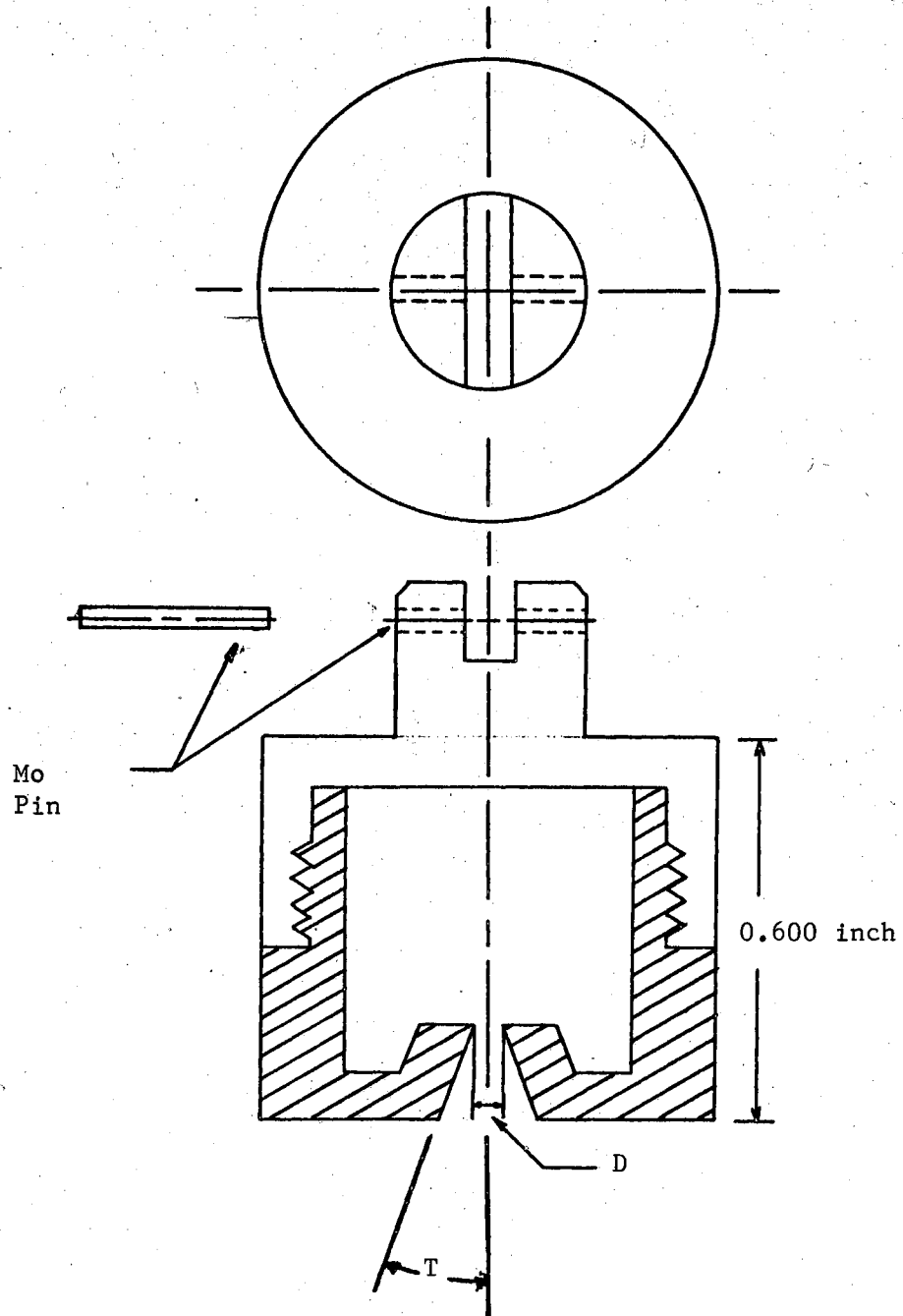
Figure 11. Miker Cell
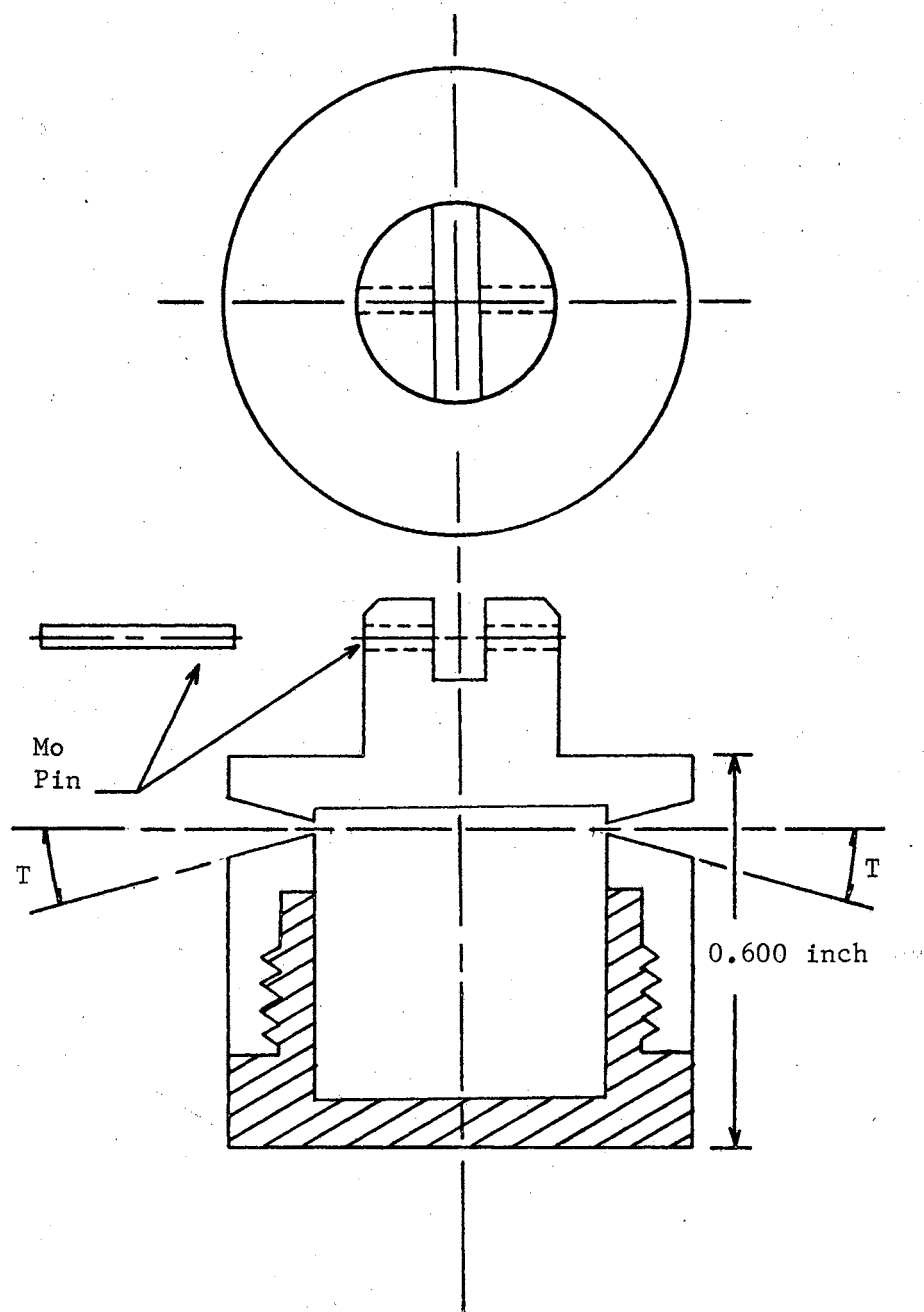
Figure 12. Double-Orifice Cell Used to Determine the
Mass that Effuses During Cooling

two diametrically opposed conical orifices in the sides of the cell,
rather than one in the bottom. With no effusion in the vertical direc-
tion, one ideally observes no recoil force with a cell of this design;
thus it may be used to determine experimentally effusion during cooling.

Ideally the orifices in both cell designs are purely conical in
shape with a sharp edge at the small end of the orifice. Meeting this
criterion was something of a problem with graphite. The cells actually
used in this experiment have a short cylindrical section at the small
end of the conical orifice. The length of this cylindrical section is
much longer than desired, especially in the double-orifice cell. Cell
parameters for the three cells are given in Table I. The volume of
the cells is approximately one cubic centimeter.

The Photopot[37]

The device which senses the null position of the balance is a light-
actuated potentiometer or Photopot. The schematic for the Photopot and
the null sensing circuitry is shown in Figure 13.

The null circuitry is basically a Wheatstone bridge with a very
stable 1.34 V mercury battery for a power supply. In one side of the
bridge is a 1-k ohm ten-turn potentiometer between two 10-k ohm resis-
tors. The ten-turn potentiometer dial has 1000 units which gives one a
bridge balancing sensitivity of approximately one ohm per unit on the
dial. The other side of the bridge is the Photopot. It has a total re-
sistance of about 20-k ohm for 0.5-inch of active length and can sense
a 0.0001-inch movement of an incident light beam, i.e., resistance
changes on the Photopot of 1-10 ohm. Thus, the sensitivity of the two
legs of the bridge are matched.

TABLE I

PARAMETERS OF MIKER CELLS

Cell	Type Orifice	Orifice Parameters[a]			Correction Factors[b]	
		L, in.	D, in.	T, deg.	W	f
1[c]	Conical	0.0782	0.0403	31	0.916	1.10
	Cylindrical	0.0123	0.0403	0	0.764	0.820
1A	Conical	0.0782	0.0403	31	0.916	1.10
4[d]	Conical	(a) 0.0660	0.0289	29.7	0.909	1.074
	Cylindrical	0.0340	0.0289	0	0.487	0.544
	Conical	(b) 0.0698	0.0282	31.2	0.918	1.085
	Cylindrical	0.0340	0.0282	0	0.482	0.538
5	Cylindrical	0.0515	0.0401	0	0.462	0.510

[a]L = length, D = smallest diameter, T = off-axis angle.

[b]Interpolated from Table III.

[c]Imperfect conical orifice.

[d]Double orifice cell with imperfect conical orifices.

The Photopot might be considered to be a frictionless potentiometer; there is no friction between the wiper (light beam) and the resistance strip. The Photopot is very simple in design, to have such unique properties. It consists of a high resistance metal strip (20 k-ohm) about 0.5-inch long and a very low resistance metal strip parallel to the first, with a photoconductive material between the strips. As a light beam moves across the potentiometer, there is a very low resistance between the high and low resistance metal strips at the point of the light beam. In analogy to a wire-wound potentiometer, the low resistance strip is the wiper terminal and the ends of the high resistance strip are the two terminals of the wound wire.

The light beam referred to here is produced by a 0.004-inch slit placed in front of a light source and by the proper lens and mirrors to refocus the slit image on the Photopot. One of the mirrors is mounted on the balance beam so that movement of the balance beam causes movement of the slit image on the Photopot. The slit image on the Photopot is 1-2 mm wide which may seem too wide to permit detection of small movements of the balance beam. But, the calibration of the detectable beam movement by the servosystem described in Chapter IV, will show this slit width to be sufficiently narrow.

Photopot Light Source and Power Supply[34]

Shown in Figure 13 is the schematic for the power supply to the constant intensity light source for the Photopot.

Initially, there was some concern with the linearity and stability of the Photopot with a fluctuating slit intensity. Therefore, a constant intensity light source seemed desirable. This power supply has a
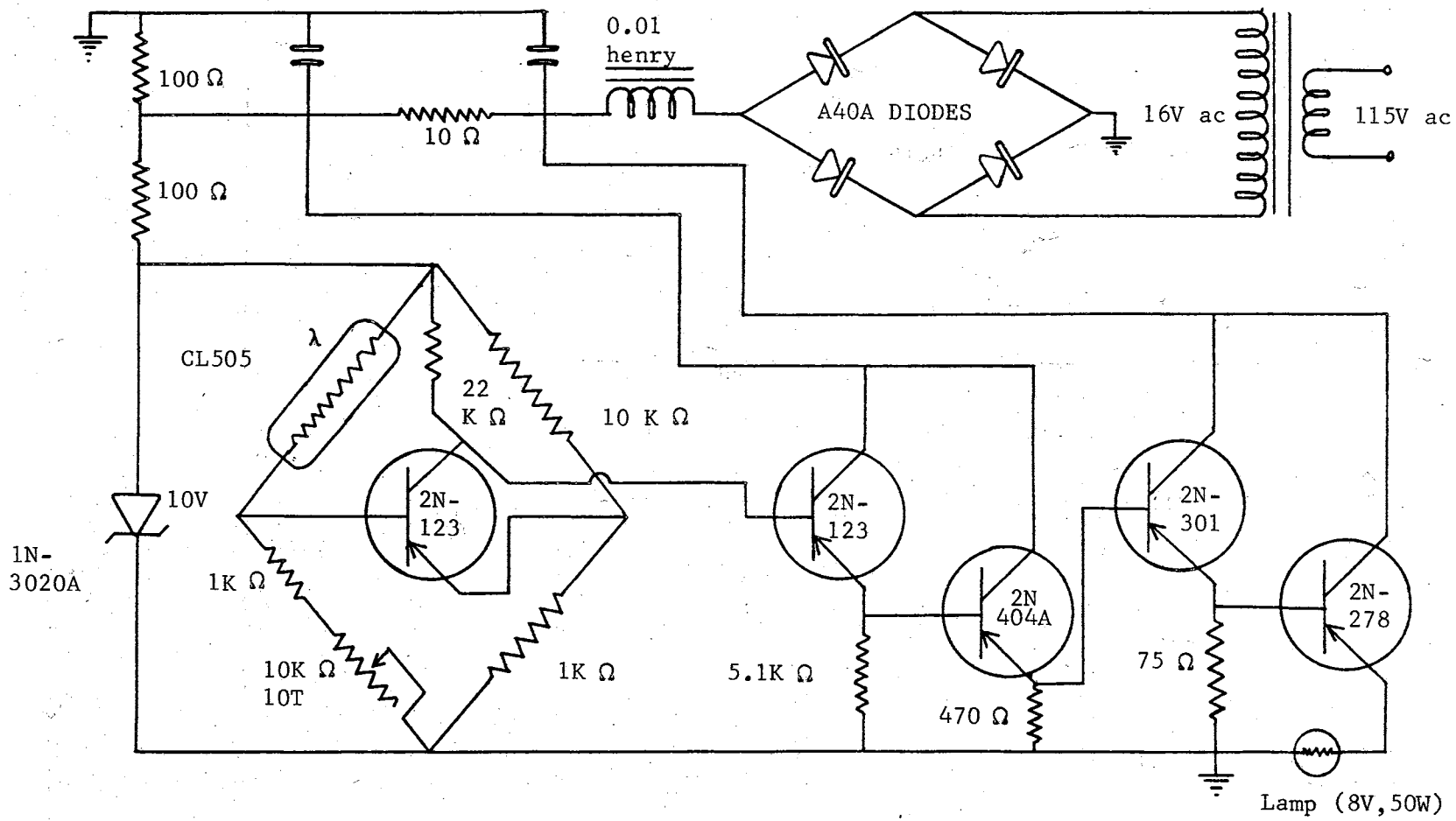
Figure 13. Regulated Power Supply for Photopot Lamp

photocell in a leg of a Wheatstone bridge regulating circuit. Fluctuations in the light intensity of the (Philips 13113 C104 8V, 50 W) lamp are detected in the photocell as a change in its conductance or resistance and the output of the bridge changed in such a direction as to compensate for the increase or decrease in light intensity with a corresponding decrease or increase in lamp current.

The Furnace Power Supply

The furnace power supply is shown in Figure 14.

The high current part of the supply is a 115 V, 100 A, ac line controlled by a bridge circuit of high current diodes, (4JA70C diodes) arranged in such a manner that conduction across the center of the bridge is always in one direction. The device in the center of the bridge, a 1N 1916 Silicon Controlled Rectifier (SCR), is a solid state device that can be controllably triggered to conduct 0°-180° of each half cycle. With the resistance of the furnace fairly constant at one ohm, the power supplied to the furnace is controlled by varying the phase angle at which the SCR is triggered[24]. The SCR is protected by a special fuse (Amptrap A25 x 100) which is fast acting and will blow in less than one half cycle (i.e., less than 1/120 of a second). Fast action is needed since solid state devices are very susceptable to voltage transients.

The SCR is triggered twice every cycle, or once every half cycle, by a Silicontrol (Model VS 6300) which is essentially a square wave generator with output variable from zero to full 180° square wave. It is very important that the line frequencies supplied to the Silicontrol and the SCR be exactly in phase with each other or the SCR may be triggered full on as soon as there is any output from the Silicontrol.
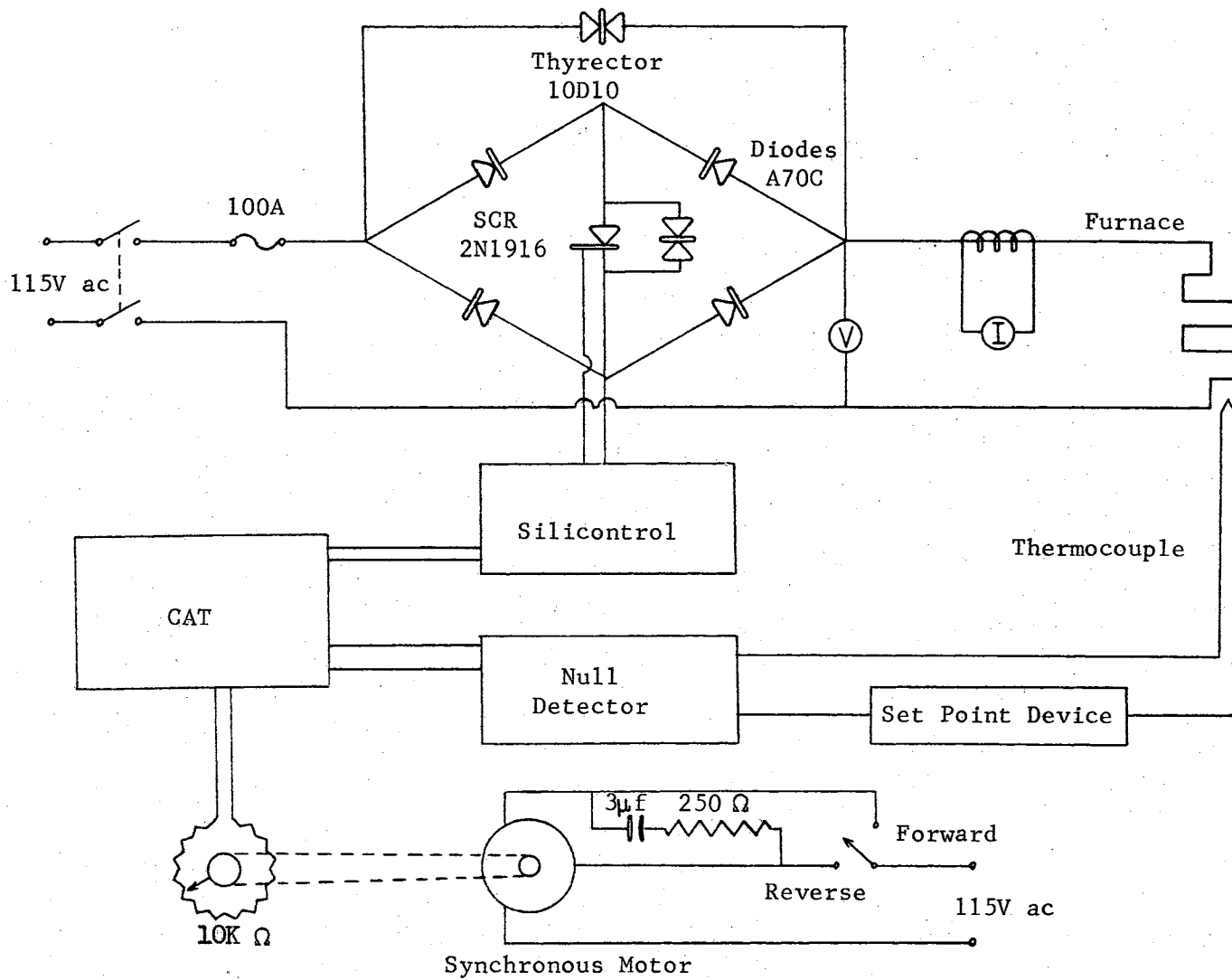
Figure 14. Furnace Power Supply

A Leeds and Northrup Current Adjusting Type (CAT) controller is used to vary the output of the Silicontrol. This instrument is a device with a current range of zero to five milliamperes. There is a bleeder resistor in parallel with the Silicontrol input to limit the current input from the CAT. This is a safety precaution that allows a satisfactory current range from the power supply but limits the possibility of accidentally shorting an expensive SCR or diode.

The CAT current output may be manually adjusted by turning a 10-k-ohm 10T potentiometer on the front of the CAT. It proved advantageous to be able to turn the power supply on and off at a slow, consistent rate. Therefore, the Manual Adjust potentiometer on the CAT has an electric servomotor attached to it so that the CAT output may be increased or decreased by turning the motor switch to "Forward" or "Reverse."

The rest of the components in the furnace power supply are a Leeds and Northrup D-C Null Detector (Model 9834-2) and a set-point device. These components complete the furnace servosystem. The thermocouple has an output that varies with the furnace temperature. The set-point device is a simple potentiometer circuit that bucks out a given thermocouple output, making the input to the null detector zero. The null detector is a differential dc amplifier commonly used with the CAT for automatic furnace control.

The Microbalance

As described in Chapter II, a balance is needed to measure recoil pressures in the range of 10^{-3} to 10^{-6} bar, which correspond to recoil forces of 1 to 10^{-3} dyne, or 10^{2} to 1 microgram _weight_, depending on the

orifice parameters. The balance must have the following characteristics: (1) operate in vacuum of 1×10^{-8} bar; (2) 1×10^{-6} gram sensitivity; (3) total load capacity of 5-10 grams, and (4) relatively sturdy and preferably unaffected by mild shocks encountered when removing from vacuum chamber. There are few, if any, commercial balances that satisfy all four of the above criteria.

One further condition is desired but is not mandatory for this technique; the balance should be automated so that weight changes can be continuously observed, and the experimenter can be free to control the furnace and measure the temperature of the cell.

The balance to be described shall bear the designation, Vacuum Microbalance 1A (VMB-1A) and is identically the same balance described by Bennett[17] with only two modifications: (1) A tare weight arm; (2) a damping coil.

The following information is a repetition of the description given by Bennett[17], with the insertion of information on the two modifications. Some comments on the sensitivity of microbalance VMB-1A are also given.

As shown in Figure 15, the balance beam A is a 6.3-inch length of stainless steel tubing with 0.094-inch i.d. and 0.120-inch o.d. Two polished diamond points C with tip radius 0.001 inch serve as center pivots. The diamond points, (mounted on small jewel screws, C), were obtained from the Moser Jewel Company. Holes were drilled and tapped in an aluminum mounting block B to accomodate the jewel screws so that the pivot tips are 0.5000 $\pm$ 0.0005 inch apart. The mounting block is attached to the beam with epoxy adhesive. Polished-sapphire cups, S, from the same source and also mounted on jewel screws, serve as bearing surfaces for the diamond pivots. The cups, or vees, are mounted in a

block so that their minima are separated by 0.5000 ± 0.0005 inch in the
horizontal plane. Point and vee alignment is fixed by lock screws D and
U, respectively.

Supports typically used at the ends of the beam are the hook type,
the quartz-on-tungsten-wire type, or the two-pivot type. To minimize
friction and to simplify the problem of adjusting all bearing surfaces
to be in a common plane, VMB-1A has a single pivot H mounted, tip upward,
at each end of the beam; these pivot tips and the center ones are ad-
justed so that they are in a common plane within 0.0005 inch. With only
one pivot at each end of the beam, this adjustment is relatively simple.
The surface which bears on the end diamond pivots is again a sapphire
cup, L (inset, Figure 15; only one is shown). A stirrup P is attached
by thin aluminum strips M to the sapphire cup at two points in a hori-
zontal plane slightly below the point of contact between the tip of the
pivot and inverted sapphire cup. Loads are suspended from the cross-
piece of the stirrups. The aluminum mounting blocks for the diamond
end-pivots are sealed in the ends of the hollow beam with epoxy adhesive.
An opening is provided at each end for evacuation of the hollow beam.

A thin front-surface mirror E, with 0.25-inch diameter, is mounted
on top of the center aluminum block and midway between the center pivots.
About 0.5-inch from one end of the beam, a small aluminum block K is
attached by epoxy adhesive to the bottom of the beam. This serves as a
mount for 0.062-inch diameter Cunife wire magnet J. The magnet is held
in the mounting block by a tight frictional fit which permits inter-
change of magnets with various lengths. When properly installed, the
magnet extends equal distances on each side of the beam.

Equidistance from the tare end of the balance beam is an aluminum
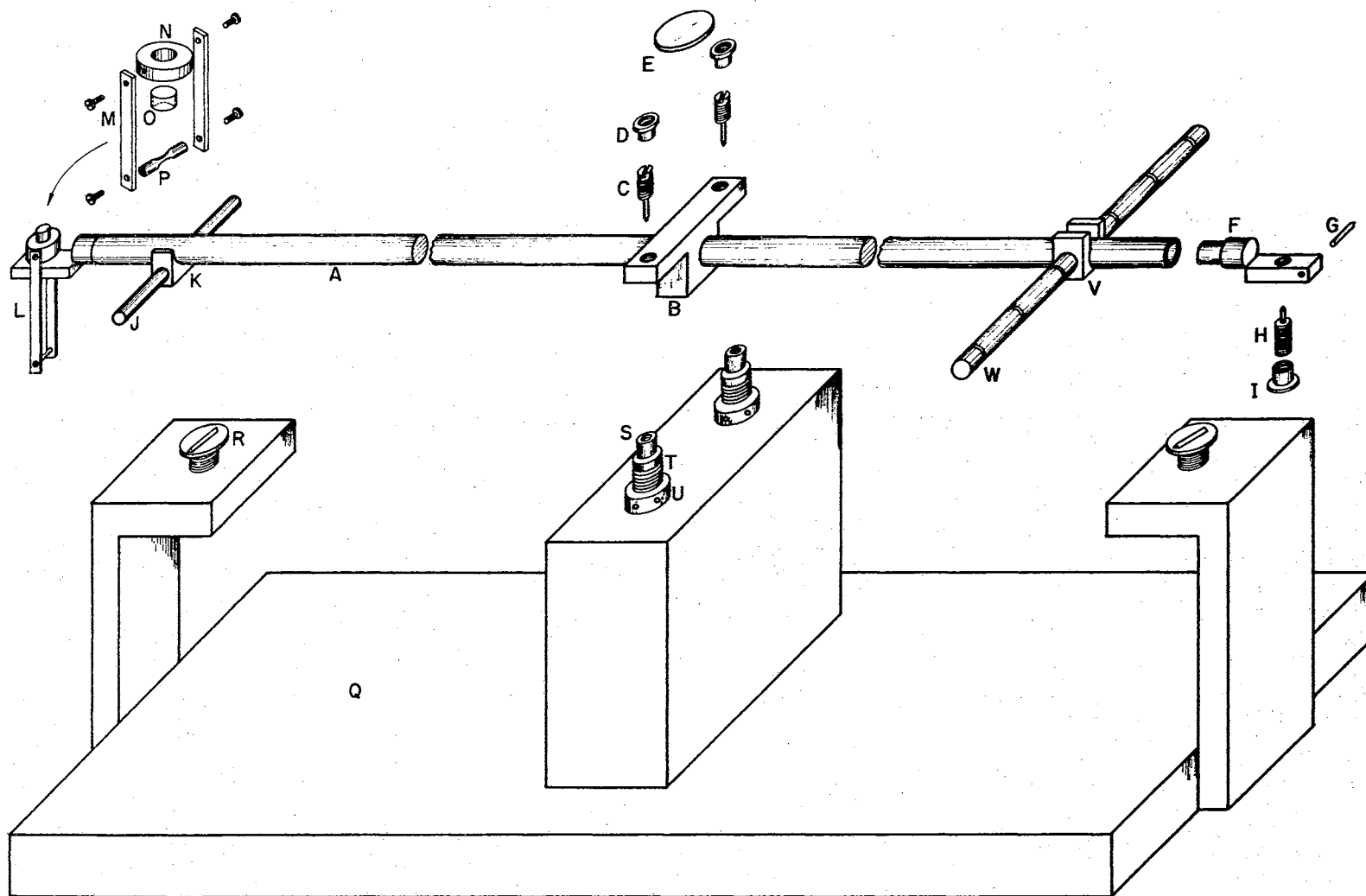
Figure 15. The Vacuum Microbalance, VMB-1A

weight arm. This arm is 2.5 inches in length and 0.125-inch in diameter. It is mounted with epoxy adhesive in the horizontal plane of the center of the balance beam via an aluminum U-shaped block. Three equally spaced grooves encircling the arm keep the tare weights from slipping or turning. This arm holds tare weights for roughly nulling the balance. Also, with the micrometer screw-bellows assembly shown in Figure 16, tare weights can be added to the arm to extend the working range of the balance. The tare weights are elongated rings of .010-inch Nichrome wire, and weigh from 20 to 25 milligrams.

The base (Figure 17) for the balance was constructed from 0.25-inch thick brass. The sapphire cups F for the center pivots are mounted on adjustable screws which are accommodated by a brass block attached to the base plate. The base plate has, in the bottom, three V-grooves which rest on ball bearings D mounted in fixed sockets of a second brass plate. This is to assure that the balance and base plate can be removed and later returned precisely to the original position. Two screw-adjustable, nylon knife edge, beam arrests, R, Figure 15, are located in the base plate. The second plate rests on four sharply pointed screws B which serve as a leveling device.

Added to the tare end of the base plate is a coil holder, a 0.500-inch i.d. copper tube with a bottom. The top is flanged to rest on a base plate extension of 0.25 inch copper that has two wedge locks that allow the holder to be aligned and then locked into position. Inside the holder is an aluminum cylindrical coil frame with approximately 400 turns of A.W.G. 32 copper magnet wire wound on it. The radius of the coil is approximately 0.200-inch. There is a 0.100-inch-radius hole through the center of the aluminim frame. A 1-inch Cunife magnet hangs
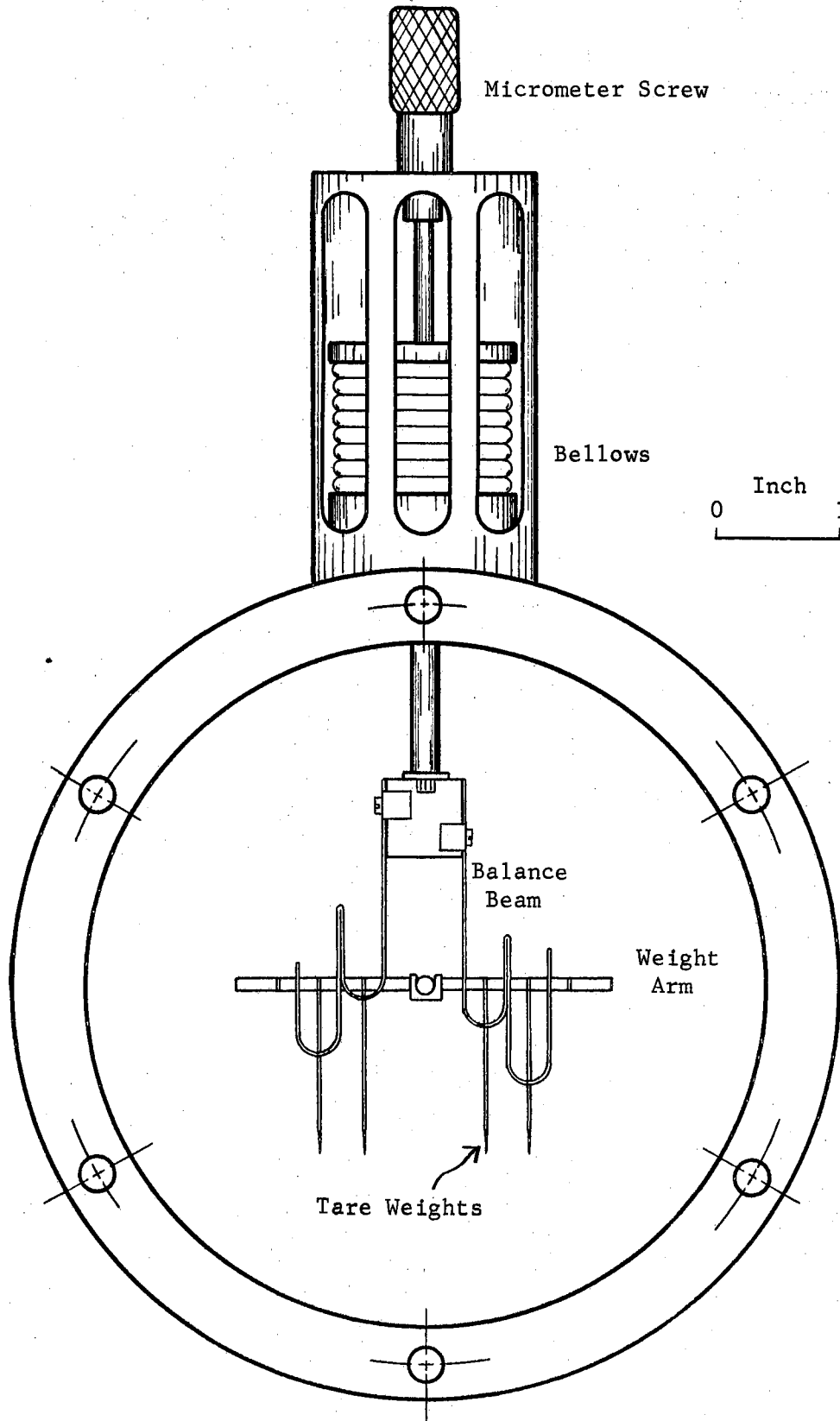
Figure 16. Mechanism for Taring Microbalance Under Vacuum
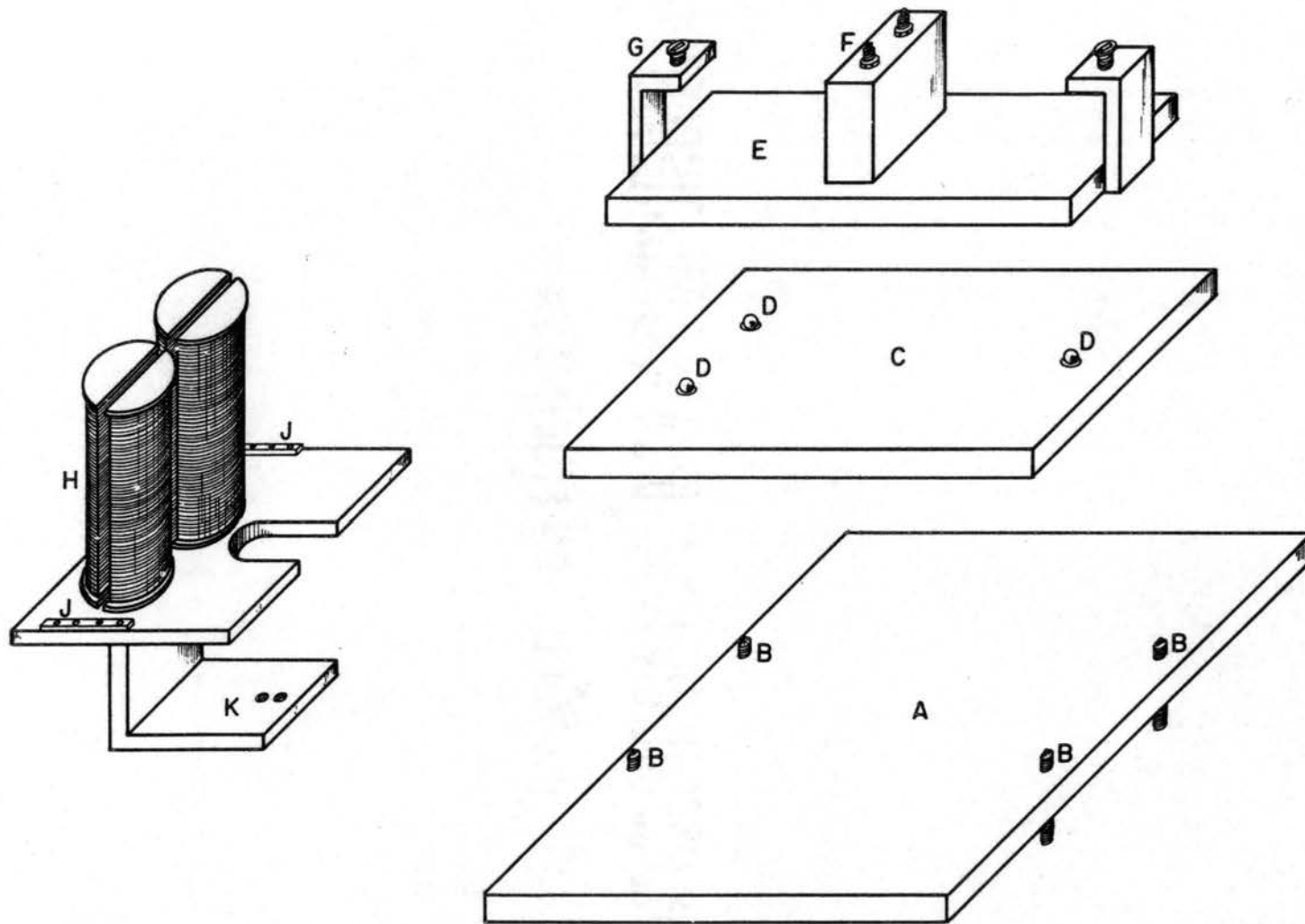
Figure 17. The Base Assembly for Supporting, Leveling, and Providing Kinematic Alignment of the Microbalance.
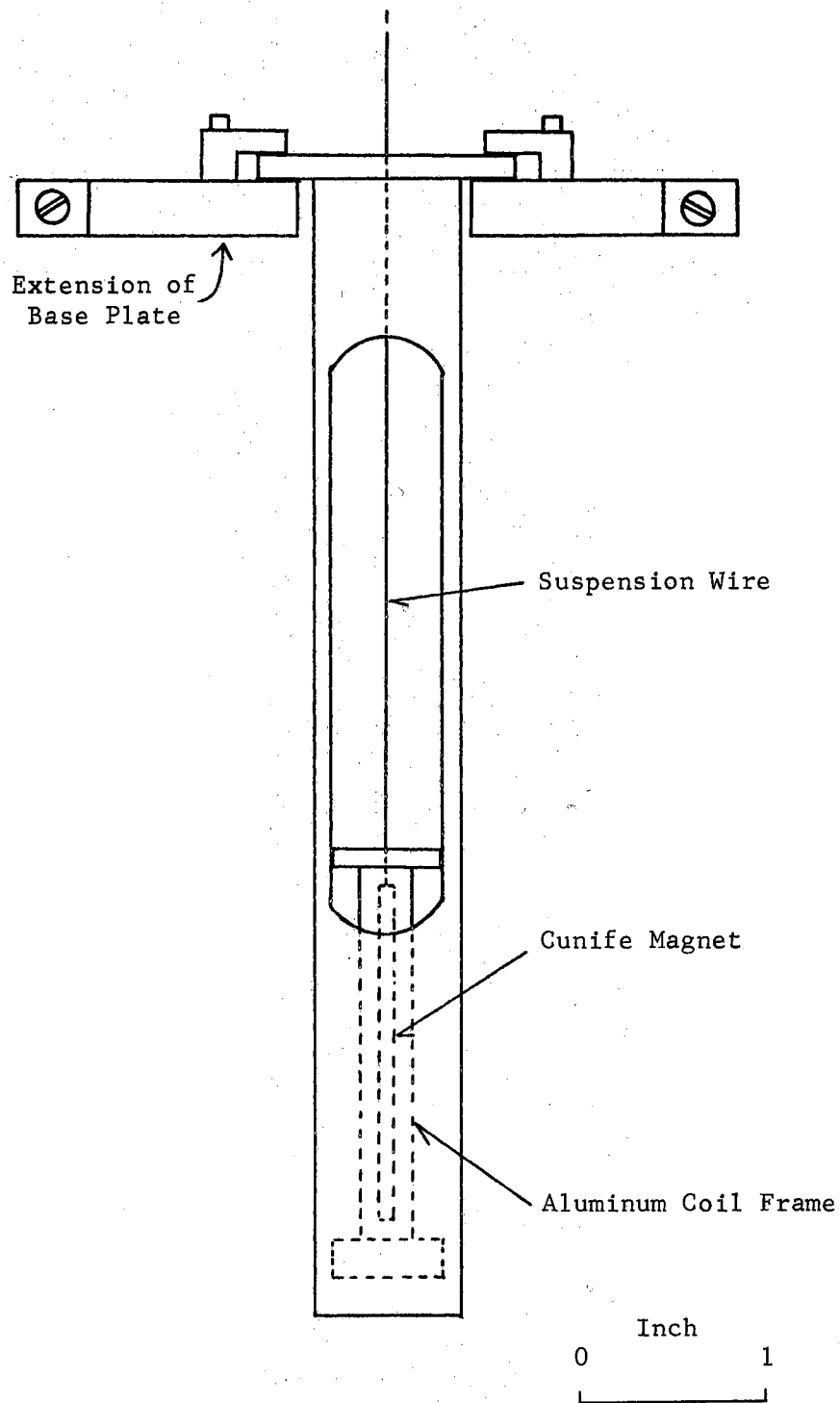
Figure 18. Damping Coil with Holder, and Base Plate Extension

from the stirrup of the balance into the coil and is centered in the coil when the balance is nulled. When an a.c. potential is applied to the coil, there is a resultant force that tends to pull the magnet to the center of the coil. The magnitude of damping is variable by adjusting the potential applied to the coil.

The damping coil has been used with a dc potential of the proper polarity to control the balance. The coupling between the balance and single coil appeared to be much better than with the four-coils system, but hystersis problems and other unknown problems offset this gain. With 50 turns of A.W.G. 32 copper wire on a copper cylinder and with a hanging magnet, the balance sensitivity is 0.35 mg/mA, whereas the 5000 turns of copper wire on the four coils produce a sensitivity of 0.28 mg/mA. The single coil arrangement has a resistance of about 0.5 ohms compared to 125 ohms for the four coils. Over the same current ranges, heat dissipation in the single coil is 250 times less than that of the four coils; this reduction is very significant in vacuum microbalance work.

One further comment on the ac damping technique. It does not work as well if the ionization gauge magnet (2000 gauss horse shoe magnet), located 12 inches from the coil, is removed. This has been approached from the pragmatic point of view that "if it works, it's okay."

Discussion VMB-1 Sensitivity

Theoretical analysis[25] of the simple beam-type balance (Figure 19) gives the equation for the sensitivity, $d\theta/dz$:

$$d\theta/dz = 1/(GS + 2ap) \tag{37}$$

where θ = turning angle in radians,

           p = load in grams on right side,

     $p + z$ = load in grams on left side,

         $2l$ = length of beam in cm,

           G = weight of beam in grams,

           S = vertical distance from center of gravity of beam

                to plane of support (cm),

           a = vertical distance from center line of beam, to

                plane of support (cm).

To simplify the discussion, the term $\underline{a}$ will be considered first. When the bearing points are co-planar with the center line of the beam, $\underline{a} = 0$, and the quantity $\underline{a(2p)}$ becomes 0. This is the first step toward making the balance sensitivity independent of load. The next is to make certain that $\underline{S}$ is not a function of the load. Ideally, the points of contact at the center pivots and those at the end pivots should be in a common horizontal plane which bisects the beam. If the beam bends under load, the situation is more complex. For any system to be mechanically stable, the center of mass must be below the center of support. Thus, if the vertical distance separating the center of mass and the center plane of support decreases with increasing load, the balance actually becomes more sensitive. If this same distance increases with increasing load, the balance becomes less sensitive.

As mentioned, the four point contacts were adjusted to lie in a common plane, within 0.0005 inch. Previously the beam was tested for bending under load by fastening it securely at the midpoint and sus- pending rather large masses from one end. With a mass of 50 g suspended from one end, no deflection, within $\pm$ 0.0005 inch, was observed. This

51
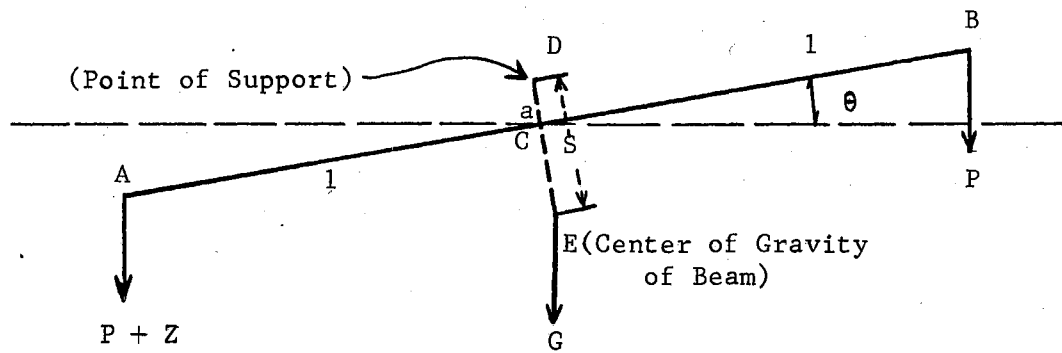
Figure 19. Diagram of a Simple Beam Balance

result, with the fact that in normal use the maximum load suspended from each end will be 5 g, indicates the balance sensitivity to be independent of beam-bending effects.

It follows that equation (37) may be simplified to

$$d\theta/dz = 1/GS \tag{38}$$

and the theoretical sensitivity may be calculated from a knowledge of $\underline{l}$, $\underline{G}$, and $\underline{S}$. Rather than calculate $\underline{S}$, the expression for the period of oscillation of the beam, which contains $\underline{S}$, will be employed. The period, $\underline{T}$ seconds, of the beam oscillating about its center pivots is given by

$$T = 2\pi I_B/gGS \tag{39}$$

where $\underline{I_B}$ is the moment of inertia, $\underline{g}$ is the gravitational constant, and $\underline{G}$ and $\underline{S}$ have been defined. Equation (39) is valid only under conditions of no load and describes the natural period of the balance.

For VMB-1 the period $\underline{T}$ was measured to be $\underline{4}$ sec; $\underline{I_B}$ was calculated to be $\underline{90}$ g cm^2; $\underline{G}$ was $\underline{4.3}$ g. The value for $\underline{S}$ calculated from equation (39) yielded $\underline{S} = 0.03$ cm, which is consistent with $\underline{S}$ values of other microbalance designs (Walker[28], $\underline{S} = 0.01$ cm; Gulbransen[29], $\underline{S} = 0.04$ cm).

The sensitivity may now be calculated from equation 38 to be $d/dz = 6.6 \times 10^{-5}$ rad/μg. For L = 8.5 cm, a 1 μg load should result in beam deflection of approximately $8.5 \times 6.6 \times 10^{-5}$ cm or about 5.6 μm/μg or 0.18 μg/μm.

The period of the balance with the new weight arm was measured to be 4.7 seconds, only slightly larger than that of the microbalance without the weight arm.

The sensitivity of the microbalance obtained directly with a cali-

brated scale of a telemicroscope, is 2.7 $\mu g/\mu m$ movement of the end of the balance beam. The observed balance beam flucuation is $\pm$ 0.7 μm in auto control. This is equivalent to about $\pm$ 1.5 μg control.

Likewise, the magnitude of the current flucuation in the balance coils is $\pm$ 3.0 μA, with good control, which is equivalent to $\pm$ 0.75 μg.

Materials

Stainless steel tubing was used in the construction of the balance beam. All other parts of the framework of the balance are aluminum, machined to very close tolerances. This material selection has proven to be a very good one; there have been no damaged parts on the balance since it was made.

The beam appeared to stick on the original brass end arrests, but this problem has been all but eliminated with the substitution of nylon beam arrests.

The pivots and cups used on the balance are diamond and sapphire, respectively. There are several reasons for the selection of diamond pivots and sapphire vees. The most important factors which determine the feasibility of any pivot-vee combination are friction, pivot load, and vibrations. Theoretically, friction is minimized by minimizing the contact area between the pivot and the vee. This principle suggests the use of infinitely sharp points, but in practice pivot points must be rounded because exceptionally sharp points deform under load. This factor more than any other limits the ultimate ratio of load capacity to sensitivity in microbalance design. Optimum design requires use of that material which yields the largest number for the ratio[32]: load at which pivot distortion occurs/pivot radius. Diamond appears a clear

choice, and Stott has determined empirically that the minimum pivot

radius suitable for a 5 g load is about 0.003 cm.

Once the pivot dimensions are selected, it is a rather simple mat-

ter to select the vee. The vee radius should be 2 to 3 times the pivot

radius to balance the necessity for minimum contact area with the need

to avoid excessive lateral play between the pivot and vee.

The depth and angle of the vee are important when vibrations are

likely to exist. Deep vees with relatively steep angles are considered

superior to shallow or side-angle vees when vibrations must be accomo-

dated.

The hardness, ready availability, and easy adaptability of sapphire

vees make them an excellent choice for the diamond pivots. Another rea-

son for choosing the diamond-sapphire combination is that, in spite of

their apparent advantages, no previous workers have stressed these

materials as microbalance components, though Honig suggested the possi-

ble use of diamond pivots, and Cochran used a sapphire cone-tungsten

point combination.

Magnetic Balancing System

The method for achieving magnetic coupling for control of the bal-

ance beam position is a modification of methods employed by Simon,

Shierrer, and Ritter[30], and by Gerritsen and Damon[31]. Each end of the

Cunife magnet extends halfway into the gap between a pair of hemicylin-

drical coils (Figure 17). Each coil has approximately 2000 turns of

A.W.G. 30 copper wire on a solid copper core. The gap between the flat

sides of a pair of coils is 0.25 inches. Control of the position of the

balance beam is achieved by varying the current through the four coils

which are wired in series. A polarity reversing switch makes it possible to drive the end of the beam to which the magnet is attached in either the downward or upward direction.

To minimize problems arising from poor heat dissipation in vacuum, the coils are mounted on a copper block which serves as a heat sink.

The magnet is mounted on the same end of the beam from which the Miker cell is suspended. This results in a constant load balance; as the mass of the Miker cell and sample decreases, a compensating increment of current is provided to the coils to retain the null. Consequently the balance always supports the same net load; if the magnet were mounted on the opposite end of the beam, this would not be the case.

Stability of Zero of Balance

It was found that the null or zero of the balance is drastically changed if one upsets the balance too much. "Too much" upset was found by this author to be that obtained by abruptly pegging the balance via instanstaneous removal of a tare, stomping the lab floor in the vicinity of the system, tapping the balance chamber with ones knuckles, etc. This indeed presented a problem, for in calibrating the balance one must remove or add small weights to a stirrup of the balance. It was found that using the micrometer screw-bellows assembly to add a weight to the weight arm eliminated this problem. Calibrations can be obtained with the weight arm-micrometer screw combination if the appropriate correction for the difference in lever arm length of the weight arm and stirrup is known.

The source of the null change upon upset appeared to this author to be the stirrups of the balance. With an abrupt pegging of the bal-

ance, the loads on the stirrups (the damping magnet and the Miker Cell) twist them on their diamond tip fulcrums and the stirrups don't twist back to the original position after settling down. Thus, the control point may be displaced 10 to 1000 μA.

It should be added here that during an experimental measurement, the largest deflections of the balance beam ever observed was approximately 70 μm. The average displacement of the balance beam was no more than 10 μm for slow effusion processes, and 20 μm for the fastest effusion rates.

This displacement varies with the rate of effusion and can be reduced to less than 10 μm by increasing the "Reset" on the CAT. This change in control setting has the disadvantage that the error signal immediately before and after a recoil measurement are drastically different, one with a constant error signal of constant polarity and the other with an error signal that oscillates about a control line. The consequence, to be discussed next in this chapter, is that one may have good control in the rate of effusion measurement but unstable control after the recoil measurement if the rate of effusion is too large (above 0.75 μg/sec.).

Automatic Control of the Microbalance

"Aladdin had no sooner rubbed the lamp, than in an instant a genie of gigantic size appeared before him, and said in a voice like thunder, "What wouldst thou have? I am ready to obey thee as thy slave."

Out of the depths of history appears one of the most potent features of civilization, man's ability to utilize the forces of nature for performing physical tasks far beyond the capabilities of his own

strength. It is the process of applying these forces, releasing, stop-

ping, and properly governing their action, which is designated under the

name control."[36]

It is the purpose of this section to elucidate very qualitatively

the servomechanism used to obtain automatic control for VMB-1A. A servo-

mechanism is a closed-cycle power amplifying electromechanical system.

Servosystems (servomechanism systems) may either be closed-loop

servosystems or open-loop servosystems. In an open-loop servosystem,

the control operation is independent of the result obtained, whereas

in a closed loop servosystem, the control operation is a function of the

result obtained. The three main components of the control system for

VMB-1A are: the balance, the error detector, and the controller.

It will be advantageous to look at a mechanical analogy to the

microbalance servosystem before discussing the control criteria and

operating parameters.

The servomechanism will be likened to a pendulum, since both de-

vices possess inertia and elasticity or the equivalent. The discussion

to follow is not original with this author, but is taken from a standard

text on "Servomechanism fundamentals."[36]

Comparison Between Viscous Damping and Error-Rate Damping

The servomechanisms to be discussed here establish a correspondence

between the positions of the input and output members of the system.

Whenever this correspondence is altered, the resulting discrepancy or

error between the positions of the input and output members causes the

controller to develop a force of such magnitude and direction as to tend

to reduce the error to zero. This force is proportional to the error,

and is thus equivalent to the elastic force of a spring, which tends to restore the spring to its original length whenever this length is altered by a stretching or compression of the spring.

Since in addition to this elasticity the system is also endowed with inertia, it will oscillate when it is disturbed from its steady-state position of equilibrium. During such oscillation the output member no longer follows accurately the position variations of the input member. To reduce the amplitude and duration of the oscillation is the function of such damping as may be introduced in the system.

Viscous damping consists in applying to the system a retarding force proportional to the speed of the output member. While such viscous damping effectively reduces transient oscillations, it also produces an undesired steady-state error, which results from the very fact that the output member is moving. In other words, viscous damping not only reduces the oscillation, but also retards the output member of the system. In order to eliminate this effect, it is then necessary to resort to other forms of damping or stabilization, which will operate only on the oscillation or transient error, but not on the steady-state motion of the system.

The difference between the two types of damping can perhaps best be understood by describing a simple mechanical system that behaves exactly like the servomechanisms here discussed. However, it should be emphasized that such a mechanical system is not a servo, and that it is described only because the characteristics of its motion are similar to those of a servomechanism.

Before such a system is described, the simple pendulum shown in Figure 20A may be considered. This consists of a mass $\underline{M}$ suspended from
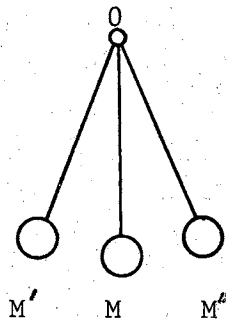
(A) Simple Pendulum
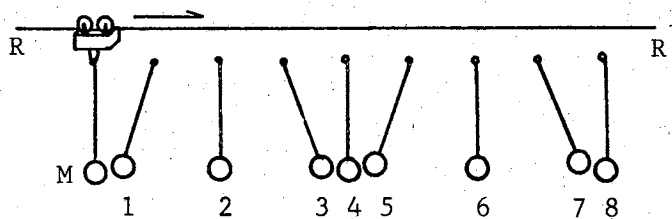
(B) Pendulum Analogy of Undamped Servomechanism
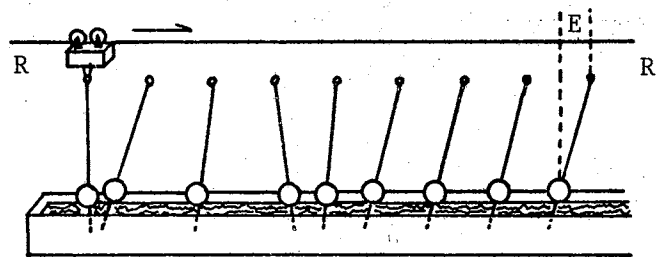
(C) Pendulum Analogy of Viscous-Damped Servomechanism
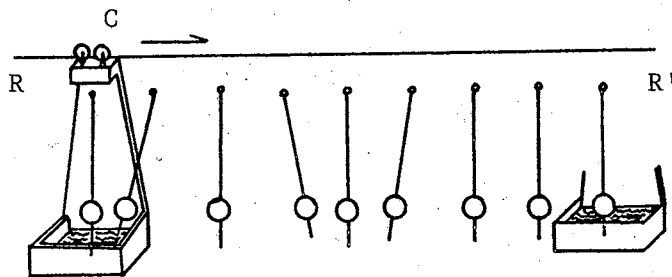
(D) Pendulum Analogy of Error-Rate-Damped Servomechanism

Figure 20. Pendulum Analogies of Servomechansims

a pivot $\underline{O}$ by a thin rod $\underline{OM}$. When the pendulum is at rest, it hangs in a vertical direction, which is its position of stable equilibrium. If the mass $\underline{M}$ is temporarily displaced to some other position $\underline{M}'$ and then released, the pendulum oscillates back and forth between positions $\underline{OM}'$ and $\underline{OM}''$ equally displaced on each side of the vertical position $\underline{OM}$.

In the absence of any friction the oscillation persists indefinitely with constant amplitude. On the other hand, if some friction is present, each swing of the mass $\underline{M}$ is smaller than the preceding one by a constant percentage, and the pendulum more or less rapidly comes to rest in its original vertical position $\underline{OM}$; i.e., the oscillation is damped.

Referring now to the system shown in Figure 20B, suppose that the pivot $\underline{O}$ of the pendulum is mounted on a carriage $\underline{C}$ that may be made to move horizontally along a rail $\underline{RR}'$. As will be shown below, the behavior of such an arrangement can be compared to that of a servomechanism, the input and output member positions of which are represented, respectively, by the position of the carriage along the rail and by the position of the pendulum mass. The difference between the positions of the carriage and of the mass along the direction of motion at any instant corresponds to the error of the servomechanism. The response of the pendulum mass to motion of the carriage is, with comparable constants, identical with the response of a servosystem to the motion of its input member.

Starting from the position of rest, shown at the left of Figure 20B and for which the pendulum is in its stationary vertical position, let the carriage be suddenly set in motion at constant velocity toward the right. The figure then shows the position of the pendulum and its support at equal intervals of time after the starting instant. By

virtue of its inertia, the mass M at first lags behind the pivot in its

motion toward the right, and the pendulum assumes a slanting position

shown at 1. As the carriage and pivot move on farther, the pendulum

swings forward, through positions 2 and 3 then backward (positions 4 and

5), oscillating back and forth indefinitely with constant amplitude.

Thus, the average position of the pendulum mass M follows the posi-

tion of the carriage C in its constant-velocity motion toward the right,

while the instantaneous position of the mass alternately precedes and

lags behind that of the carriage. This creates an alternately positive

and negative discrepancy or error, between the positions of the mass M

on the one hand, and the pivot O and carriage C on the other. The sys-

tem is thus comparable to an undamped servo-control system, in which the

carriage and pivot represent the input member, while the mass repre-

sents the output member, and the zero-error position is that for which

the pivot and mass are on a common vertical line.

Similarly, the system in Figure 20C may be taken as equivalent to a

viscous-damped servosystem. It differs from the system of Figure 20B in

that the mass M is provided with a small vane that dips in some damping

liquid, such as oil, contained in a tank beneath the rail RR'. As the

carriage is suddenly started from the position of rest shown at the left,

the pendulum at first oscillates, as in the previous example. However,

the retarding force between the vane and the liquid damps the oscilla-

tion more or less rapidly, and the pendulum mass M then simply follows

the constant-velocity motion of the carriage and pivot toward the right.

But, under these conditions, the pendulum does not assume a vertical

position. The friction arising between the vane and the liquid, because

of the motion, produces a retarding force on the mass M as the vane is

dragged through the liquid by the motion of the carriage, thus, the position of the mass M lags behind that of the pivot 0 in the motion of the system toward the right, and the resulting error between the instantaneous position of the mass and pivot is proportional to the velocity of motion. A force equal and opposite to the retarding friction force must be constantly applied to the carriage in order to keep the system moving at constant velocity. Under steady state conditions the pendulum assumes a slanting position of equilibrium for which the torques due to friction and gravity are equal and opposite.

From the preceding remarks, it is seen that the mass M, which represents the output member of a servosystem as studied before, is subjected to two kinds of motion superimposed upon each other and constituting its actual motion as just described. One of these two component motions is a constant-velocity translation toward the right. The other is a temporary or transient damped oscillatory motion, lasting only during and directly following the accelerating period of the system. Both these motions are affected by the friction, which is proportional to the velocity of the mass M with respect to the damping liquid in the tank.

Since the steady-state error is due to the constant-velocity translatory component of the motion of the mass and its vane with respect to the liquid, it becomes obvious that no such error will arise if this relative translatory motion between the mass and the damping liquid can be of oscillations due to acceleration (or deceleration) of the input member, or carriage C.

Such a system is illustrated in Figure 20D. Instead of using a stationary tank to contain the damping liquid, as was done in the case

of Figure 20C the present arrangement employs a smaller tank permanently

attached to the carriage C, or input member of the system. When the

carriage is suddenly started from rest and set in constant-velocity mo-

tion toward the right, the pendulum at first oscillates in the same

manner as described before. The friction arising from the resulting

motion of the vane in the liquid soon damps out this oscillation. But

since the motion of the carriage C does not drag the pendulum mass

through the damping liquid (which it did in the case of Figure 20C), the

pendulum reverts to a vertical position of rest. In other words, while

an oscillation of the pendulum produces a relative motion of the mass

and the liquid, which motion is then damped out, there is no relative

translatory motion and therefore no steady-state error. The carriage,

pendulum, and damper all move together at the same constant velocity

toward the right, and the mass M and pivot O retain their original re-

lative positions on a common vertical line.

In order to apply to the design of a servomechanism the principles

involved in such an arrangement, it is necessary to analyze further the

particular type of damping illustrated here. This damping affects only

the oscillatory component of motion, without operating on the constant-

velocity translatory motion component. It will be recalled that the

frictional force, which produces the damping, is proportional to the

velocity of the mass and its vane with respect to the damping liquid.

Since the damping liquid is carried along by the carriage in its uniform

translatory motion, the damping force is proportional to the velocity

of the mass with respect to the carriage, which is actually the velocity

of the error. Thus, in the rate of change of the error, instead of

being proportional to the output velocity as in the case of the systems

studied previously.

In a servosystem employing such error-rate damping, the controller must therefore produce a driving force or torque proportional to the sum of the following two components:

1. The input-output position error. The corresponding force causes the output member to follow the input member when the input member position is changed, i.e., when the input member is moved with respect to the output member. (Note that in the preceding pendulum analogies the output position restoring force is the force of gravity, which tends to bring the pendulum back to the vertical position. For small oscillation angles of the pendulum this force is proportional to the displacement of the mass $\underline{M}$ from the vertical, i.e., the force is proportional to the position error between the pendulum mass and pivot.)

2. The rate of change of the input-output position error. This component of the controller torque has been shown, in the pendulum analogy, to provide damping without introducing a steady-state error.

The total torque is thus expressed mathematically by the relation

$$T = KE + L \, dE/dt \tag{40}$$

where $\underline{T}$ is the torque produced by the controller, $\underline{E}$ and dE/dt are the input-output error and time rate of change of the error, respectively, and the proportionality factors $\underline{K}$ and $\underline{L}$ are two controller constants.

Suppose, as shown in Figure 21, that the carriage $\underline{C}$ is filled with sand and that its floor is provided with two small funnels $\underline{H}$ and $\underline{K}$, through which the sand may escape when either lower orifice is open. The pendulum operates a slide $\underline{S}$, which closes the openings of both funnels when the pendulum is in a vertical position, but opens either the forward funnel $\underline{K}$ or the rear funnel $\underline{H}$, depending on whether the pendulum
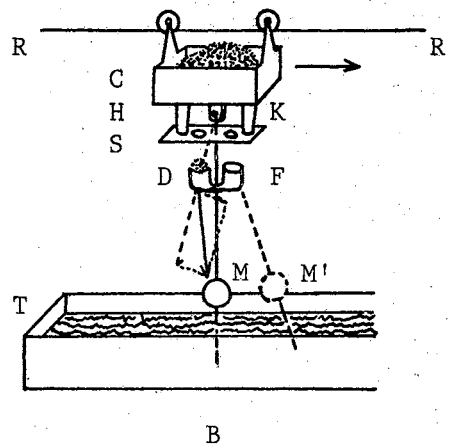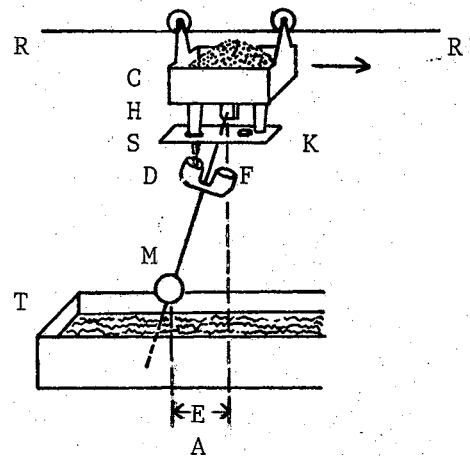
Figure 21.   Pendulum Analogy of Viscous-Damped
             Servomechanism with Added Integral
             Control

is displaced forward or backward of the vertical position. Attached to the pendulum are also two cups D and F into which the sand escaping through H or K, respectively, may fall. As in the case of Figure 20D, a vane is fixed to the pendulum mass and dips in the damping fluid contained in the stationary tank T.

Let now the carriage C be driven at constant velocity from left to right along the rail RR' against the friction of the vane in the damping fluid. As in the simple viscious-damped system of Figure 20C, the pendulum will tend to assume a backward slanting position, as shown in the sketch A of Figure 21, producing a position error E between the mass M and pivot. This, however, displaces the slide S and opens the rear funnel H, through which sand then escapes from the carriage C into the cup D. The resulting unbalance of the pendulum tends to bring it into a vertical position, as shown in the sketch B of the figure. As the pendulum approaches the zero-error, or vertical, position, the slide S gradually closes the funnel H and finally cuts off the flow of sand when the pendulum reaches the vertical position. A similar erro-canceling action would take place, through the forward funnel K, if the pendulum should swing forward of the vertical position.

It may be assumed that the opening of the funnel H and the flow of sand into the cup D are proportional to the instantaneous deviation or error E of the pendulum from the vertical position. The weight of sand collected by the cup during the period of time required for the error to be reduced to zero and for the pendulum to be brought to the vertical position can then readily be calculated. Thus, consider this period of time to be made up of a succession of elementary time intervals t so short that the funnel opening may be looked upon as remaining constant

during any one of them. If a_1 is the area of the opening during one such time interval Δt_1, the weight of sand w_1 flowing out of the funnel during this time interval is proportional to the product $a_1 \Delta t_1$. Since the opening area a_1 is proportional to the corresponding error value E_1, the weight w_1 is also proportional to the product $E_1 \Delta t_1$, or equal to this product if a suitable unit of weight is used.

If a_2, a_3, ...a_n are the areas of the opening during the succeeding time intervals Δt_2, Δt_3, ... Δt_n when the error assumes the corresponding values E_2, E_3, ... E_n, the respective weights of sand flowing during these time intervals are

$$w_2 = E_2 \Delta t_2$$

$$w_3 = E_3 \Delta t_3$$

$$\cdots$$

$$w_n = E_n \Delta t_n$$

The total weight of sand collected by the cup is then

$$W = w_1 + w_2 + w_3 + \ldots + w_n$$

$$= E_1 \Delta t_1 + E_2 \Delta t_2 + \ldots + E_n \Delta t_n$$

$$= \sum_{n = 1, 2, \ldots} E_n \Delta t_n \qquad (41)$$

The assumption that the funnel opening remains constant during any elementary time interval is, of course, more closely justified as these time intervals are made smaller. If they are made infinitesimally small and infinitely numerous, the preceding summation becomes equal to the time integral of the error,

$$W = \sum E dt \qquad (42)$$

Hence the name <u>integral</u> <u>control</u> is given to this method of correcting

the input-output error of the system to zero.

There is a fundamental difference between the operating conditions

of the servos previously studied and those of a servo employing integral

control: while the driving force (or torque, in case of rotary motion)

in the steady-state condition is proportional to the error in these

earlier servosystems and becomes equal to zero with the error, a finite

driving force may be operating in an integral control system, even when

the error is zero.

Another characteristic feature of a servo employing integral con-

trol is that the system will not come to rest, when the input member is

stopped, until the time integral of the error has become equal to zero.

This may be illustrated by referring again to the pendulum analogy pic-

tured in Figure 21. As explained in relation to the diagram <u>B</u> of that

figure, the pendulum is subjected to the retarding friction drag be-

tween the pendulum vane and the damping liquid, caused by the transla-

tory motion of the system toward the right. This drag tends to give to

the pendulum an oblique position similar to that shown in Figure 20C.

However, the pendulum is maintained in the vertical position because it

is unbalanced by the weight of the sand which has accumulated in the cup

D during the transient period.

When the system is stopped, the frictional drag disappears, but the

unbalance remains, which tends to give to the pendulum a forward slant-

ing position, shown as <u>M</u>' in dotted line. This, in turn, opens the

funnel <u>K</u>, allowing sand to flow from the carriage <u>C</u> into the cup <u>F</u> un-

til a weight of sand equal to that contained in the cup <u>D</u> restores the

balance of the pendulum. The pendulum then assumes its normal vertical

position of rest.

As described above, integral control is applied to servomechanisms with viscous output damping for neutralizing the steady-state error resulting from the output frictional drag. It can be applied as well to servomechanisms having both viscous and error-rate damping. It is this general case which will be analyzed mathematically in the paragraphs that follow, after which practical means for obtaining integral control will be described and discussed briefly.

The servomechanism to be discussed here has viscous and error-rate damping along with integral control. The mechanical model for this system is shown in Figure 21. The block diagram and schematic are shown in Figures 22 and 23 respectively. To achieve good servocontrol, the error, i.e., the pendulum displacement, should be as small as possible for as short a length of time as possible. If the area of the funnel opening is too small, it will take a long time before E becomes zero. If the area of the funnel opening is too large, the cup will become too full on the left side and the pendulum will go past the $E = 0$ point and requires addition of sand to the right cup and this cycle would continue indefinitely, if the pendulum were not damped properly. The oscillating of the pendulum about the $E = 0$ point is referred to as "hunting." One can perhaps see that to obtain the optimum servocontrol, he has to consider many factors. (i.e.,the magnitude of viscous damping, the error-rate damping, the period of the pendulum, the size of the error when the cart starts to some velocity U and stops instantaneously, the rate of deposition of the sand, the velocity U of the cart, etc.)

The Microbalance Servosystem
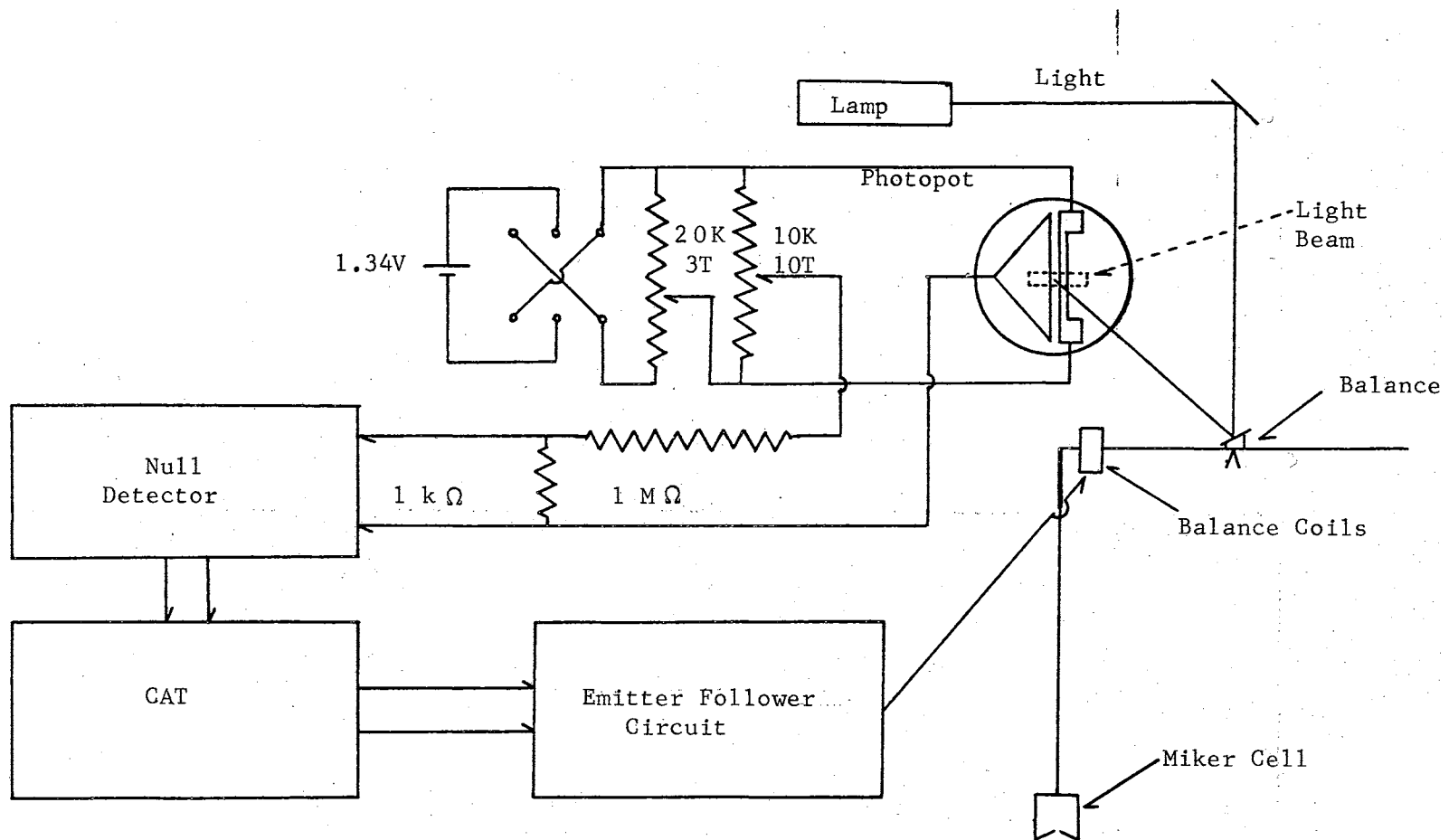
Figure 22. Block Diagram of Microbalance Servosystem
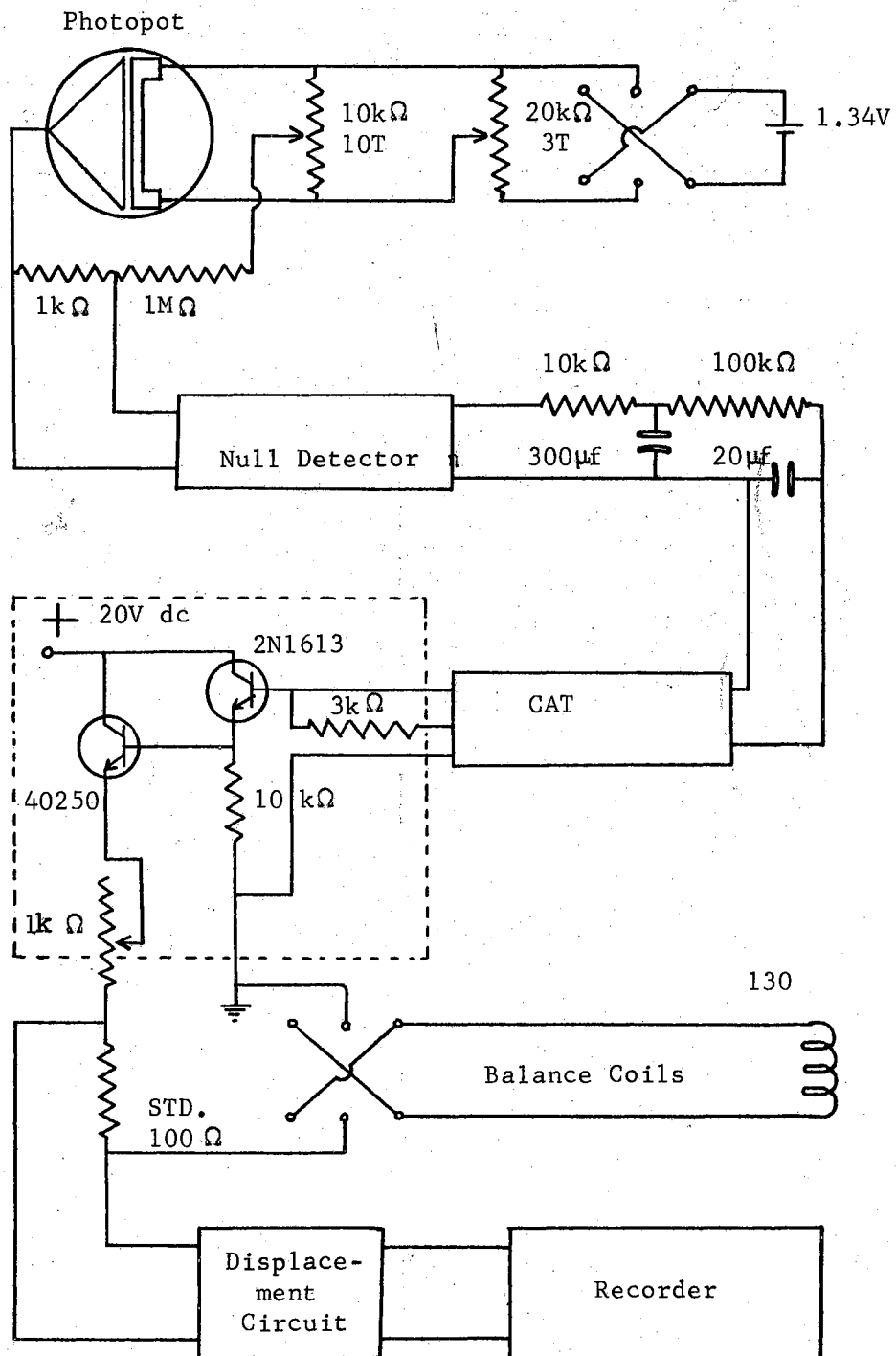
Figure 23. Schematic Diagram of Microbalance Servosystem

In a dynamic servosystem, it is impossible for the error, $\underline{E}$, to ever become zero. The first step then in determining the operating parameters for a servosystem with optimum control is to determine the error (displacement from the desired control line) that one can tolerate in the experiment to be performed.

As previously indicated, the sensitivity of the microbalance to be used here is about 2.7 $\mu g/\mu m$ movement of the end of the balance. Therefore, the first requirement to be satisfied was that the servosystem control the balance beam to $\pm$ 1 μm movement. The balance is operated as null seeking device; weight loss from the Miker cell causes current to change in the controlling coils to keep the balance in a null position.

The major components on the balance are retained from VMB-1: the Cunife wire magnet, the four coils, the front surfaced mirror on the beam, and the beam itself. Two components have been added to VMB-1 as previously discussed; the weight arm and the damping magnet and coil.

The error detection components have been drastically altered from VMB-1. The components are: The light source and slit, the Photopot and mounting, the Wheatstone Bridge circuit, and the Leeds and Northrup Null Detector.

A constant intensity lamp (Philips 1B113C-04 projector lamp) illuminates the slit which serves as light source for the Photopot. The regulated power supply is shown in Figure 13 and has been previously described in this chapter. About one inch in front of the lamp is a 0.004 x 1.0 inch slit. This arrangement insures that the maximum amount of light goes initially through the slit. The light beam is then reflected into the vacuum system, from the balance mirror, and onto the Photopot. Focus on the Photopot is adjusted primarily by a lens of 18-

cm focal length located just above the vacuum window in the top of the balance chamber. It might be noted here that the optical path is just the reverse of that presented by Bennett for control system II[17]. The Photopot is inside the vacuum chamber and the light starts from the top of the chamber.

The Photopot is one side of a Wheatstone bridge circuit. Movement of the balance beam causes the light beam to traverse the Photopot, changing the output of the Wheatstone bridge. A 1-Mohm and a 1-kohm resistor are in series across the output of the bridge. The error signal developed across the 1-kohm resistor is fed into a dc null detector where it is amplified. A 1.34 V mercury battery is used for the power source of the bridge circuit because of its constant voltage characteristics.

The output of the null detector is fed into a current adjusting type (CAT) controller. The CAT output varies from zero to five milliamps. With the instrument in the AUTO control position, the dc output decreases or increases depending upon the polarity of the null detector output (+ or -).

The output of the CAT controls the output of an emitter-follower (E.F.) circuit shown in Figure 22. The load in the E.F. circuit is the coils that control the position of the microbalance.

Thus, the servo-loop has been closed. A brief summary of the components and their operation will perhaps bring the components back into perspective. The balance is operated in a null position. A deviation from the null position is sensed by the detector circuitry as a positive or negative output of the Wheatstone bridge. This signal is amplified and inverted in polarity by the null detector and fed into the CAT.

The CAT responds in such a fashion as to bring the balance back to the null position. Alas, one cycle is complete.

Now, each component of the servosystem will be discussed in detail, with the instrument settings used for optimum control included.

The Photopot[37]

This device is the latest model of the half-inch stroke unit as of May, 1966. It does not outgas appreciably and is unaffected by high vacuum. For light intensities above about 1000 $\mu W/cm^2$, the voltage output of the Photopot is linear. The response time of the Photopot is in the order of one millisecond and the resolution is about 1×10^{-4} cm. The Photopot was obtained from Gianni Controls Corporation as Model No. 8118j.

The Photopot Circuitry

As shown in Figure 23, the Photopot is one side of a Wheatstone bridge circuit. The other side of the bridge has two 10-kohm resistors in series with a 1-kohm ten-turn potentiometer. As recommended by the supplier, the output of the bridge has a 1-Mohm resistance in it.

The Null Detector

The null detector is a Leeds and Northrup Model 9834-2 differential amplifier. This device has two modes, linear and non-linear. The linear mode is used in auto-control of the balance. In the linear mode, the gain of the amplifier may be adjusted from a setting of "2" (with a voltage gain of approximately 500) to "6" (with a gain of 8000) or even higher to "10". Considerable work was done to determine the stability

of the null detector because drift in the zero of this instrument will
not be compensated for elsewhere in the servo loop. Conversely, drift
in the CAT or emitter follower circuit or power supply will automatical-
ly be compensated for by the null detector. Tests were made with the
input of the null detector shorted and the output fed into a recorder.
It was found that the higher gain settings produced larger drift rates.
It was also determined that cooling the instrument with a muffle fan
stabilized it on all gain settings, to the extent of decreasing the
noise by a factor of ten. To reduce drift, a gain setting of "2" was
employed and was later found to be quite satisfactory since with that
gain the servosystem has a sensitivity of 0.7 to 1.0 μg weight change.

The R-C Filter

On the output of the null detector is an R-C filter, which is an
error-rate stabilization network, or electronic damping used in the
absence of significant viscous damping in the servosystem. The values
for the resistance and capacitances used in the circuit were determined
by Harvard Tomlinson[38]. This author does not fully appreciate the
techniques used to determine these values. However, the servosystem
is completely unstable if the filter is removed. It has been assumed
that the servosystem parameters have not changed significantly since
1964 and that the values used in this circuit are still near the opti-
mum values for the servosystem.

The CAT Controller

The current adjusting type (Leeds and Northrup Model 10877) con-
troller is commercially used in process control in industry. The in-

strument may be set at some current output in its "Manual" mode, then switched to its "Auto" mode and the current will remain constant if the output impedance in both modes is matched and if there is no input signal. An input signal to the CAT from the null detector causes the control current out of the CAT to change, increasing or decreasing, depending upon the polarity of the error signal from the null detector. The rate at which the output of the CAT changes is dependent upon the magnitude of the error signal and the dial settings on the CAT.

There are three settings located on the front of the CAT. They are:

1. Proportional Band. The proportional band adjustment controls the extent of influence which the instantaneous magnitude of the error signal has on the output. Proportional Band is simply that portion of the measuring instrument scale (expressed in percent of full scale) that when traversed by the indicator, will cause a change from 0% to 100% output in the control system. Under proportional control and without reset of any kind, when the measured variable is at a value which coincides with the desired control point, the output level of the system usually will be at 50% of maximum. Consequently the control point is in the middle of the proportional band.

2. Reset. The reset adjustment controls the extent of influence which the time integral of the error has on the output. Automatic reset is calibrated in "repeats per minute". For a static or fixed proportional band error, the setting indicates the number of times per minute that automatic reset control action will repeat the same change in output level that the proportional band error created.

3. Rate. The rate adjustment controls the extent of influence

that the derivative, or rate of change of the error, will have on the output.

It should be noted here that reset action adds to proportional band action and is largest when the error is largest; whereas rate action subtracts from proportional action and is largest when the error signal approaches zero.

The Emitter Follower Circuit[34]

A two-stage emitter follower circuit was originally designed as a calorimeter heater power supply (with a 1-A output) to be used in conjunction with a CAT. A "dummy" load of 50 ohms is in parallel with the balance coils so the circuit will have a sufficient current output to make it stable. The power supply for the E.F. circuit is a Sorensen Model QB-28-1 voltage-regulated supply, set for 20 volts output. This circuit has presented one minor control problem. With direct coupling between the emitter follower and the CAT, the feedback for the CAT is changed and the CAT drifts appreciably in "Auto" control with no null detector imput signal. The problem has been very minor because the null detector automatically compensates for the drift.

The Recorder

A Sargent Model TR recorder continuously monitors the current in the compensating coils by recording the voltage across a 100-ohm standard resistor in series with the coils. At the maximum coil current of 50 mA there will be a 5 volt input to the recorder. A displacement circuit with four mercury batteries in series is used to oppose this potential. The large standard resistor is used because there is evidence

that the lower recorder scales are non-linear. They push the amplifier in the recorder to near maximum output. Using a larger resistor, one can use a higher recorder scale with lower gain setting and measure the same coil current.

Drift

Considerable drift in the control point was encountered in the servosystem (i.e., the null detector) until the null detector was supplied with Voltage-regulated ac power. Leaving the electronic circuitry on continuously helped to stabilize the system a great deal, too.

Optical Pytometer Corrections and Measurements

Shown in Figure 24 is the device used to obtain the Wien's Law correction factor for a given prism used between the Miker Cell and the optical pytometer. As noted previously in this chapter, there is a prism mounted in the bottom of the furnace chamber. The prism permits the optical pyrometer to be positioned horizontally when the orifice in the bottom of the Miker Cell is being observed.

The device used to determine the temperature correction is a rather simple one. It consists first of a circular board, about 20 inches in diameter, with three leveling screws 120 degrees apart. Bolted to the center of the circular board is an aluminum arm that is free to rotate around the board. Mounted in the free end of the aluminum arm is an electrical socket that will accept a tungsten strip lamp. Finally, a Variac and stepdown transformer are used to supply the proper current and voltage to the lamp.

In measuring the transmittance of a prism (or window), it is de-
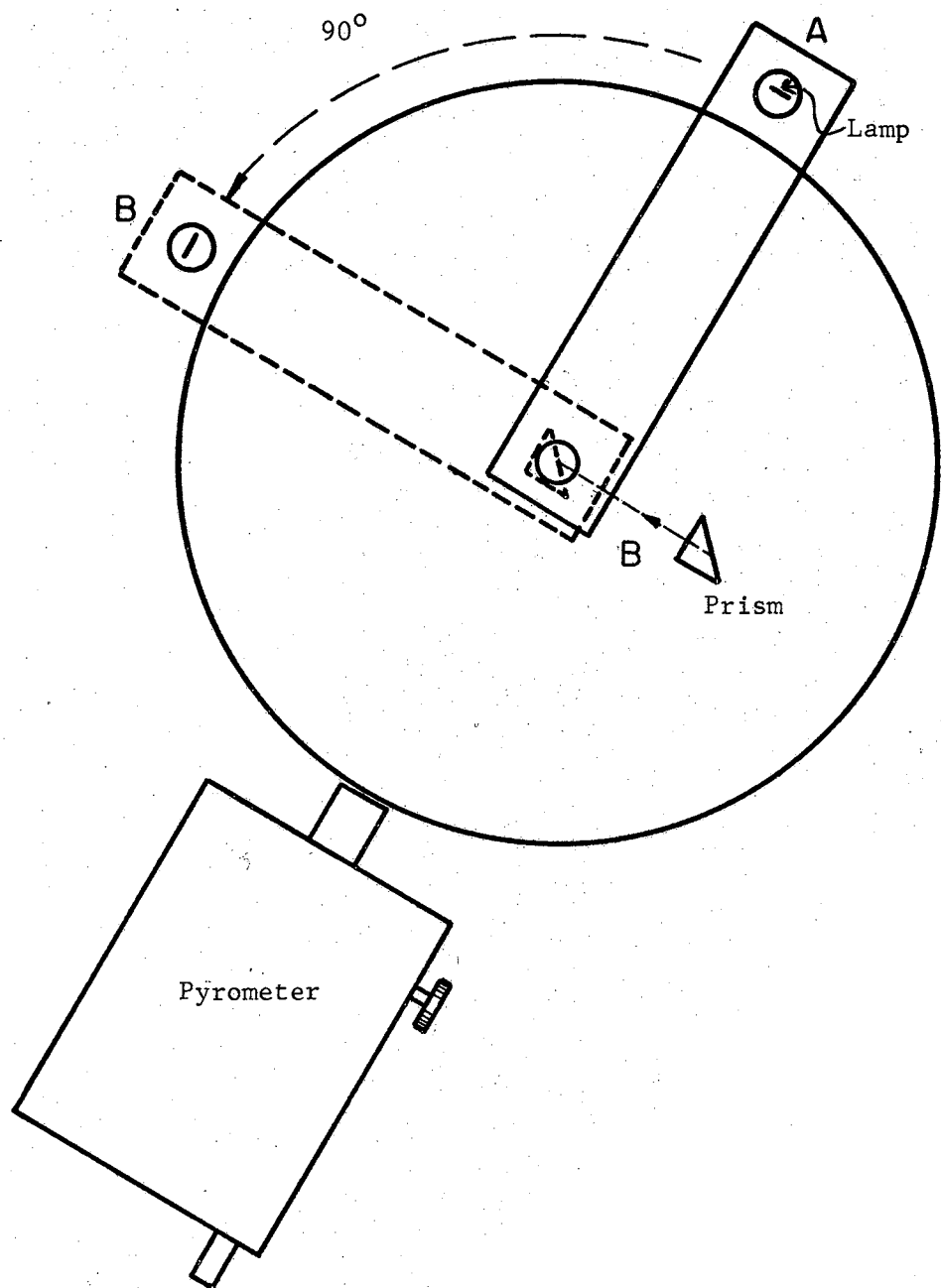
Figure 24. Apparatus Used to Determine Wien's Law Constant for Prisms

sirable to observe exactly the same spot on the tungsten filament with and without the prism between the lamp and the pyrometer. It is also desirable to observe the tungsten filament through the same portion of the lamp tubulation and at the same angle to the tubulation, with and without the prism. With an ordinary, planar quartz window this is easily done, but with a prism the problem becomes quite involved. With the above apparatus, the tungsten strip can be perpendicular to the pyrometer and in the line with the swivel bolt. With the board horizontal and the 90° prism inserted just above the swivel bolt, the lamp filament can be viewed through the prism with the above criteria satisfied (i.e., the same spot on the filament through the same portion of the glass tubulation).

The temperature is measured with an automatic photoelectric "Photomatic" pyrometer manufactured by Pyrometer Instrument Co., Inc., Serial No. A111. This instrument was calibrated at the factory and has been checked in this laboratory against a Leeds and Northrup Catalog No. 8622c manual optical pyrometer. The two agree generally in 10°C at 1200°C. The automatic pyrometer consistently reads 10°C higher than the manual pyrometer. Further plans include recalibration of the photoelectric pyrometer.

Temperature corrections for light transmittance of less than one hundred percent through a window or prism have been tabulated in Appendix C.

CHAPTER IV

EXPERIMENTAL PROCEDURE AND RESULTS

Microbalance Calibration

There are two techniques used to calibrate the microbalance. One involves the addition of known tare weights to the cell end of the microbalance. The other involves addition of a known tare weight to the weight arm via the micrometer screw weight adder.

In the first technique, tare weights are added to the stirrup of the microbalance. These weights are weighed precisely on a Sartorius-Werke semi-microbalance before being added to the microbalance with tweezers. As a tare is added or removed from the stirrup, the current in the coils is manually adjusted to bring the balance back to null. Thus one obtains experimentally current change for various known weight changes on the microbalance. The null position is determined by the position of the light beam (slit image) on the Photopot, which is sensitive to better than $\pm$ 1 μm displacement.

There are several disadvantages to this technique.

(1) This is the only technique that can give one an absolute balance calibration. This is true because it involves weight changes from the end of the balance where weight changes actually occur in the experiment.

(2) Addition of a weight, regardless of how small it may be, usually upsets the balance, which can very easily result in a

change of the null position.

(3)   The brass plate on the end of the balance chamber must be re-
moved so that weights can be added or removed, which makes
the balance susceptible to air currents and the Photopot sus-
ceptible to stray light.

The following technique was finally used to obtain a satisfactory
balance calibration.

(1)   Since the balance does not have a beam arrest, the balance
beam was carefully brought to rest (by manual control of com-
pensating coil current) on the appropriate end rest, and kept
there during addition or removal of a tare weight. This
limited the change in null point because of upsetting the bal-
ance.

(2)   Tare weights were added or removed very carefully with a pair
of ivory tweezers, thus limiting the magnetic attraction be-
tween the metal tweezers and balance magnets which also upsets
the balance.

It should be noted here that the balance null point changed from
time to time if the balance was upset severely. This null point change
was apparently due to twisting of the end stirrups of balance, which did
not come to rest in the same position relative to the balance beam.
Since the saddle rests on a diamond pivot point, rather than a knife
edge, there was no way to limit this twisting except to not jar the
balance.

The second technique for calibrating the balance is to add tare
weights to the weight arm. This is a very convenient procedure. The
weight can be added incrementally and the total displacement of the bal-

ance beam can be limited. This technique is comparable to using a pan arrest on a regular pivot balance. The one severe disadvantage to this technique is that there are unequal lever arms that must be considered to determine the true balance calibration. The advantages are:

(1) The end plates can be in place on the balance chamber.

(2) There is very little beam displacement as the weight is added or removed if the weight adder acts as an end stop 3 to 4 microns off null while the coil current is changed to compensate for this displacement.

(3) The balance can be calibrated in automatic control, if desired.

The reproduceability of the balance calibration is $\pm$ 0.010 mg/mA with the first technique and $\pm$ 0.003 mg/mA with addition of the tare to the weight arm. Over a period of one year, the calibration constant of the balance, determined via addition of a tare to the weight arm, decreased 0.007 mg/mA.

No direct comparison can be made here to Bennett's[17] calibration since all Cunife wire magnets on the balance were resaturated at the onset of this authors work and thus one would expect the balance calibration to change. There _is_ a slow decay of the magnetic field strength of a bar magnet with time, but this appears neglible with the present magnet and coil configuration. The four coils have also been repositioned since Bennett's work. The calibration constant obtained by Bennett[17] was 0.289 mg/mA and the value obtained in this work was 0.265 mg/mA.

Figure 25 shows the calibration curve for the microbalance.

Servosystem Sensitivity
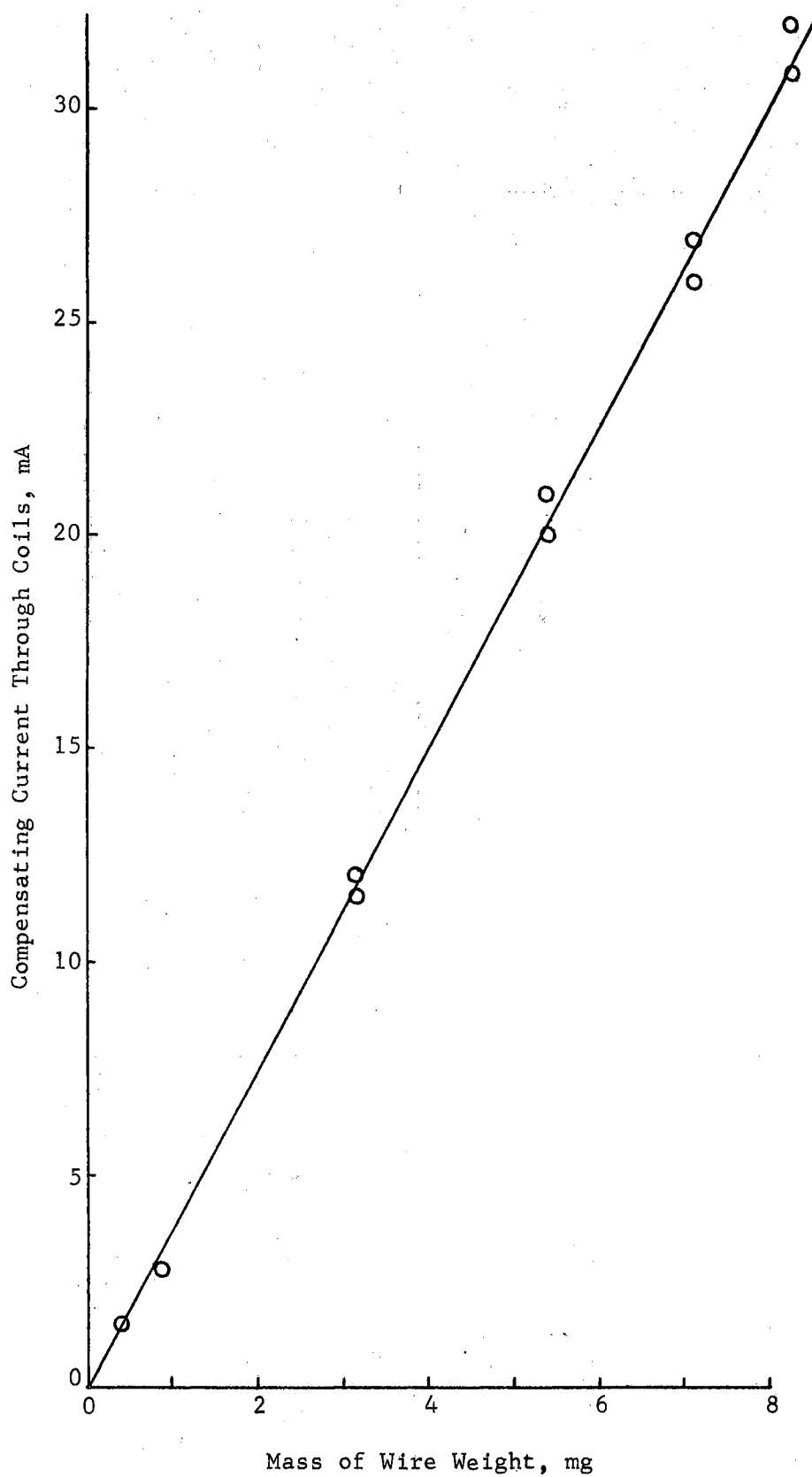
Figure 25. Calibration of Microbalance

Some comments need to be made at this time about the sensitivity

of the automatic control system, which will certainly be the determining

factor in the evaluation of any experimental data in terms of the ac-

curacy of the measurements. These factors should be considered as order

of magnitude factors, since it was impossible to observe balance move-

ment much less than 100 μm (0.004 inches) to more than two significant

figures with the telemicroscope.

As shown in Figure 26, the sensitivity of the microbalance in

micrograms per micrometer movement of the balance is about 2.7 μg/ μm.

There are two methods that one may use to determine the sensitivity

of the servosystem. One can observe the nominal oscillations of the

N.D. output meter or he can observe the nominal oscillation of the cur-

rent through the balance coils.

To determine the servosystem sensitivity by observing the N.D. out-

put, the ratio of N.D. output to balance movement is needed. The ratio

of N.D. output to balance movement may be determined by observing the

N.D. output and the corresponding current change through the coils, and

then multiplying the current change by the coil calibration (0.265

μg/μm) and dividing by the beam sensitivity (2.7 μg/μm).

Doing this, it was determined that 70 μm of balance movement would

cause approximately 0.2 scale division output on the N.D. meter.

With the aid of a microammeter the servosystem was observed to con-

trol to ± 0.2 mV N.D. output. Since 0.2 scale division on the N.D.

meter corresponds to 20.0 mV, this implies that the servosystem controls

within ±0.002 scale division on the N.D. output, or within ± 0.7 μm.

At 2.7 μg/μm sensitivity of the balance, ± 0.7 μm corresponds roughly

to control within ± 1.9 μg.
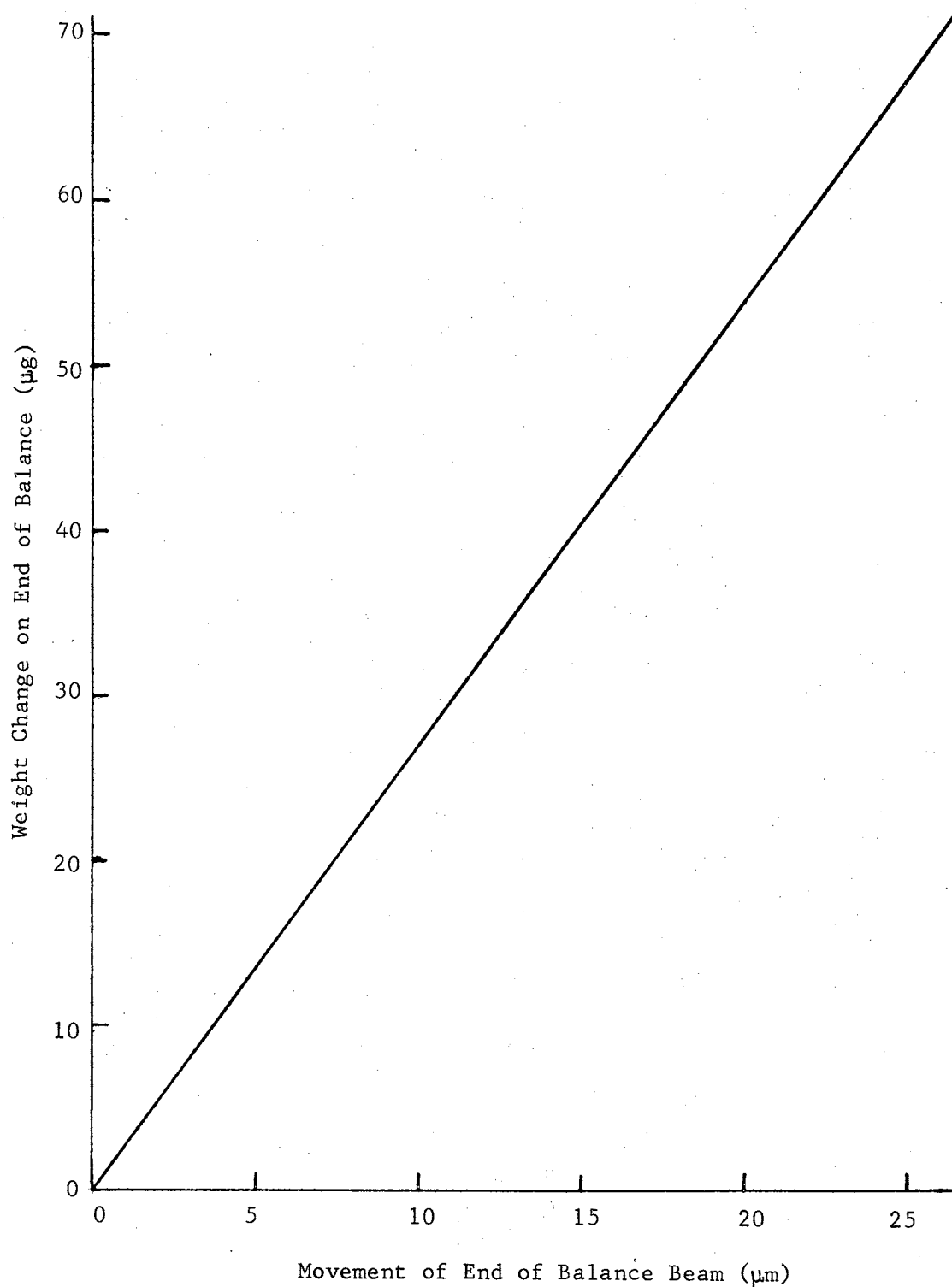
Figure 26. The Experimental Sensitivity of the Microbalance

The easiest way to estimate the sensitivity of the servosystem, if one <u>knows</u> the error detection circuitry is sensitive enough, is to observe the nominal current oscillation in the balance coils. An oscillation of $\pm$ 3 μA has been observed for the microbalance, which would correspond to control within $\pm$ 0.8 μg. A "rough" dynamic control might have oscillations of $\pm$ 5.0 μA or $\pm$ 1.3 μg control.

Weighing Range of VMB-1A

The weighing range over which the microbalance can work is much larger than needed. The coil current has been limited to 50 mA maximum to keep down hystersis in the bar magnet, which will change the magnet strength. This limits the total weighing range of the cell to about 13 milligrams. A 5-milligram weighing range is usually sufficient for a two hour series of vapor pressure and recoil force determinations, usually 20 to 30 determinations. If a large weighing range is needed, 4 tare weights of about 13 milligram equivalent weight may be removed from the weight arm and the solenoid current can be reversed to offer another 13 milligrams. A total of 78 milligrams weight change could be determined without opening the vacuum system.

Operating Procedure

The operating procedure used to obtain optimum control of the Servosystems and to obtain the best experimental data is given in Appendix B.

The tin used in this experiment received no special treatment before use. The graphite cells were baked out at high temperature before initial use. Initially the tin was granular (100 mesh) in form, but

after heating to a high temperature formed a single drop of sample.

Two to three hundred milligrams of sample were normally used. The

following specifications were given by the supplier: (Baker): Sn

99.99% Lot No. 1537.

Auxiliary Determinations

Several questions have arisen as a result of this work.

Some are concerned with pseudo-recoil effects. They are:

1. Are there furnace current-cell interactions?

2. What effect does the residual gas have on the measurements?

3. What effect does light from the furnace have on the Photopot?

4. What effect does decomposition of the furnace have on the cell?

5. What are the resulting pseudo-recoil effects?

The second auxiliary determination is that of determining the ef-

fusion during cooling experimentally and applying this information to

regular recoil measurements.

Pseudo-Recoil Forces

The first indication of a spurious furnace-cell interaction came in

Run 5 which was the first attempt to measure the effusion during cooling

with a double orifice cell. Theoretically, one should see no recoil

force with a double orifice cell when the furnace is cut off, but a very

large recoil was in fact, observed. Run 6, with an empty cell, showed

the apparent recoil force to vary approximately linearily with furnace

current as shown in Figure 27. It seemed apparent that there was some

sort of electromagnetic interaction of the furnace with the balance.

After extensive work, the largest part of this pseudo-recoil force
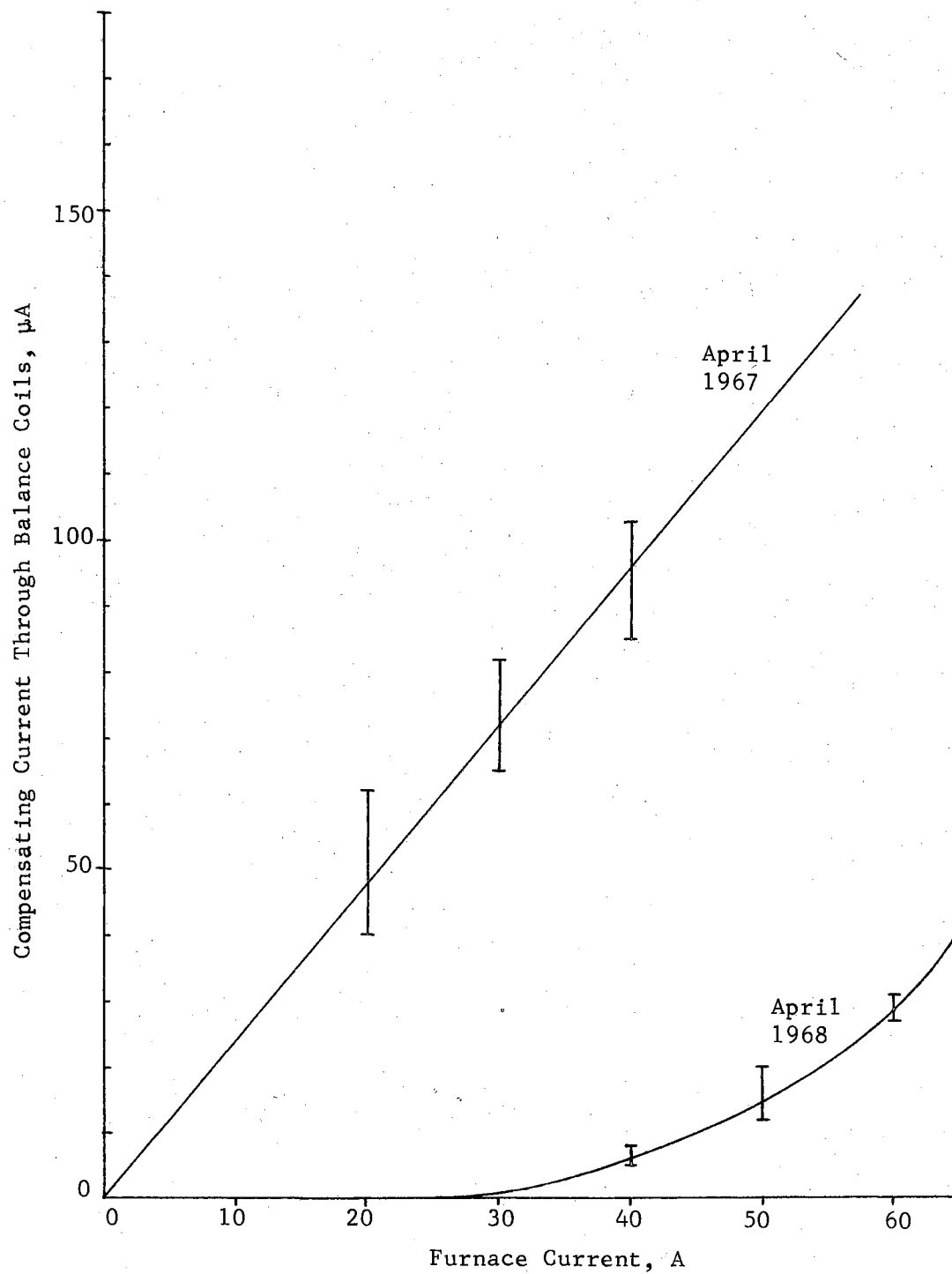
Figure 27. Pseudo-Recoil for the Microbalance

was found to originate primarily from nonsymmetrical furnace leads, furnace vacuum feed-through attachments and furnace power supply leads. The final arrangement shown in Chapter Three has reduced this part of the spurious interactions by a factor of ten or more.

The second source of pseudo-recoil force was found to originate from the residual gas in the system. The author has observed with this experimental apparatus that the control position of the microbalance will change in direct **relation to the system pressure.** This effect was observed with an empty cell _in_ the furnace, _above_ the furnace, or _below_ the furnace. It was _not_ observed when the cell was in the balance chamber. Pressure _changes_ in the furnace chamber of 1.0×10^{-8} bar when the furnace was cut on were detected as apparent weight changes of the cell, and each change was reproducible and reversible. Once the cell had reached operating temperature and the pressure had stabilized, the apparent weight change would not be seen again. One may interpret this effect as just degassing of the cell and furnace. But, one must also consider the remarkable consistency of pressure change and control point change, which point to vacuum "winds" even in the 10^{-8} bar range.

A third source of a psuedo-recoil effect was determined to be caused by light from the furnace reflecting onto the Photopot. With the balance beam, and hence the slit image on the Photopot, locked in position, the output of the Photopot detector circuit changed as the furnace current was changed, if the current was above 30 amperes, i.e., if the furnace temperature was 1000 $^{\circ}$C. The changes were quite reproducible and appeared to be exponential in form. Consequently, the Photopot was shielded as much as feasible from stray light.

These are then the known sources of spurious interactions in this

particular experimental apparatus. They have been dealt with, yet have

probably not been completely eliminated. The effect of the sum total of

these three interactions, and perhaps some other unknown ghosts, are

shown in Figure 27. The pseudo-recoil mass to be described in the

treatment of the data is taken from this figure and is interpreted to be

primarily a function of the current in the furnace elements (i.e., the

temperature of the elements).

Effusion During Cooling

The data shown in Tables IV, V, VI for effusion during cooling have

been determined from a theoretical extrapolation. The details of this

approach are given in Appendix A.

Basically, the calculation amounts to assuming that the effusion

from a cell during cooling is directly proportional to its rate of

effusion at a given temperature. A second assumption here is that any

cell of given geometry will cool at the same rate as another from a

given temperature $\underline{T}$ and that this rate is reproducible.

At a given temperature the first assumption can be rigorously

shown to be true, if the second assumption is true. A great deal of

trouble has been taken to assure that the second assumption is valid.

Thus, using the results of Appendix A.

$$m_{c1}^* / m_{c2}^* \; = \; \dot{g}_1 / \dot{g}_2 \tag{43}$$

where $\underline{m}_{c1}^*$ and $\underline{m}_{c2}^*$ are the actual masses lost during cooling from a given

initial temperature at which $\underline{\dot{g}}_1$ and $\underline{\dot{g}}_2$ are the rates of effusion for

two different cells cooling from the same initial temperature. The

actual mass during cooling $\underline{m}_c^*$ referred to here is the observed effusion

during cooling minus the pseudo-recoil of the balance.

The result of this approach is that one may use a cell with orifices in its sides to measure an apparent effusion during cooling and rate of effusion for various temperatures and furnace currents (pseudo-recoil). Then, the results with this cell, which sees no recoil force because of the position of the orifices, may be used to determine the effusion during cooling from a Miker Cell.

The raw data used in the calculation of $\underline{m}_c$ for the Miker cells is shown in Table II. Cell number 4 was used to obtain this information. Also listed in the table is the pseudo-recoil mass determined with an empty Miker cell under the same conditions of an experimental run.

Temperature Measurement

The temperature of the Miker cell was measured with an optical pyrometer. The pyrometer used was an Automatic Optical Pyrometer Serial No. A111 manufactured by Pyrometer Instrument Company. The detailed procedure of these measurements is given in Appendix B.

It may be noted here that the orifice of the cell appeared to be darker than the cell. Further investigation showed this was possibly caused by reflection of light from the furnace elements, which are at least one hundred degrees hotter than the cell.

The temperature that one measures here is referred to as the observed cell temperature T_o. The correct cell temperature T_c is actually higher because the prism in the pyrometer-cell path does not transmit all the light it receives from the cell.

One determines T_c from T_o by the use of Wiens' Law[*]. A tabulation

---

[*]Chapter III.

TABLE II

EFFUSION DURING COOLING[+]

Run	T °K	Furnace Current (A)	Rate of Effusion (μg/sec)	Apparent Effusion During Cooling (-) μg	Pseudo-Recoil Mass (-) μg	Actual Effusion[*] During Cooling (-) μg
1	1395	40	0.148	2.91	1.58	1.33
2	1395	40	0.148	2.91	1.58	1.33
3	1395	40	0.146	3.44	1.58	1.86
4	1395	40	0.154	2.51	1.58	0.93
5	1425	42	0.280	6.09	1.99	4.10
6	1425	42	0.287	6.62	1.99	4.63
7	1465	44	0.428	12.2	2.38	9.82
8	1465	44	0.428	12.2	2.38	9.82
9	1465	44	0.437	12.7	2.38	10.32
10	1500	46	0.697	22.8	2.78	20.0
11	1500	46	0.693	22.0	2.78	19.2
12	1530	48	1.077	38.9	3.31	35.6
13	1530	48	1.121	33.4	3.31	30.1
14	1560	50	1.536	59.6	3.71	55.9
15	1560	50	1.553	54.3	3.71	50.6

[*]See Appendix A.

[+]Experimental Data for Double Orifice Cell Number 4.

has been made, part of which is given in Appendix C, of ΔT_c (temperature correction) where

$$T_c = T_o + \Delta T_c \qquad (44)$$

for various values of AK (Wien's Law Constant).

The prism used in obtaining the results presented here had an AK value of about $7.0 \times 10^{-6}/{}^\circ K$.

Experimental Results

The experimental results are shown in Tables IV, V and VI. The three tables present vapor pressure data and average molecular weights determined with three different effusion cells.

Cell 1 has a conical orifice with a short cylindrical section at the top of the cone. Cell 1A has the same conical orifice with the cylindrical section shortened to less than 0.002 inches in length. Cell 5 has a standard cylindrical orifice that is long compared to the usual thin cylindrical orifice.

There are several points of interest in a comparison of these tables:

1. All three sets of data were tabulated in the same manner.

2. Cell 1 and cell 1A give nearly the same results for the average molecular weight. (About 40-45 g/mole).

3. Cell 5 gives values for M* only slightly less than that reported by Freeman[39] and Bennett[17] of 90 g/mole $\pm$ 14. The values obtained are significantly larger than those obtained with the conical orifices.

4. At the same temperature, the rate of effusion for cell 1A is at least double that for cell 1, where the only difference in the two

TABLE III

TRANSMISSION PROBABILITIES AND RECOIL FORCE
CORRECTIONS FOR CONICAL ORIFICES[19]

T $(L/r_m)^*$	0° W	30° W	40° W
0.1	0.9523	0.9869	0.9927
0.2	0.9092	0.9761	0.9871
0.4	0.8341	0.9597	0.9790
0.6	0.7711	0.9481	0.9739
0.8	0.7178	0.9396	0.9704
1.0	0.6720	0.9334	0.9681
2.0	0.5142	0.9177	0.9629
4.0	0.3566	0.9095	0.9607
6.0	0.2754	0.9073	0.9603
8.0	0.2253	0.9065	0.9601
10.0	0.1909	0.9060	0.9599

T $(L/r_m)^*$	0° f	30° f	40° f
0.1	0.9683	1.009	1.014
0.2	0.9373	1.016	1.027
0.4	0.8785	1.027	1.047
0.6	0.8247	1.036	1.062
0.8	0.7762	1.043	1.074
1.0	0.7327	1.049	1.084
2.0	0.5725	1.069	1.116
7.0	0.4024	1.091	1.146
6.0	0.3125	1.104	1.162
8.0	0.2564	1.114	1.172
10.0	0.2177	1.121	1.172

$^*r_m$ refers to the smallest radius of the concial orifice.

TABLE IV

VAPOR PRESSURE AND RECOIL FORCE DATA FOR TIN CELL

NUMBER 1 (CONICAL AND CYLINDRICAL ORIFICE)

Run	T_c °K	Rate of Effusion (g) (μg/sec)	Recoil Mass (μg)	Ave. Effusion During Cooling $-(\mu$g)	Ideal Recoil Mass [+] μg	P_K μbar	P_R μbar	M^* g/mole
3	1421	0.227	11.1	3.97	15.1	2.42	3.33	62.8
4	1428	0.225	10.1	3.97	14.0	2.41	3.10	71.5
5	1427	0.230	10.6	3.97	14.5	2.45	3.22	69.0
6	1428	0.225	10.6	3.97	14.5	2.41	3.22	62.9
8	1457	0.358	21.4	9.00	30.4	3.86	6.73	39.0
10	1459	0.362	18.0	9.00	27.0	3.91	5.97	50.9
11	1459	0.388	22.0	9.00	31.0	4.19	6.85	44.5
12	1455	0.371	21.6	9.00	30.7	4.00	6.79	41.2
14	1488	0.605	31.8	16.9	48.8	6.60	10.80	44.3
15	1488	0.613	31.2	16.9	48.3	6.69	10.68	46.6
16	1488	0.605	31.5	16.9	48.6	6.60	10.74	44.8
17	1486	0.587	29.1	16.9	46.2	6.40	10.22	46.6
18	1486	0.578	28.3	16.9	45.4	6.31	10.04	46.8
19	1517	0.927	47.4	30.7	78.1	10.20	17.27	41.4
20	1517	0.944	45.3	30.7	76.0	10.40	16.81	45.4
21	1518	0.944	49.8	30.7	80.5	10.40	17.80	40.5
22	1547	1.46	76.3	49.5	126.	16.19	27.88	40.0
23	1548	1.46	74.9	49.5	125.	16.29	27.58	41.4
24	1576	2.28	118.4	78.1	196.	25.56	43.45	41.1
25	1576	2.08	119.2	78.1	197.	23.34	43.63	34.0

[+]Algebraic sum of the measured recoil mass $\underline{m}_r$ and the mass that effuses during cooling $\underline{m}_c$.   Ave 45.5
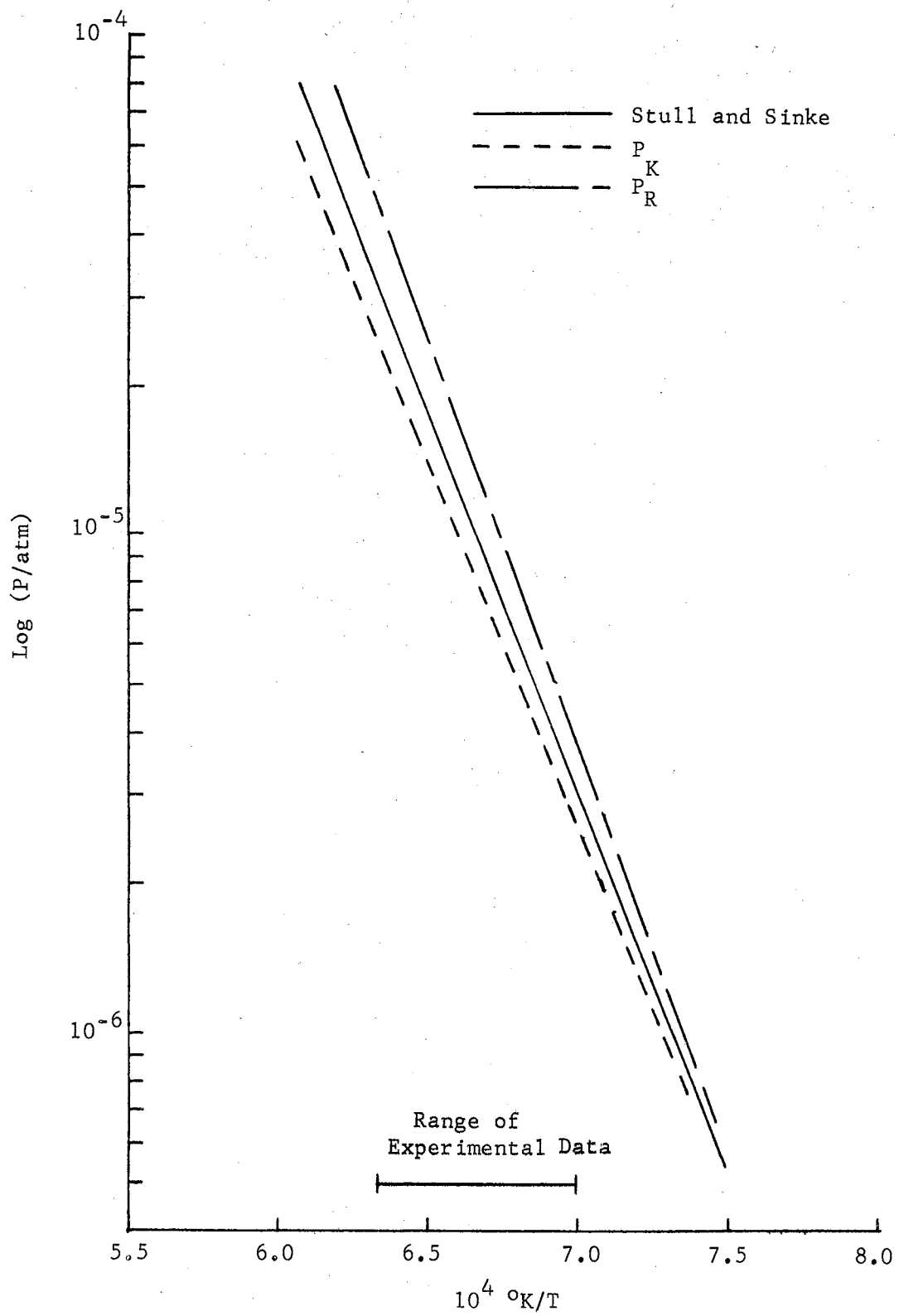
Figure 28. Vapor Pressure of Tin, Cell 1

TABLE V

VAPOR PRESSURE AND RECOIL FORCE DATA FOR SN
CELL 1A (NEAR=IDEAL CONICAL ORIFICE)

Run	T_c °K	Rate of Effusion (g) (µg/sec)	Recoil Mass (µg)	Effusion During Cooling (-µg)	Ideal Recoil Mass[+] (µg)	P_K µbar	P_R µbar	M^* g/Mole
1	1396	0.304	8.87	4.37	13.2	2.39	2.77	88.0
2	1392	0.309	12.2	4.37	16.5	2.42	3.47	57.7
3	1434	0.512	22.4	9.93	32.0	4.06	6.72	43.4
4	1425	0.503	21.2	9.80	31.0	3.98	6.51	44.4
5	1424	0.521	23.3	10.1	33.4	4.12	7.02	40.9
6	1420	0.490	19.9	9.53	29.6	3.87	6.22	46.0
7	1423	0.530	21.3	10.2	31.5	4.19	6.62	40.1
8	1449	0.878	29.7	22.5	52.2	7.01	10.96	40.9
9	1447	0.909	33.4	23.3	56.6	7.25	11.89	37.1
10	1455	0.830	34.2	21.4	55.6	6.63	11.68	38.3
11	1455	0.838	32.3	21.6	53.9	6.71	11.32	41.6
12	1454	0.794	31.1	20.6	51.8	6.35	10.88	40.4
13	1455	0.883	24.2	22.6	56.8	7.06	11.93	41.5
14	1455	0.794	30.7	20.6	51.3	6.35	10.77	41.2
15	1456	0.838	33.9	21.7	55.5	6.71	11.66	39.3
16	1455	0.812	32.3	20.9	53.3	6.49	11.19	39.9
17	1425	0.425	21.8	10.1	32.0	4.16	6.72	45.4
18	1427	0.560	22.6	10.6	33.3	4.44	6.99	47.8
19	1427	0.481	20.1	9.53	29.6	3.81	6.22	44.5
20	1398	0.278	10.6	4.10	14.7	2.18	3.09	59.1

[+]Algebraic sum of the measured recoil mass m_r and the mass that effuses during cooling m_c.　　Ave 45.9
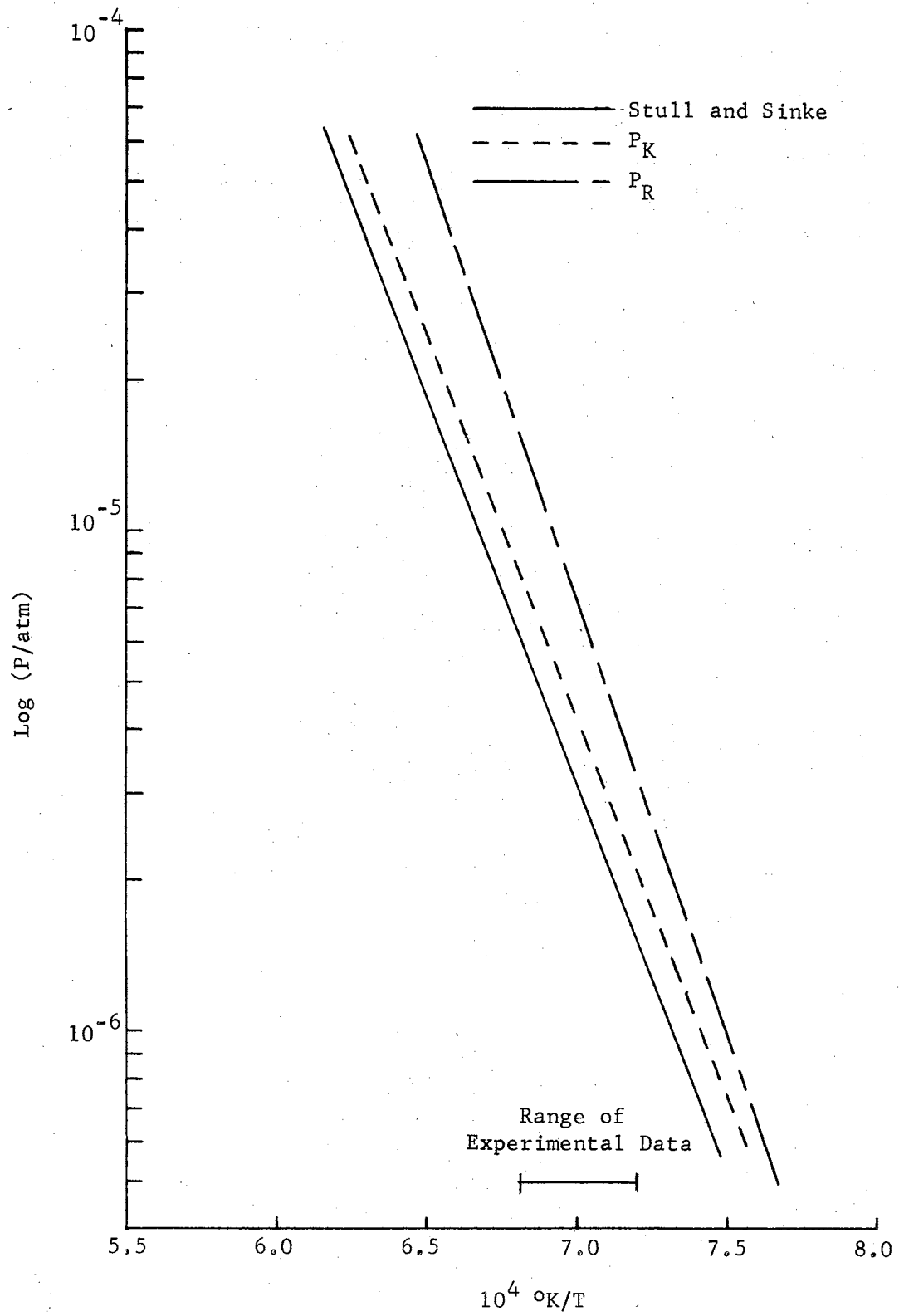
Figure 29. Vapor Pressure of Tin, Cell 1A

TABLE VI

VAPOR PRESSURE AND RECOIL FORCE DATA FOR SN

CELL NUMBER 5, (CYLINDRICAL ORIFICE)

Run	T_c °K	Rate of Effusion (g) (μg/sec)	Recoil Mass (μg)	Effusion During Cooling $-(\mu g)$	Ideal Recoil Mass[+] (μg)	P_K μbar	P_R μbar	M^* g/Mole
1	1498	0.596	15.1	18.8	33.8	12.9	16.0	76.9
2	1498	0.609	17.7	19.1	36.8	13.2	17.5	67.8
3	1498	0.605	17.2	18.9	36.2	13.1	17.2	76.3
4	1500	0.609	15.6	19.1	34.7	13.2	16.5	76.3
9	1498	0.613	13.2	19.2	32.4	13.3	15.4	88.7
10	1500	0.644	14.3	20.0	34.3	14.0	16.3	87.4
11	1500	0.631	15.9	19.7	35.6	13.7	16.9	77.9
12	1501	0.631	16.7	19.7	36.4	13.7	17.3	74.5
13	1503	0.635	15.9	19.9	35.7	13.8	16.9	66.4
14	1532	0.949	27.0	33.5	60.5	20.8	28.7	62.2
15	1530	0.958	26.0	33.8	59.7	21.0	28.3	65.0
16	1531	0.980	24.1	34.4	58.5	21.5	27.8	70.9
17	1533	0.953	24.9	33.6	58.6	20.9	27.8	67.0
18	1536	0.958	26.2	33.8	60.0	21.0	28.5	64.6
19	1468	0.384	9.00	11.1	20.2	8.45	9.59	92.2
20	1470	0.397	10.9	11.5	22.3	8.53	10.6	77.0
21	1471	0.393	9.80	11.4	21.2	8.44	10.1	83.4
22	1475	0.380	15.4	11.1	26.4	8.16	12.5	50.4
23	1471	0.340	10.3	10.2	20.5	7.30	9.73	66.8
24	1470	0.358	15.9	10.6	26.4	7.68	12.5	44.5

[+]Algebraic sum of the measured recoil mass $\underline{m}_r$ and the mass that effuses during cooling $\underline{m}_c$ Ave 71.8
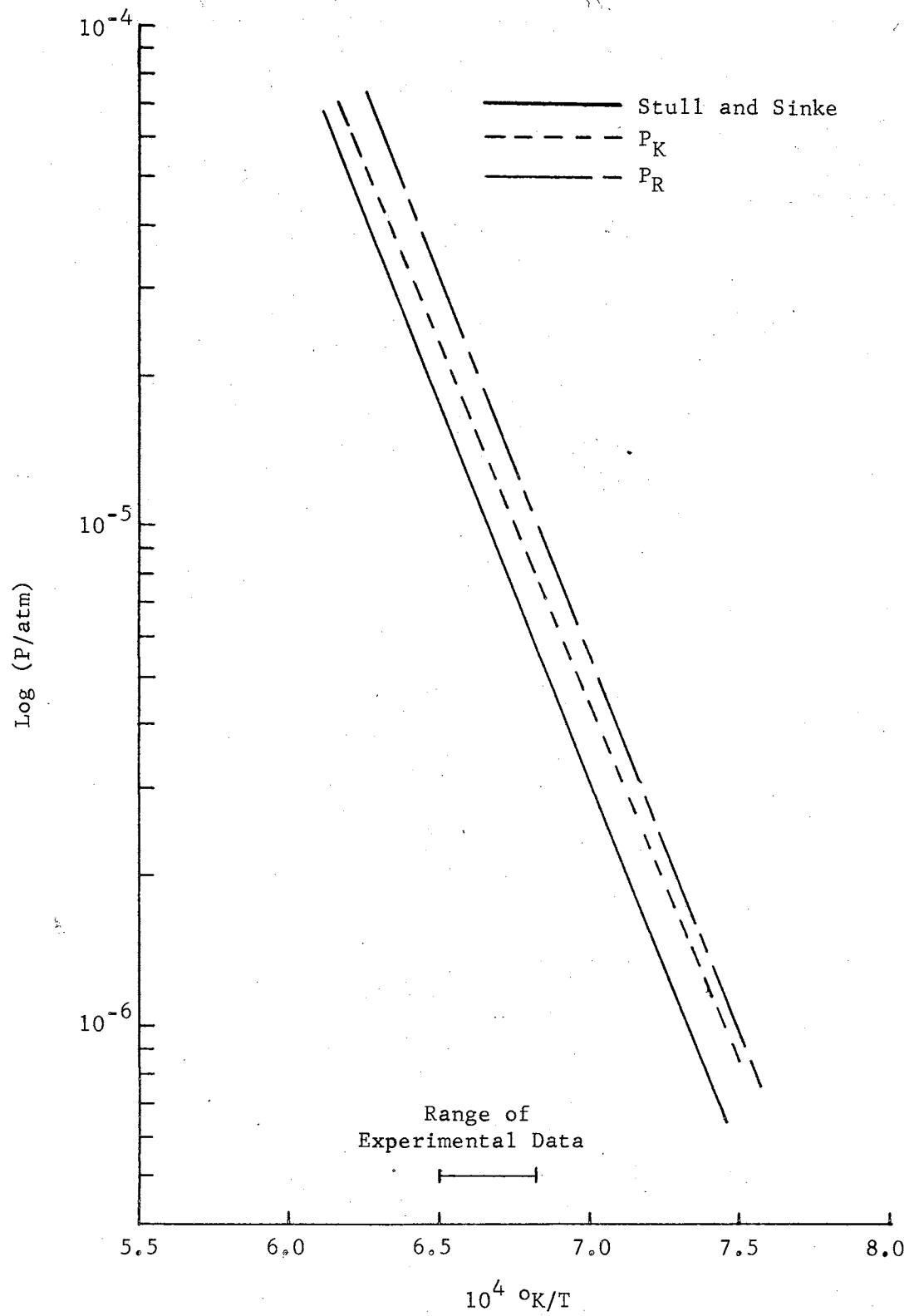
Figure 30. Vapor Pressure of Tin, Cell 5.

cells is a cylindrical section approximately 0.012 inches in length at the top of the conical orifice of cell 1.

5. Correction factors $\underline{f}$ and $\underline{w}$ were taken from Table III which is an excerpt of a recent publication by Freeman[19]. Figures 28, 29 and 30 present conventional Log $\underline{P}_K$ vs. 1/T plots for the three cells. Also included here is the Log $\underline{P}_R$ vs. 1/T plot for comparison purposes. $\underline{P}_K$ was determined in each case by assuming tin vapor to be monatomic.

The tabulated data of Stull and Sinke[40] is used for a comparison in each case.

The least squares solution to each of the plots is:

For cell 1; $\text{Log } P_K = 4.924 - 15045/T$ (45)

For cell 1A; $\text{Log } P_K = 5.567 - 15626/T$ (46)

For cell 5; $\text{Log } P_K = 5.306 - 15291/T.$ (47)

CHAPTER V

INTERPRETATION OF RESULTS

Discussion

Tin was chosen as the material to be studied in this experiment because it was thought to satisfy the requirements of this system. Tin has been shown by mass spectrometric studies[45-47] to be primarily monomeric in nature. It also has the proper vapor pressure in the $1000^{\circ}K$ to $1600^{\circ}K$ tmperature range to be studied by this present mechanical system. Some modifications of the furnace would be required to attain higher temperatures.

Runs were made with a cylindrical orifice in a Miker cell so as to be able to compare the results with the results (Freeman[14]) of other workers using the Torker technique. Also, several runs were made with conical orifices in an attempt to compare the experimental results obtained with conical and cylindrical orifices.

This author has used some nomenclature in this thesis that may be misleading. An "ideal" orifice is an infinitely thin cylindrical orifice. It is this "ideal" orifice that the theory of Chapter II treats. The term "ideal conical" orifice used in parts of this thesis might best be phrased as a "perfect" or "near-perfect" conical orifice. In other words, a "perfect" conical orifice is not an "ideal" orifice, but it is an orifice that is "perfectly" conical from inside to outside.

Cell 5

The average molecular weight of tin determined with the cylindrical orifice cell is 25.1% low (based on monatomic tine of 118.7). This compares well with the work of Freeman[14] and Bennett[17], even though the result is physically impossible if the cell (graphite) itself isn't evaporating appreciably. It should be noted that Freeman[14] used the Torker technique, and that Bennett[17] used a theoretically determined value for $\underline{m}_c$ whereas the empirical approach discussed in Appendix A was used in these calculations. This comparison of results for average molecular weight indicates that there is some validity in the approach used here, at least compared with other work.

The $\underline{P}_k$ values obtained with the cylindrical orifice cell agree very well with compilation of Hultgren[42]. The ΔH^o_s of 71.56 ± 0.32 kcal/mole obtained from the 3rd Law calculation and shown in Table VII are in agreement with $72.2^o \pm 0.50$ kcal/mole from Hultgren and 72.00 kcal/mole from circular 500[43].

There is some discrepancy in the ΔH^o_s of 72.900 kcal/mole calculated from the slope of the log $\underline{P}_k$ plot for cell $\underline{5}$, but very little can be accredited to this because of the relatively narrow temperature range.

Cell 1

Little comment is needed about cell $\underline{1}$. The results of this run are typical of the results obtained in all previous runs. The vapor pressure is low, making ΔH^o_s high. The problem here is that the orifice in this cell is a hybrid between the conical and cylindrical orifices; thus theoretical values for $\underline{f}$ and $\underline{W}$ for neither conical or cylindrical orifices would give one a valid correction for this particular physical

TABLE VII

HEAT OF SUBLIMATION OF TIN FROM RATE

OF EFFUSION DATA, CELL NUMBER 5

T_c °K	G_T^o/T	$(-)fef(g)^*$	$(-)fef(1)^*$	H_{298}^o/T	H_{298}^o
1498	22.39	45.42	20.10	47.71	71.47
1498	22.35	45.42	20.10	47.67	71.41
1498	22.37	45.42	20.10	47.69	71.44
1500	22.35	45.43	20.11	47.67	71.51
1498	22.34	45.42	20.10	47.66	71.40
1500	22.24	45.43	20.11	47.56	71.34
1500	22.28	45.43	20.11	47.60	71.40
1501	22.28	45.43	20.11	47.60	71.45
1503	22.27	45.44	20.12	47.59	71.53
1532	21.45	45.44	20.15	46.74	71.61
1530	21.43	45.54	20.14	46.83	71.65
1531	21.39	45.54	20.14	46.79	71.64
1533	21.44	45.55	20.15	46.84	71.81
1536	21.43	45.56	20.16	46.83	71.93
1468	23.24	45.30	19.97	48.57	71.30
1470	23.24	45.31	19.98	48.57	71.40
1471	23.31	45.32	19.98	48.65	71.56
1475	23.27	45.33	20.00	48.60	71.69
1471	23.53	45.32	19.98	48.87	71.89
1470	24.48	45.31	19.98	48.81	71.75
				Average	71.56
					± 0.32

$(-)fef(g) = -(G_T^o - H_{298}^o)/T$ (g)

$(-)fef(1) = -(G_T^o - H_{298}^o)/T$ (1)

*Hultgren[42]

orifice.

Cell 1A

The average molecular weight of tin determined with cell 1A is 61.4% low, but the values are very consistent. If one throws out the temperatures below $1400^{\circ}K$, the deviation is about $\pm$ 5 g/mole in the remaining seventeen measurements. The data of cell 1 gives results very close to that of cell 1A for molecular weights, as have all previous runs with conical orifices, regardless of the presence or absence of pseudo-recoil effects.

The ΔH_s^o of 74.454 kcal/mole calculated from the slope of the log P_k plot for cell 1A is high compared with the ΔH_s^o of 71.33 $\pm$ 0.52 kcal/mole obtained from the 3rd Law calculation and shown in Table VIII. The ΔH_s^o of 71.33 $\pm$ 0.52 kcal/mole is again in agreement with other compilations[42,43].

Conclusions

There are several discrepancies which remain in this work. While the "perfect" conical orifice (cell 1A) gives apparently reliable values for the rate of effusion of the sample, the recoil pressures appear to be too large by a factor of 1.61 for all the conical orifice runs. There are several possible explanations for this:

(1) The recoil force correction factor for the conical orifice could be too low. The value of 1.09 used in these calculations for cell 1A must be changed to 1.85 to account for the discrepancy. If there is specular reflection[22] occurring in the effusion process, the recoil force correction factor

TABLE VIII

HEAT OF SUBLIMATION OF TIN FROM RATE
OF EFFUSION DATA, CELL NUMBER 1A

T_c °K	G_T^o/T	$(-)fef(g)^*$	$(-)fef(1)^*$	H_{298}^o/T	H_{298}^o
1396	25.75	45.02	19.64	51.13	71.38
1392	25.73	45.01	19.62	51.12	71.16
1434	24.70	45.17	19.81	50.06	71.79
1425	24.74	45.14	19.77	50.11	71.41
1424	24.67	45.13	19.77	50.03	71.24
1420	24.79	45.12	19.75	50.16	71.23
1423	24.63	45.13	19.76	50.00	71.15
1449	23.61	45.23	19.88	48.96	70.94
1447	23.54	45.22	19.87	48.89	70.74
1455	23.72	43.25	19.91	49.06	71.38
1455	23.70	45.25	19.91	49.04	71.35
1454	23.80	45.25	19.90	49.15	71.46
1455	23.60	45.25	19.91	48.94	71.21
1455	23.81	45.25	19.91	49.15	71.51
1456	23.70	45.26	19.91	49.05	71.42
1455	23.76	45.25	19.91	49.10	71.44
1425	24.65	45.14	19.77	50.02	71.28
1427	24.52	45.15	19.78	49.89	71.19
1427	24.83	45.15	19.78	50.20	71.64
1398	25.93	45.03	19.65	51.31	71.73
				Average	71.33
					±0.52

$(-)fef(g) = -(G_T^o - H_{298}^o)/T$ (g)

$(-)fef(1) = -(G_T^o - H_{298}^o)/T$ (1)

*Hultgren[42]

would very likely be larger[41] than 1.09 for the orifice of

cell 1A. The exact change in f if one considers specular

reflection for low incident angle particles rather than

"cosine law" reflection is not known at this time, but a

rough estimate[41] has indicated a change of only + 0.1 to f.

(2) A second possibility is that the technique used to evaluate

m_c and m_r is not valid. This is a very likely possibility,

but the technique used here was the best technique available

when this work was done, in view of the various pseudo-recoil

effects, etc.

(3) The third possibility is that the relationship between the

force of the effusing molecules and the recoil force trans-

ferred to the cell is not properly interpreted. If one looks

at the equation for the recoil pressure in terms of the force

of the effusing molecules (i.e., the force they would exert

if they were to impinge and condense on a target)

$$P_R = 2 F_m/a \tag{48}$$

where F_m is the force of the effusing molecules, P_R is the

recoil pressure, and a is the area of the orifice, an impor-

tant observation can be made. Pressure is defined[21] as the

force imparted to a surface per unit area. But here, we have

$P = 2 F_m/a$. Where does the factor of 2 come from? This fac-

tor is legitimate because we are talking about the force F_m

these molecules would impart to a surface, were they just to

impinge on the surface. But, from kinetic molecular theory[21],

the pressure includes the force exerted by particles reflect-

ing from the surface, thus the factor of 2.

The question now arises, "How does one relate the force of the effusing molecules F_m to the recoil force given to the cell F_c?" First, one must realize that there is no force exerted on the Miker cell by the effusing molecules, only because of the effusing molecules. The vertical force exerted upward on the Miker cell because of the effusing molecules is the result of molecules impinging on and reflecting from an area a (equal to the orifice area) on the wall inside the Miker cell and opposite the orifice, (i.e., $F_c = 2F_m$). There is also some minor force exerted by molecules impinging on the inside of the orifice and reflecting with either "cosine" or "specular" distribution.

F_c is determined as the apparent mass change of the cell under the acceleration of gravity that is ideally observed when effusion is stopped by cooling the cell instantaneously, i.e., $F_c = m_i g$.

Thus, equation (48) may be restated as

$$P_R = 2 F_m/a = F_c/a = m_i g/a \qquad (49)$$

The most deceptive part of the derivation is the assumption that force is transferred to the Miker cell by the effusing molecules, not because of the effusing molecules.

It is interesting to note that if one uses the Knudsen pressures P_K, which seem to agree with the results of other workers, to determine the recoil force on, and then the corresponding "recoil mass" of, the cell using an equation from basic theory of rocketry "propulsion",[44]

$$F_R = P_R \, af, \qquad (50)$$

one can predict the observed recoil mass within 10% for cell $\underline{1A}$ and within 25% for cell $\underline{5}$.

Another observation can now be made, with hope that someday some researcher will pursue the problem.

In comparing $\overset{\circ}{\underline{g}}_1$ for cell $\underline{1}$ and $\overset{\bullet}{\underline{g}}_{1A}$ for cell $\underline{1A}$, one sees that $\overset{\bullet}{\underline{g}}_1 = \frac{1}{2} \underline{g}_{1A}$ at a similar temperature. Both cells have essentially the same orifice areas, since cell $\underline{1A}$ is just cell $\underline{1}$ with the orifice sanded down (i.e., $\underline{a}_1 = \underline{a}_{1A}$). The transmission probabilities for cell $\underline{1}$ are: $\underline{W} = 0.77$ for cylindrical portion of orifice ($L/r = 0.61$); $\underline{W} = 0.916$ for conical portion of orifice; for cell $\underline{1A}$, $\underline{W} = 0.916$. Since the areas of the orifices are essentially identical, one might expect from the observed rates of effusion ($\underline{g}_1 = \frac{1}{2} \underline{g}_{1A}$) that the transmission pro-bability of cell $\underline{1}$ should be one-half that of cell $\underline{1A}$. This problem can be stated forthrightly: theoretical correction factors ($\underline{f}$ and $\underline{W}$) are available for conical and cylindrical orifices, but neither of these orifices is practical, especially for graphite cells. Cylindrical orifices must be very short ($L/r = 0.2$) to have a reasonably valid $\underline{W}$[22]. This is rather difficult to achieve with graphite. Conical ori-fices must have perfectly sharp (0.001-inch) edges at the top of the cone for the W's to be correct. This too is rather difficult to ach-ieve. It seems to this author that the orifice of cell $\underline{1}$ is a very useful one, especially when using graphite. It would also be an easy orifice to describe mathematically.

It appears that the most difficult task in effusion studies is to fabricate a perfect orifice so that the theoretical $\underline{f}$'s and $\underline{W}$'s will apply. Results with cell $\underline{1}$ and $\underline{1A}$ have shown that one of the most

critical requirements in the calculations is that the <u>orifice</u> fit the theoretical <u>model</u>. Thus, one very apparent conclusion from this study is the praticality and need for correction factors for an orifice, such as that in cell <u>1</u>, that is not perfectly conical or cylindrical but a hybrid. These factors would be useful for cells fabricated from non-metallic materials that exist as densely packed, minute crystals that defy fabrication of the sharp, well-defined edges which are needed in perfectly conical or cylindrical orifices.

Evaluation of the Miker Technique

There are several advantages:

1. Rate of effusion and recoil force are determined essentially simultaneously <u>with the same detector</u>, i.e., the microbalance.

2. A single Miker run consists of a continuous null determination (automatic balance control), which provides continuous confirmation of the rate of effusion. A knudsen determination with a conventional cell, on the other hand employs only the initial and final weight of the cell to determine the rate of effusion, and any deviation from this "average" rate of effusion during the run is never detected.

3. Errors in balance calibration and orifice area measurement cancel in the calculation of molecular weight of the vapor since it is the <u>ratio</u> of rate of effusion to recoil force which is required.

4. Measurements of rate of effusion and of recoil force can be made rapidly and over a wide temperature range without intermittent opening of the vacuum system.

5. The Miker cell serves as an excellent black body for pyrometric determinations of temperature.

6. The orifice is located "within the cell", which should minimize cold orifice problems.

7. Effusion downward, away from the microbalance, minimizes difficulties with condensation on suspension wires.

8. Temperature gradients should be minimized by the cylindrical symmetry of the Miker cell, coupled with the cylindrical resistance heating element.

The apparent disadvantages of the technique are:

1. Furnace current, vacuum "winds", and stray light in the vacuum system appear to affect the recoil measurements severely and must be carefully defined or eliminated.

2. With the above effects tempered as much as possible, the mass change attributable to effusion during cooling $\underline{m}_c$ is a rather large part of the ideal "recoil mass." The furnace <u>can</u> cool over one hundred degrees in six to ten seconds and such rapid cooling would minimize $\underline{m}_c$, but the accompanying rapid decrease in the furnace current "upsets" the microbalance.

3. The transmission probability $\underline{W}$ and recoil force correction factor $\underline{f}$ have not been checked experimentally for conical orifices at high temperature. Erbar[20] has done angular distribution studies on conical orifices at room temperature and has seen some rather interesting effects.

Automation of the microbalance, while presenting many problems[*],

---

[*]Chapter III

has taken some of the human error out of the measurements. As can be seen in Tables VI, VII, and VIII, the experimental data is in general extremely consistent for a given cell. One might expect then that the largest descrepancy between the three runs, since they were all done using similar techniques, would be $\underline{f}$ and $\underline{W}$.

The large apparent error in the value obtained for $\underline{M}^*$ with the conical orifice cell might be thought to lie in the determination of the factor $\underline{m}_c$ as postulated by Bennett[17]. However, in view of the inconsistency of the results of the conical and cylindrical orifices, and of an evaluation of the Technique used to determine $\underline{m}_c$ and then $\underline{M}^{*\dagger}$, it is believed by this author that the largest source of error lies elsewhere.

<center>Suggestions for Future Work</center>

Future work with the Miker Technique should be divided into two areas: (1) vapor pressure measurements extended to other systems; (2) continued modification and development in the experimental technique.

Measurements of rate of effusion appear to be limited only by the availability of the proper container materials. This is only a technical problem that will perhaps be resolved with time. These measurements are not affected by pseudo-recoil effects or effusion during cooling and can thus be determined without knowledge of these effects.

There are a couple of suggested areas of work here:

1. Cells could perhaps be stamped from some thin sheet metal

(0.001-inch molybdenum or tungsten or tantalum). Metal cells

$\dagger$
See Appendix A

that are inert and lightweight might help to eliminate diffus-
ion through the cell wall, and one would certainly be able to
fabricate a more nearly perfect orifice.

2. Theoretical work on the determination of f and W for hybrid
conical-cylindrical orifices would be very helpful, especially
if graphite or other non-metallic cell material (such as boron
nitride) is to be used.

In the modification and development of the experimental apparatus
and technique, there are several suggestions:

1. A triple-orifice cell should perhaps be used to determine the
effusion during cooling as a check of the double-orifice cell.
The double orifice cell is arranged such that there is an ori-
fice on the opposite wall from an orifice, rather than a solid
wall. It is not known if this affects the rate of effusion
from the cell appreciably.

2. The CAT and null detector could be replaced by solid state
operational amplifiers, which should improve the stability of
the control system.

3. More work needs to be done in comparing f and W for conical and
cylindrical orifices using different cell materials. There
definitely appears to be a discrepancy in at least one of these
correction factors.

SELECTED BIBLIOGRAPHY

1. Gilles, P. W. in "The Characterization of High Temperature Vapors, "J. L. Margrave, Editor, John Wiley and Sons, Inc., New York (1967).

2. Beckett, C. W., in "The Characterization of High Temperature Vapors, "J. L. Margrave, Editor, John Wiley and Sons, Inc., New York (1967).

3. Union Carbide Corporation, Carbon Products Division, P.O. Box 22127, Houston, Texas, 77027.

4. Knudsen, M., Ann. d. Physik. 6, 129 (1930).

5. Knudsen, M., Ann. d. Physik. 31, 205 (1910).

6. Knudsen, M., Ann. d. Physik. 31, 633 (1910).

7. Carlson, K. D., in "The Characterization of High Temperature Vapors, "J. L. Margrave, Editor, John Wiley and Sons, Inc., New York (1967).

8. Langmuir, I., Phys. Rev. 2, 329 (1913).

9. Paule, R. C. and Margrave, J. L., in "The Characterization of High Temperature Vapors," J. L. Margrave, Editor, John Wiley and Sons, Inc., New York (1967).

10. Freeman, R. D., in "The Characterization of High Temperature Vapors," J. L. Margrave, Editor, John Wiley and Sons, Inc., New York (1967).

11. Grimley, R. T., in "The Characterization of High Temperature Vapors," J. L. Margrave, Editor, John Wiley and Sons, Inc., New York (1967).

12. Volmer, M., Z. Physik. Chem., Bodenstein Festband, 863 (1931).

13. Sheer, M. D., J. Phys. Chem. 61, 1184 (1957).

14. Freeman, R. D., Ph.D. Thesis, Purdue University (1954).

15. Meschi, D. J. and Searcy, A. W., J. Phys. Chem. 63, 1175 (1959).

16. Margrave, J. L., Editor, "The Characterization of High Temperature Vapors," John Wiley and Sons, New York (1967).

SELECTED BIBLIOGRAPHY (Continued)

17. Bennett, J. E., Ph.D. Thesis, Oklahoma State University (1965).

18. Edwards, Ph.D. Thesis, Oklahoma State University (1964).

19. Freeman, R. D., "Molecular Flow and the Effusion Process in the Measurement of Vapor Pressures," Technical Documentary Report ASD-TDR-63-754, Pt. III (1967).

20. Erbar, R., Ph.D. Thesis, Oklahoma State University, to be published.

21. Kennard, E. H., "Kinetic Theory of Gases," McGraw-Hill Book Company, Inc., New York (1938).

22. Wang and Wahlbeck, to be published, J. Chem. Phys.

23. Freeman, R. D., "Molecular Flow and the Effusion Process in the Measurement of Vapor Pressures," Technical Documentary Report ASD-TDR-63-754, Part II (1965).

24. Silicontrol Gate Drive, Sprague Electric Co., Special Components Division, North Adams, Massachusetts, 01248.

25. Gulbransen, E. A., in "Surface Studies with the Vacuum Microbalance: High Temperature Reactions," Advances in Catalysis, Vol. V (W. G. Frankenburg, et. al., ed.) Academic Press, New York 1953, pp. 119-175.

26. Winterbottom, W. L. and Hirth, J. P., J. Chem. Phys. 37, 784 (1962).

27. Stott, V., "Collected Researches," Vol. XXIV, Standards of the National Physical Laboratory, London.

28. Walker, R. F. in "Vacuum Microbalance Techniques," Vol. 1, (M. J. Katz, ed.) Plenum Press, New York (1961).

29. Gulbransen, E. A. and Andrew, K. F., Vacuum Microbalance Techniques, Vol. 2, (R. F. Walker, ed.), Plenum Press, New York (1962).

30. Simons, Shierrer and Ritter, Rev. Sci. Instr. 24, 36 (1953).

31. Gerritsen, A. N. and Damon, D. H., Rev. Sci. Instr. 33, 301 (1962).

32. Honig, J. M. and Czanderna, A. W., Anal. Chem. 29, 1026 (1957).

33. Cochran, C. N., in "Vacuum Techniques," Vol. 1, (M. J. Katz, ed.) Plenum Press, New York (1961).

34. Prosen, E. J. (Private Communication).

35. Rosenthal, L. A., Rev. Sci. Instr. 36, 1329 (1965).

36. Laver, Lesnick, and Matson, "Servomechanism Fundamentals," 2nd Edition, McGraw-Hill Book Company, Inc., New York (1960).

37. Photopot, Giannini Controls Corporation, Sales Engineering Office, 6170 Sherry Lane, Dallas, Texas.

38. Tomlinson, H. L. Master Thesis, Oklahoma State University (1964).

39. Freeman, R. D., M.S. Thesis, Purdue University (1952).

40. Stull, K. R. and Sinke, G. C., "Thermodynamic Properties of the Elements," American Chemical Society Advances in Chemistry Series No. 18, Washington (1956).

41. Wang, K. C., Private Communication.

42. Hultgren, R., Orr, R. L., Anderson, P.D., and Kelley, K. L., "Selected Values of Thermodynamic Properties of Metals," John Wiley & Sons, Inc., New York (1963).

43. Circular 500, National Bureau of Standards (1952).

44. Hill, P. G., and Peterson, C. R., "Mechanics and Thermodynamics of Propulsion," Addison-Wesley Publishing Company, Inc., New York (1965).

45. Honig, R. E., J. Chem. Phys. 21, 573 (1953).

46. Brewer, L., "The Chemistry and Metallurgy of Miscellaneous Materials," Mc-Graw Hill Book Company, Inc., New York (1950).

47. Hildenbrand, D. L., Aeronutronic Report No. U-1497, Contract AF 04(611)-8523, 1961.

APPENDICES

APPENDIX A

EFFUSION DURING COOLING

In the usual Knudsen equation, which we write in differential form:

$$dw = aW(M/2\pi R)^{\frac{1}{2}} P_K T^{-\frac{1}{2}} dt \qquad (50)$$

$\underline{dw}$ is the mass of vapor which effuses in time $\underline{dt}$ from a Knudsen cell which has an orifice with area $\underline{a}$ and transmission probability $\underline{W}$, and in which the vapor is at pressure $\underline{P}$ and temperature $\underline{T}$. While the cell is cooling, the temperature $\underline{T}$ is a function of the time: $\underline{T} = g(t)$; conversely, this relation may be expressed by $t = f(T)$, from which

$$dt = f'(T)dT \qquad (51)$$

If we assume that equilibrium between vapor and condensed phase is maintained during cooling, the vapor/dissociation pressure $\underline{P}$ is conveniently related to the temperature by the integrated Clausius-Clapeyron equation, $\ln\underline{P} = \underline{C}-(\underline{B}/\underline{T})$, which we write in exponential form

$$P = Ae^{-B/T} \qquad (52)$$

Substituting the relations into the Knudsen equation,

$$dw = aW(M/2\pi R)^{\frac{1}{2}} Ae^{-B/T} T^{-\frac{1}{2}} f'(T)dT \qquad (53)$$

Thus, one needs only to define $f'(T)$ to be able to calculate the effusion during cooling for a material.

This is, of course, a very difficult task. The rate of cooling of a cell depends upon things such as the heat capacity of the cell and

118

furnace, the rate at which power is cut in the furnace, the heat capacity of the sample, the given masses, heat loss by conduction, heat loss by radiation, etc. Thus, it is very difficult to determine a function that explicity covers all of the factors.

The most simple approach to the problem is to assume cooling by either conduction or radiation alone. Freeman[23] has treated both of these approaches. In the treatment of the cooling of the cell by radiation only, the cooling rate is determined by the familiar T^4 relation.

$$dT/dt = -k_r(T^4 - T_f^4) \tag{54}$$

where $\underline{k}_r$ is the cooling constant, $\underline{T}$ is the temperature at time $\underline{t}$, and $\underline{T}_f$ the final temperature.

From equations (54) and (51) it follows that

$$f'(T) = -1/ k_r(T^4 - T_f^4) \tag{55}$$

which when substituted into equation (53) yields

$$w_r = (-)(aWA/k_r)(M/2\pi R)^{\frac{1}{2}} f(u) \tag{56}$$

where $f(u) = e^{-B/T} T^{-\frac{1}{2}}(T^4 - T_f^4)^{-1} dT$.

The ratio of the effusion during cooling of one cell to the effusion during cooling of a second cell with the same sample is

$$w_{r_1}/ w_{r_2} = \frac{(a_1 W_1/ k_{r_1}) f(u_1)}{(a_2 W_2/ k_{r_2}) f(u_2)} \tag{57}$$

From the standard Knudsen equation, the ratio of the rates of effusion for two different cells containing the same sample is

$$\mathring{g}_1/\mathring{g}_2 = \frac{a_1 W_1 P_1 T_1^{\frac{1}{2}}}{a_2 W_2 P_2 T_2^{\frac{1}{2}}} \tag{58}$$

Solving equation (58) for the ratio $(a_1 W_1/a_2 W_2)$ and substituting into equation (57), one gets

$$\frac{w_{r_1}}{w_{r_2}} = \frac{\mathring{g}_1}{\mathring{g}_2} \quad \frac{P_2}{P_1} \quad \frac{T_1}{T_2}^{\frac{1}{2}} \quad \frac{k_{r_2}}{k_{r_1}} \quad \frac{f(u_1)}{f(u_2)} \tag{59}$$

One now makes the substitution in notation $w_{r_1} = m_{c1}$ to correspond to the notation used in this thesis. If one now assumes that: (1) the cells cool at the same rate, $k_{r1} \cong k_{r2}$, by a similar mechanism, $f(u_1) = f(u_2)$; (2) the cells have the same initial temperature, $T_1 = T_2$, and samples, $P_1 = P_2$; then equation 59 reduces to

$$m_{c1}/m_{c2} = \mathring{g}_1/\mathring{g}_2 \, . \tag{60}$$

This same result can be obtained by assuming that the cell cools by conduction alone and is thus not limited to cooling by radiation only.

As indicated in Figure 31 there is a pseudo-recoil effect (m_{PR}) that enters into this calculation. As indicated in the figure,

$$m_c^* = m_c - m_{PR} \tag{61}$$

$$m_r^* = m_r + m_{PR} \tag{62}$$

and, $\quad m_i = m_c^* + m_r^* = m_c + m_r \tag{63}$

where the asterisk refers to the mass of effusion during cooling and the recoil mass, both corrected for the pseudo-recoil effect. One has to
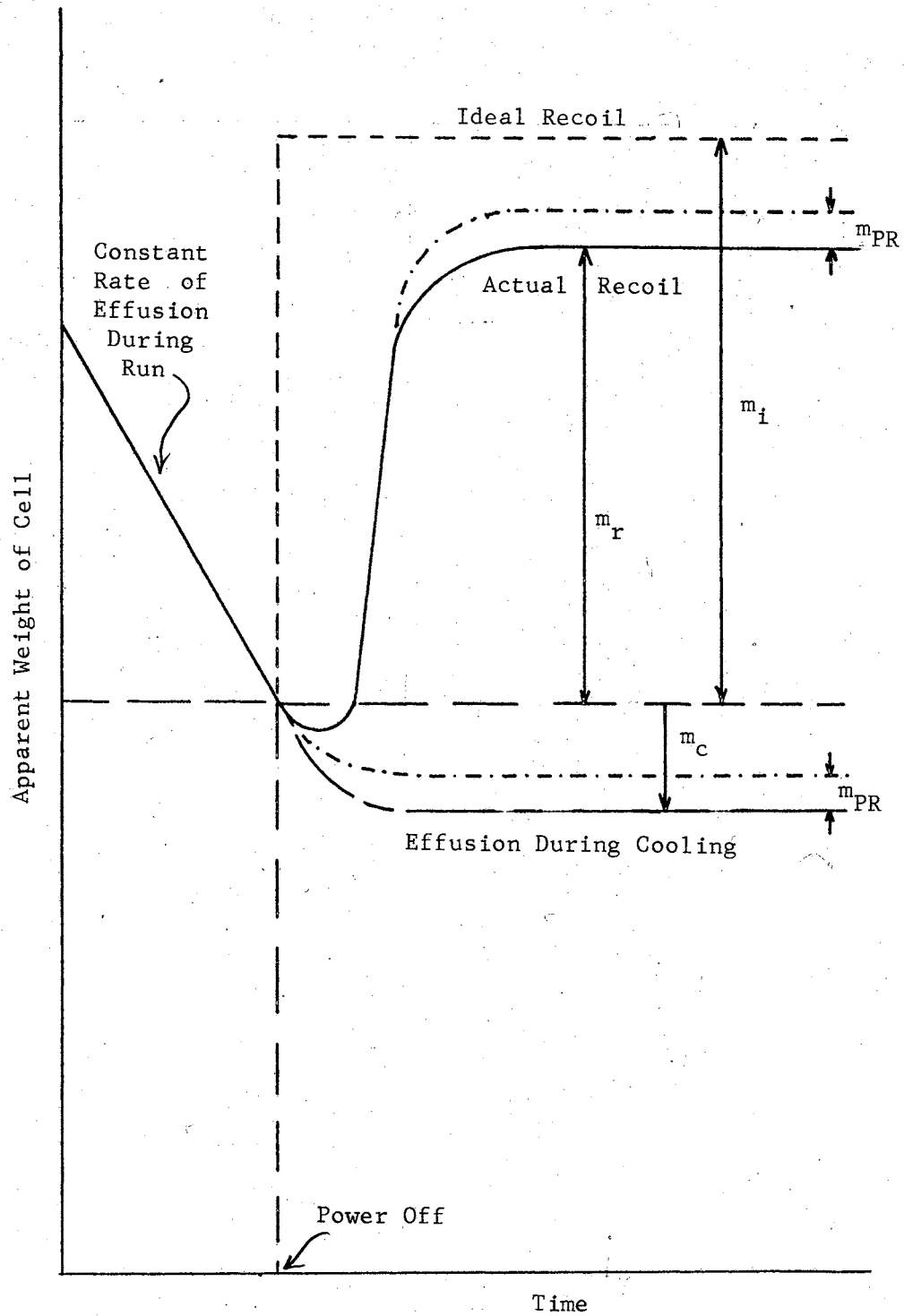
Figure 31. The Effect of the Pseudo-Recoil on the Actual
Recoil and Effusion During Cooling

use values of m_c^*, not m_c, for extrapolation of effusion during cooling from one cell to another.

It is also important to note that m_i is the algebraic difference of m_c and m_r, so that a base line could be chosen at any time before the cell begins to cool and one could determine $\underline{m}_i$ without having values of $\underline{m}_c$ and $\underline{m}_r$ which represent "reality". The only restriction here is that the experimenter be consistent in all of his measurements. This author verified this in his initial experimental runs.

Since the cell will never cool instantaneously at power cut off, it is perhaps improper to speak of $\underline{m}_c$ as the actual mass during cooling but simply the apparent mass change after some time $\underline{t}_o$ if one uses a double orifice effusion cell. The same argument applies for $\underline{m}_r$ with an inverted orifice cell. The only truly significant value is the algebraic difference between these two, $\underline{m}_i$, for an inverted effusion cell.

APPENDIX B

GENERAL EXPERIMENTAL PROCEDURE

Preliminary Work

1. Load cell with sample.

2. Hang from balance.

3. Tare balance with wire weights.

4. Check stirrups, light slit, free movement, etc.

5. Close vacuum system.

6. Begin roughing pump.

7. Begin oil diffusion pump (50 ubar).

Bake Out

1. Pump down to at least the 10^{-8} bar range.

2. Turn water on to all cooling coils.

3. Turn on furnace power supply and cooling fan.

4. Begin bake out of the cell.

   a. Turn furnace on to 10-15 amps.

   b. When pressure returns to 10^{-8} bar range, turn current up to 20-25 amps.

   c. Again, when the pressure is in 10^{-8} bar range, turn current up to 30-35 amps and leave at least two to three hours.

   d. Bake out may continue at 40 amps if the system pressure still flucuates as the furnace is cut on and off. Fifty or sixty

123

amps may be desirable for short periods of time.

Preparation for Experimental Run

1. The servosystem should be left on at all times or at least twelve hours before a run.

2. Liquid nitrogen should be used in all runs so the system pressure will remain low.

3. The automatic pyrometer should be cut on at least thirty minutes before a run.

4. The following procedure may be used to align the pyrometer.

   a. The furnace should be at 30-35 amps.

   b. Open the shutter in the bottom of the furnace chamber.

   c. With the pyrometer telescope on low power, position the telescope so that the bottom of the Miker cell is in full view.

   d. One should be careful not to leave the shutter open too long because of deposition of sample on the prism window.

   e. The black dot in the eyepiece of the pyrometer telescope should should be positioned near the orifice of the cell. At $8\frac{1}{2}$ inches from the cell, the effective dot size is about 0.022 inches in diameter, which makes it smaller than the 0.040 inch orifice.

   f. Switch the pyrometer to high magnification and refocus the telescope on the edge of the cell. Turn the dot back to the orifice of the cell.

   g. Close the shutter, zero the pyrometer controller periodically, and one is prepared to make temperature measurements of the cell.

5. The final step in preparing for a run is to put the microbalance in-
    to automatic control. The following procedure may be used.

    a. The fan on the null detector (N.D.) should be cut on at least
        thirty minutes before "Auto" control is used to allow the N.D.
        to equilibrate.

    b. After equilibration, the following procedure may be used to
        zero the N.D. (The zero should be checked every 30 minutes or
        so.)

        1. Switch the N.D. input to the shorted position.

        2. Make sure the N.D. is on its linear scale.

        3. Zero the instrument roughly using the N.D. meter and the
            zero adjust knob on the instrument.

        4. Switch the auziliary microammeter in parallel with N.D.
            meter and re-zero the instrument.

        5. Switch the microammeter out of the N.D. output circuitry.

        6. Switch the N.D. back into the servo-loop and continue the
            run. Care should be taken never to drive the N.D. output
            meter to its limits, since this tends to polarize the
            electrolytic capacitors in the detector, thus causing some
            drift in the instrument.

    c. The Photopot lamp should be on five to ten minutes in advance
        to equilibrate. Both ports on the microbalance chamber must be
        covered.

    d. The damping coil should be turned on to about 10 Vac.

    e. With the solenoid selector switch in the "4" (four coils) posi-
        tion, the Photopot bridge voltage on maximum, the N.D. on a
        sensitivity on 2.00 in the linear position, and the lamp current

at 4.8 to 5.0 amps, the servo-system is ready for transfer to "Auto" control.

f. The C.A.T. is adjusted manually to zero the N.D. meter, and then switched from "Man" to "Auto". The optimum C.A.T. settings are: Rate time, 0.0-0.5; Reset, 1-20 (depending on the rate of effusion); and Proportional Band, 100-150 (depending on viscous damping).

g. It takes several minutes for the servo-system to stabilize. If it does not, increasing the proportional band, decreasing the reset, or decreasing the Photopot bridge voltage will help overcome the problem. The later two suggested changes are the best alternatives.

h. Once the Servosystem is operating smoothly, one is ready to make the experimental measurements.

Procedure Used to Obtain Experimental Data

1. A Sargent TR recorder is used to record the needed information.

    a. This recorder is used to measure the potential across a 100 ohm standard resistor which is in series with the compensating coils of the micro-balance; hence, the recording gives a direct measure of the current through the coils.

    b. The 12.5, 25.0 and 50 mV scales are used on the recorder as needed. These correspond to 0.125, 0.250 and 0.500 mA scales.

2. The furnace is turned on gradually by switching the synchronous motor switch on the "on" position.

3. The furnace current can easily be maintained at a constant level $\pm$ 0.5 A with manual adjustment of the C.A.T. output; the corres-

ponding temperature stability is $\pm$ 10 $^{\circ}$K.

4. As the cell heats and effusion begins, the recorder pen moves in the direction of decreasing coil current. The most consistent rates of effusion have been recorded using a chart speed of one inch per minute and a recorder scale such that the pen traverses the chart in two or three minutes. These are perhaps the optimum conditions for the shortest run time with the greatest precision.

5. After one obtains several rate of effusion curves or is reasonably sure the rate of weight loss is at a constant value (at least two minutes after furnace turn on), the recoil force data is obtained.

6. It has appeared advantageous to measure the recoil force with the recorder set on the most sensitive scale feasible and with a fast chart speed.

7. With the above parameters satisfied, the synchronous motor switch is turned to the "OFF" position at a time carefully marked on the recorder chart and the furnace current is reduced to 20A. The following observations suggest this turn-off procedure.

   a. An instantaneous furnace cut off upsets the balance servo-system a great deal.

   b. A slow turn off rate was found to be satisfactory. Since it is necessary that this rate be reproducible, a synchronous motor is used. (The turn off rate has not been optimized.)

   c. If there is still some minute furnace current-balance inter-action, cutting the current to 20A instead of zero would help minimize the interaction; a current of 20A produces a tempera-ture (700°C) too low for any appreciable effusion of the sam-ples of interest here.

8. One now has rate of effusion and recoil data. The final experimental measurement is the observed temperature of the cell. With the automatic optical pyrometer, this is a very simple task. Since the pyrometer has been aligned previously, one needs only to activate the shutter in the bottom of the furnace chamber and read the temperature from the pyrometer meter. This measurement can be made at any time during the run and in just a few seconds. This author chose to do it at the end of the last rate of effusion measurement, just before the recoil measurement.

The above series of operations express in detail the procedure used in the experiment. This corresponds to the best procedure as of April, 1968.

APPENDIX C

TEMPERATURE CORRECTIONS TO OPTICAL PYROMETER READINGS

FOR WINDOWS WITH LESS THAN 100% TRANSMITTANCE

An example of temperature corrections to optical pyrometer readings

for windows with less than 100% transmittance is shown in Table IX.

These corrections are determined from a series expansion of Wien's Law,

$$AK = 1/T_o - 1/T_c \qquad (64)$$

where $\underline{AK}$ is Wien's Law constant for a given prism, $\underline{T}_o$ is the observed

temperature, and T_c is the correct temperature.

Rearranging equation (64),

$$\frac{1}{T_c} = \frac{1}{T_o} -AK = \left[1 - (AK)(T_o)\right]/T_o \qquad (65)$$

or

$$T_c = T_o/ 1 - (AK)(T_o)$$

Using the binomial expansion for $(1-X)^{-1}$,

$$T_c = T_o \; 1 + (AK)(T_o) + (AK)^2(T_o)^2 + \ldots + (AK)^n(T_o)^n +\ldots \qquad (66)$$

Thus, T_c is expressed in a form readily programmed on a computer.

For a tabulation, it was felt that a temperature correction $\underline{\Delta T_c}$ would be

more useful than the corrected temperature $\underline{T_c}$, thus

$$\Delta T_c = (T_o)^2 (AK)\left[1.0 + (AK)(T_o) + (AK)^2(T_o)^2 + \ldots (AK)^n(T_o)^n\right] \quad (67)$$

where

$$T_c = T_o + \Delta T_c \tag{68}$$

Table IX shows values of ΔT_c for various $\underline{AK}$ and T_o values. All $\underline{\Delta T_c}$ values tabulated are correct to ± 0.01 ^{o}K.

The following is a list of the computer program in Fortran IV language used to generate the temperature corrections of Table IX. Fortran IV words and their English Equivalents.

Fortran IV Word	English Equivalent
AK	Wien's Law Constant
TEMPO	Temperature observed with the pyrometer
TEMPC	Correction to observed temperature for less than 100% light transmittance of the prism.

TABLE IX

TEMPERATURE CORRECTIONS TO OPTICAL PYROMETER READINGS FOR WINDOWS WITH LESS THAN 100 % TRANSMITTANCE

Temp. Obs. °K		1.0	2.0	3.0	4.0	AK Values 5.0	6.0	7.0	8.0	9.0	10.0
1000.0	=	1.00	2.00	3.01	4.02	5.03	6.04	7.05	8.06	9.08	10.10
1025.0	=	1.05	2.11	3.16	4.22	5.28	6.34	7.41	8.47	9.54	10.62
1050.0	=	1.10	2.21	3.32	4.43	5.54	6.66	7.77	8.89	10.02	11.14
1075.0	=	1.16	2.32	3.48	4.64	5.81	6.98	8.15	9.33	10.50	11.68
1100.0	=	1.21	2.43	3.64	4.86	6.08	7.31	8.54	9.77	11.00	12.23
1125.0	=	1.27	2.54	3.81	5.09	6.36	7.65	8.93	10.22	11.51	12.80
1150.0	=	1.32	2.65	3.98	5.31	6.65	7.99	9.33	10.68	12.03	13.38
1175.0	=	1.38	2.77	4.16	5.55	6.94	8.34	9.74	11.15	12.56	13.97
1200.0	=	1.44	2.89	4.34	5.79	7.24	8.70	10.17	11.63	13.10	14.57
1225.0	=	1.50	3.01	4.52	6.03	7.55	9.07	10.60	12.12	13.66	15.19
1250.0	=	1.56	3.13	4.71	6.28	7.86	9.45	11.03	12.63	14.22	15.82
1275.0	=	1.63	3.26	4.90	6.54	8.18	9.83	11.48	13.14	14.80	16.47
1300.0	=	1.69	3.39	5.09	6.80	8.51	10.22	11.94	13.66	15.39	17.12
1325.0	=	1.76	3.52	5.29	7.06	8.84	10.62	12.40	14.20	15.99	17.79
1350.0	=	1.82	3.65	5.49	7.33	9.17	11.02	12.88	14.74	16.60	18.47
1375.0	=	1.89	3.79	5.70	7.60	9.52	11.44	13.36	15.29	17.23	19.17
1400.0	=	1.96	3.93	5.90	7.88	9.87	11.86	13.86	15.86	17.87	19.88
1425.0	=	2.03	4.07	6.12	8.17	10.23	12.29	14.36	16.43	18.51	20.60
1450.0	=	2.11	4.22	6.34	8.46	10.59	12.73	14.87	17.02	19.17	21.33
1475.0	=	2.18	4.36	6.56	8.75	10.96	13.17	15.39	17.61	19.84	22.08
1500.0	=	2.25	4.51	6.78	9.05	11.34	13.62	15.92	18.22	20.53	22.84
1525.0	=	2.33	4.67	7.01	9.36	11.72	14.08	16.46	18.83	21.22	23.62
1550.0	=	2.41	4.82	7.24	9.67	12.11	14.55	17.00	19.46	21.93	24.60
1575.0	=	2.48	4.98	7.48	9.99	12.50	15.03	17.56	20.10	22.65	25.20
1600.0	=	2.56	5.14	7.72	10.31	12.90	15.51	18.12	20.75	23.38	26.02
1625.0	=	2.64	5.30	7.96	10.63	13.31	16.00	18.70	21.40	24.12	26.84
1650.0	=	2.73	5.46	8.21	10.96	13.73	16.50	19.28	22.07	24.87	27.68

TABLE IX (Continued)

AK in Mireds x 1.0 x 10^6, Temperature in Degrees Kelvin

```
    DIMENSION TEMPO(84),AK(10),TEMPC(10),B(10),C(10),D(10),E(10)
106 FORMAT(1H1,////////,45X,23HTEMPERATURE CORRECTIONS,/39X,35HFOR LES
   2S THAN 100 0/0 TRANSMITTANCE)
107 FORMAT(24X,10F7.1,/)
108 FORMAT(16X,F7.1,2H = ,10F7.21
109 FORMAT(/31X,51HAK IN MIREDS*1.0E 06, TEMPERATURE IN DEGREES KELVIN
   3)
110 FORMAT(F7.1)
111 FORMAT(F5.1)
112 FORMAT(24X,6P10F7.1,/)
114 FORMAT(//14X,10HTEMP. OBS.,30X,9HAK VALUES)
115 FORMAT(16X,F7.1,2H =,10F7.1)
    WRITE(6,106)
    WRITE(6,114)
    READ(5,110) TEMPO(1)
    DO 10 I=2,81
 10 TEMPO(I) = TEMPO(I-1) + 25.0
 11 READ(5,111) AK(1)
    IF(AK(1).EQ.55.0) GO TO 13
    DO 12  J=2,10
 12 AK(J) = AK(J-1) + 1.0
    GO TO 15
 13 DO 14 J=2,10
 14 AK(J) = AK(J-1) + 5.0
 15 WRITE(6,107)(AK(J),J=1,10)
    DO 16 J=1,10
 16 AK(J) = AK(J)   /   1000000.0
    DO 18 I = 1,81
    DO 17 J=1,10
    B(J) = AK(J)  *  TEMPO(I)
    C(J) = B(J)*B(J)
    D(J) = B(J)* C(J)
    E(J) = B(J)* D(J)
```

```
      TEMPC(J)=TEMPO(I)*B(J)*(1.0+B(J)+C(J)+D(J)+E(J)+B(J)*E(J)+          C(
     5J) * E(J) + D(J) * E(J))
   17 CONTINUE
      IF(AK(J).LE.50.E-06) GO TO 21
      WRITE(6,115) TEMPO(I),(TEMPC(J),J=1,10)
      GO TO 22
   21 WRITE(6,108) TEMPO(I),(TEMPC(J),J=1,10)
   22 IF(I.FQ.27) GOTO 20
      IF(I.FQ.54) GOTO 20
      IF(I.EQ.81) GOTO 20
      GO TO 18
   20 WRITE(6,109)
      WRITE(6,106)
      WRITE(6,114)
      IF(I.EQ.81) GO TO 18
      WRITE(6,112) (AK(J),J=1,10)
   18 CONTINUE
      GO TO 11
      STOP
      END
$ENTRY
 1000.0
    1.0
   11.0
   21.0
   31.0
   41.0
   55.0
$IBSYS
```

VITA

2.

Eugene Albert Elphingstone

Candidate for the Degree of

Master of Science

Thesis: THE MIKER TECHNIQUE FOR DETERMINING VAPOR PRESSURES AT HIGH
         TEMPERATURE

Major Field: Chemistry

Biographical:

    Personal Data: Born in Marianna, Arkansas, August 19, 1943, the
        son of Mr. and Mrs. Edwin Aubrey Elphingstone.

    Education: Graduated from T. A. Futrall High School, Marianna,
        Arkansas, in May, 1961; received the Bachelor of Science
        degree from Arkansas State University in August, 1965, with
        a major in Chemistry; completed requirements for the Master
        of Science degree at Oklahoma State University in May, 1969.

    Professional Experience: Graduate teaching assistant, Department
        of Chemistry, Oklahoma State University, 1967-68.